# Mechanisms Regulating Development and Homeostasis of Mammary Epithelium Organization

By
Alexander Pfannenstein

Dissertation
Submitted to the Faculty of the
Graduate School of Vanderbilt University
in partial fulfillment of the requirements
for the degree of
DOCTOR OF PHILOSOPHY
in
Cell and Developmental Biology

August 11, 2023
Nashville, Tennessee

Approved:
Ian G. Macara, PhD, Advisor
Kathleen L. Gould, PhD, Committee Chair
Rebecca A. Ihrie, PhD
Robert J. Coffey, MD
W. Kimryn Rathmell, MD PhD

## Acknowledgements

This work was supported by these funding sources: Integrated Biological Systems Training in Oncology grant T32CA119925 to AP, and NIH CA197571 from the NCI to IGM. At Vanderbilt, I would like to thank both the office of biomedical research education and training, and the department of cell and developmental biology for providing an environment that supported my growth as a graduate student and scientist. I would also like to thank my committee members for their scientific and career feedback, and for dedicating time to be a part of my committee.

I thank Ian Macara and the rest of the Macara lab members through the years. Ian has been a great mentor and supportive of scientific exploration while providing solid perspective and feedback. His passion for interdisciplinary science sets the tone. He is a science machine, never short of useful insight. The lab members have been critical. Special thanks to Lindsey Seldin, who guided my introduction to the lab and rotation project. Fellow graduate students Christian de Caestecker, Erica Tross, and Maria Fomicheva, and postdocs Lindsey Seldin, Mukhtar Ahmed, Armelle Le Guelte, Chih-chao Yang, Loic Fort, Paola Molina, and Aishwarya Venkataravi, as well as lab manager Mikiyas Daniel, provided support for my growth as a scientist. Special thanks to Loic Fort, who accommodates my pace on our mid-week runs.

I thank my family and friends. I have made many wonderful connections in my time in Nashville and enjoyed the happy hours, long weekends, occasional pontoon boat excursions, and other numerous shenanigans. Shoutout to Marylanders Sam Miskiel and Dan Ashirov for their support and coming to visit. My family has been critical in my success as a person including during graduate school. Greg, Vicki and Pat have been great role models and parents that have helped with science projects. We have come a long way from feeding plants Gatorade and coffee. My wonderful siblings, Adam and Kelly, their significant others Jen and Jay, and my wonderful nieces and nephews Aubrey, Camden, Dahlia, Kenzi, and Gio are thanked for their support and for providing the occasional human subject for experimentation. I cannot thank my wife Veronika enough. We met in graduate school, and she always brings out the best in me. I'd also like to thank Ollie who accompanies us on long walks.

I would also like to thank my previous advisors in science Charles Bieberich at UMBC and Jonathan Keller at the NCI, as well as high school AP bio teacher Ed Neuman who fostered my interest in science research. My first lab research experience was with Jonathan Keller at the NCI in Frederick MD. His guidance fostered my passion for research. He is extremely generous with his mentoring, feedback, time, and resources and I aspire to be as supportive of an advisor.

## Table of Contents

## List of Tables and Figures

## Abbreviations

| | |
|---|---|
| 2D | 2 dimensional |
| 3D | 3 dimensional |
| AJ | Adherens junction |
| Akt | Stock A strain K mouse thymoma/transforming serine/threonine protein kinase |
| ANOVA | Analysis of variance |
| aPKC | Atypical protein kinase C |
| BrdU | Bromodeoxyuridine |
| CDK | Cyclin-dependent kinase |
| CFSE | Carboxyfluoroscein succinimidyl ester |
| Crb | Crumbs |
| CRISPR | Clustered regularly interspaced short palindromic repeats |
| DCIS | Ductal carcinoma *in situ* |
| DLG | Discs large |
| DMEM | Dulbecco's modified eagle medium |
| DMSO | Dimethyl sulfoxide |
| DNA | Deoxyribonucleic acid |
| ECM | Extracellular matrix |
| EGF | Epidermal growth factor |
| EGFR | Epidermal growth factor receptor |
| Eph4 | Ep-1 (IM-2 derivative) clone H4 |
| ERK | Extracellular signal-regulated kinase |
| FBS | Fetal bovine serum |
| FGF | Fibroblast growth factor |
| Gai | Inhibitory G protein alpha |
| GFP | Green fluorescent protein |
| H2B | Histone H2B |
| HER2 | Human epidermal growth factor receptor 2 |
| IDC | Invasive ductal carcinoma |
| IGF1 | Insulin-like growth factor 1 |
| ILK | Integrin linked kinase |
| JNK | Jun N-terminal kinase |
| KO | Knockout |
| LGL | Lethal giant larvae |
| LGN | Leucine glycine asparagine |
| LTR | Long terminal repeat |
| MAPK | Mitogen activated protein kinase |
| MCC | Multiciliated cell |

| | |
|---|---|
| MDCKII | Madin Darby canine kidney II |
| MEC | Mammary epithelial cell |
| MEM | Minimum essential media |
| MLCK | Myosin light chain kinase |
| MMTV | Mouse mammary tumor virus |
| Muc1 | Mucin 1 |
| MYPT | Myosin phosphatase |
| NT | Non-targeting |
| NuMA | Nuclear mitotic apparatus |
| OCD | Oriented cell division |
| Pals | Peptidoglycan-associated lipoprotein |
| Par | Partitioning deficient |
| Patj | PALS1-associated tight junction |
| PCR | Polymerase chain reaction |
| PFA | Paraformaldehyde |
| PH | Pleckstrin homology |
| pHH3 | Phosphorylated histone H3 |
| PI3K | phosphatidylinositol-4,5-bisphosphate 3-kinase |
| PIP3 | Phosphatidylinositol-3,4,5-trisphosphate |
| PLC | Phospholipase C |
| Pten | Phosphatase and tensin homolog |
| PyMT | Polyomavirus middle T antigen |
| ROCK | Rho-associated protein kinase |
| Scrib | Scribble |
| SD | Standard deviation |
| SEM | Standard error of the mean |
| sgRNA | single guide RNA (ribonucleic acid) |
| TEB | Terminal end bud |
| TGFb | Transforming growth factor beta |
| TJ | Tight junction |
| WT | Wildtype |
| ZO-1 | Zonula occludens 1 |

# Chapter 1: Introduction

## 1.1 Epithelial Function and Organization

The organization of cells into tissues characterizes all Metazoa (animals) and one main tissue type is epithelium. Epithelia line the internal and external surfaces of the body and perform critical roles at the interfaces of these separated domains. The epithelium is thought to have arisen over 600 million years ago in multicellular organism evolution, before that of neural, muscular, and connective tissues [1]. This ancient origin is supported by its presence in some non-metazoan organisms such as *Dictyostelium discoideum* (Amoebozoan) [2]. In complex animals, the epithelium is a critical component of all organ systems, and a range of types are present with diverse functions.

### 1.1.1 Epithelial Tissue Types and Functions Overview

The arrangement of cells within epithelium supports its function. Defining characteristics of epithelial cells include their adherence to a basement membrane, adherence to other epithelial cells, polarity, and organization into sheets [1]. While these features define all epithelial cells, the cells themselves may differ drastically in shape and function between various organs. Cells may be of squamous, columnar, and cuboidal shape and may form simple (single/mono-layer), stratified, or pseudostratified arrangements. Squamous cells have a large surface area, allowing for gas exchange in lung epithelia; columnar cells are tall and commonly have microvilli arranged in a brush border to facilitate absorption; and the relatively symmetric cuboidal cells tend to be found in tissues where either secretion or solute exchange is emphasized such as in glandular or kidney epithelium, respectively. Stratified epithelia usually form protective barrier regions such as in the skin, while simple epithelia usually perform absorption and secretion roles like in the gastrointestinal tract, kidneys, and glands for example.

### 1.1.2 Cellular Processes that Control of Development and Homeostasis of Epithelium

In section 1.1.2.1-5, characteristics and behaviors supporting normal growth and development will be introduced to provide insight and perspective on the processes shaping epithelium. How cells apply polarity and junctional characteristics to support a collective organization is not well understood.

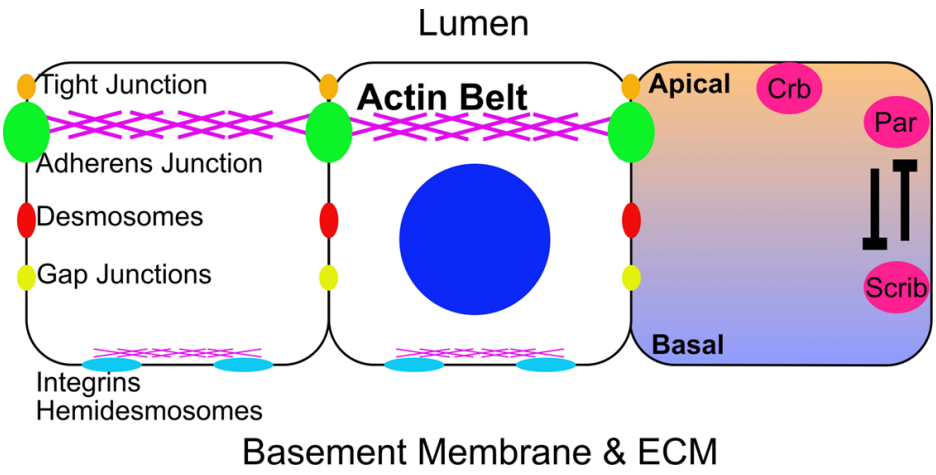


**Figure 1.1 Epithelial Cell Polarity and Junctions**

#### 1.2.1.1 Cell Polarity

The polarization of cells within an epithelium supports many of their functions including directional absorption and transport of molecules extracellular space, or release or secretion of cellular content such as hormones or milk components. These processes are just a few examples of epithelial functions that rely on a conserved set of proteins that establish and maintain apical-basal cell polarity. Polarity proteins and the overarching system of establishing asymmetric distributions within cells was first characterized in a landmark screen of *C. elegans* development where random gene mutations – often disrupting gene function – were probed at the zygotic stage to determine which disrupted the asymmetric partitioning of the first cell division. These studies identified the Par proteins (partitioning-deficient) in *C. elegans* and their homologues were later discovered in other organisms [3-6]. Since these studies, other

critical regulators of cell polarity have been found, elucidating an intricate system where different apical or basal polarity protein complexes support the establishment and maintenance of polarized domains of the cell through mutual antagonism of opposing polarity complexes [7, 8].

In the canonical model of apical-basal polarity in epithelia, the Crumbs and Par complexes maintain the apical domain while a basal Scribble (Scrib) complex determines basal identity. The Par complex consists of Par3, Par6, and atypical protein kinase C (aPKC). The Crumbs complex consists of the transmembrane protein Crumbs (Crb), PatJ, and Pals1. The Scrib group consists of Scrib, LGL, and DLG (which do not form a stable complex). Crb interacts with and helps form the apical junctional complex consisting largely of the apical-most tight junction proteins and linkage to the cytoskeleton. Par3 and Par6 are large scaffolding proteins supporting the interaction of the serine/threonine kinase aPKC with many potential targets for phosphorylation or other apical interacting proteins. The basal polarity proteins Par1 and LGL are targets of aPKC and their phosphorylation leads to their inactivation and re-localization to the basal domain by Par5. Likewise, Par1 may phosphorylate Par3, where it is recycled into the cytoplasm by binding through Par5 and dephosphorylated, supporting its reactivation. This regulatory network of constant antagonism and feedback helps establish and maintain polarized epithelial domains, which in turn, supports tissue organization. Through different interacting partners, lipid moieties in polarized domains, and mutual antagonism, these complexes establish apical-basal polarity, support epithelial development and maintenance, are also important for processes such as migration and division orientation.

#### 1.1.2.2 Cell-Cell Junctions

Of critical importance to epithelial structure and integrity is the linkages cells make to one another through homotypic cell adhesion molecules. These junctions support the defining characteristics of epithelium. Tight junctions form a barrier to solutes and help establish a fence for polarized membrane protein localization. Adherens junctions provide much of the structural rigidity within the tissue sheet and

form connections with the dynamic actin-myosin cytoskeleton, important for collective behaviors such as migration. Desmosomes provide structural stability and integrate into the cytoskeleton through binding to keratins. Gap junctions facilitate exchange of small molecules and ions between cells. These processes help to keep epithelium in a polarized, adherent sheet (Fig. 1).

The adherens junction is composed of the cell-cell adhesion molecules Cadherin and Nectin, stabilized on the intracellular side by Catenin and Afadin, respectively. E-cadherin works in a calcium dependent manner and is interacts at the intracellular side with the catenin family proteins alpha-, beta-, and delta- (p120) catenins. Beta-catenin and p120-catenin support E-cadherin stabilization at the cell membrane and prevent it from being endocytosed while alpha-catenin attaches the cadherin-catenin complex to the actin cytoskeleton. The importance of E-cadherin in epithelial tissues is well established and most tissues would not be maintained in the absence of cadherin-based junctions. Indeed, when Cdh1 (the gene encoding E-cadherin) is knocked out, development is halted before the implantation stage (embryonic day 4) in mice [9]. Loss of E-cadherin in the luminal cells of the mammary gland prevents their incorporation into normal epithelial structures [10].

This junction is also supported on the intracellular side by a strong crosslinking to the actomyosin (actin and myosin) belt that sits around the perimeter of the apical domain. The perijunctional actomyosin belt is critical for many processes involving motility or collective migration by myosin contraction on its actin filament substrate. This ability to constrict the apical domain supports many developmental processes such as convergent extension and tube folding [11].

In mammary epithelial cells, loss of E-cadherin-based adhesion is highly detrimental to epithelial order. Disruption of E-cadherin by blocking antibodies, loss of p120, or genetic ablation all destroy epithelial integrity in mammary glands as luminal cells disassociate [10, 12, 13]. Adherence to the basal/cap cell layer is also disrupted when P-cadherin, which is expressed in basal and cap cells, is inhibited by introducing a specific blocking antibody *in vivo* [12]. Desmosomes also play a role in luminal-basal cell organization. Preventing desmosome formation using blocking antibodies disrupts the aggregation of mammary luminal cells with basal cells around the exterior [14].

Adherens and desmosome junctions are both thought to play a role in mammary cell migration within the epithelial context [15, 16].

A fundamental question in the mammary biology field is how the motile properties of cells contribute to morphogenesis of the tissue. Junction-dependent motility in other models of epithelial morphogenesis may involve buckling, folding, or convergent extension of sheets of cells to form tubes and ducts [17]. Many well studied epithelia form tubes through these processes which require existing epithelial sheets of cells, while in the mammary gland the generation of epithelial architecture arises from multilayered masses in the TEB [18], as is described below (Section 1.2). While there are different mechanisms involved in generating tissue shape, it is likely that the production of forces through adherens junctions is common to all epithelia including the mammary gland. It is possible that intercalation of the cells is a driving force to generate epithelial architecture, but it still remains unclear if this alone is sufficient for morphogenesis or whether other junctions such as the tight junction are involved [19].

While transformed or cancer cells are typically more motile and unconstrained than their normal epithelial parents, many still retain their cell-cell junctions such as E-cadherin, at least at the earlier stages of ductal carcinoma *in situ* (DCIS) and invasive ductal carcinoma (IDC) in the breast [20, 21]. The presence of E-cadherin in these cells may support their motility around the tumor and surrounding environment. In support of this idea, recent studies have also shown that distant metastasis does not require an epithelial to mesenchymal transition as once thought, and that in some cases E-cadherin is required for efficient metastasis [22, 23]. These findings suggest mammary cell migration occurs in the context of cells maintaining adherens junctions and these behaviors may be important in development, homeostasis, and disease. Other types of junctions may also be important for cell motility in normal and diseased state in the mammary gland.

#### 1.1.2.3 Cell-Matrix Junctions

Many cells adhere to non-cellular substrates, a process which is critical for cell anchorage, motility, and signaling. In epithelial cells, specialized junctions between the basement membrane and the cell control adhesion. Integrins are transmembrane receptors that usually bind to extracellular matrix (ECM) proteins but may also make cell-cell connections [24]. In epithelial cells, integrin binding is essential to prevent anoikis (cell death through loss of attachment) and promote proper development [25, 26]. In mammary epithelium, this process is largely mediated through ERK and JNK signaling downstream of integrin attachment [27-29]. Loss of JNK signaling promotes excessive mammary branching and causes a delay in the rate of lumen clearance of cells in developing mammary glands, indicating there may be a role for apoptosis in mammary gland development [28]. Integrin connections are also important for establishing cell polarity. In the skin loss of beta-1 integrin results in loss of stratifying oriented cell divisions through failure to alter mitotic spindle position [30, 31]. In mammary epithelial cells, blocking or deleting beta-1 integrin results in lumen formation defects in 3D acinar culture by failure to correctly orient cell polarity and the microtubule network [32]. This was determined to be dependent on activation of integrin-linked kinase (ILK) signaling. These results show the importance of integrin signaling in establishing polarity, division orientation, and in promoting survival in mammary epithelial cells.

Cell-matrix interactions are a key player in shaping the mammary gland during development and may also play a role in forming the ductal monolayer. Organoids and *ex vivo* culture techniques have become useful models to study epithelial morphogenesis in relation to ECM composition. Early experiments using mammary epithelial cells show culture of luminal cells only in collagen-I gels results in no lumen formation while addition of basal cells rescues lumen formation due to increased deposition of laminin-1 [33]. These experiments show the ECM composition greatly affects mammary epithelial morphogenesis. In these same studies, it was shown basal cells from patient tumors often failed to interact with and polarize luminal cells due in part to lack of laminin deposition, implicating changes in ECM to breast cancer and

epithelial dysplasia [33]. Luminal cell dependence on basal cell and ECM deposition may be a vital cue during mammary gland development as cells form a ductal monolayer.

One important model that has emerged is salivary gland budding morphogenesis which shares several similarities with mammary gland morphogenesis. The development of the salivary gland can be studied using 3D *ex vivo* culture, a system which has been hard to replicate for the mammary gland [34]. Recent evidence suggests that cells in budding regions sort based on the strength of cell-matrix and cell-cell adhesion, mediated at least in part through beta-1 integrin [35]. Interestingly, these cells are highly motile and cycle between interior and exterior layers of the bud – a property which may also be present in luminal cells in the developing mammary gland TEB.

In the mammary gland, ECM is thought to influence the bifurcation angle of the TEB and present a physical constraint around the neck region in order to shape the developing mature duct [15, 36]. This hypothesis fits nicely with a need for a physical constraint to direct multilayered cells of the TEB into a uniform monolayer, but more work is needed to parse apart the physical cues that control this process and how these cues arise in the ECM arise. Not only composition but also ECM alignment may be an influence on the migration of tumor cells. Studies show radial alignment of collagen in the stroma adjacent to primary tumors has worse prognosis than does unaligned collagen [37, 38]. *In vitro* studies have shown the tendencies for mammary-derived normal and cancer cells to migrate along collagen but whether this mechanism is causal to worse cancer outcome is challenging to determine [39, 40].

#### 1.1.2.4 Oriented Cell Division

Mitosis is perhaps the most dramatic event a cell can undergo. A complete cell cycle involves the growth of the cell organelles and duplication of the entire genome, along with the process of segregating all these intercellular components properly through establishing the massive mitotic spindle apparatus. Complex regulatory networks guide the cell into and through mitosis, but the focus of this section will be on

the physical separation of the mother cell into two daughters and its consequences in epithelium. Cell division in epithelia is a carefully controlled process with a host of proteins involved in alignment of the mitotic spindle and cytokinetic ring. The asymmetric and highly adherent nature of epithelial cells presents a unique challenge to cell division.

There are several different considerations for dividing epithelia cells. One being how to ensure the architecture of the tissue is maintained during and after division, and another consideration is how to maintain junctional order and barrier function through division. Cells within a simple monolayer must maintain both daughter cells within the tissue plane and to do this they commonly rely on planar division orientation so both daughter cells land within the tissue plane. To accomplish this, a conserved set of proteins regulate the orientation of the mitotic spindle during metaphase to properly turn and align the spindle, resulting in oriented cell division (OCD) [41]. This is essential because it controls the relative position of the nuclei directly after division and spindle position also regulates the plane of the division itself or cytokinesis. Early experiments detailed this spindle-position-dependent control of cleavage in urchin eggs by rolling the egg while pressing gently to induce a new spindle-aligned axis, which, remarkably, altered the position of the newly forming cleavage furrow [42]. Even earlier theories by Oscar Hertwig proposed a rule of alignment of the division plane (cytokinesis) perpendicular to the long axis of the cell [43, 44]. While some studies support this rule [45, 46], there seem to be exceptions, with cell tension being a critical cue in some epithelial cells [47-49]. One often overlooked dimension in these studies is the apical-basal axis – which for many epithelia, is the long axis. Indeed, when considering the shape of the average (columnar) enterocyte, rules such as these may lead to multilayering issues. Intestinal cells divide in the plane of the monolayer which, within the cell, is approximately half the length of their long apical-basal axis [50]. The regulation of OCD has long intrigued scientists due to its potentially impactful effects on tissue development.

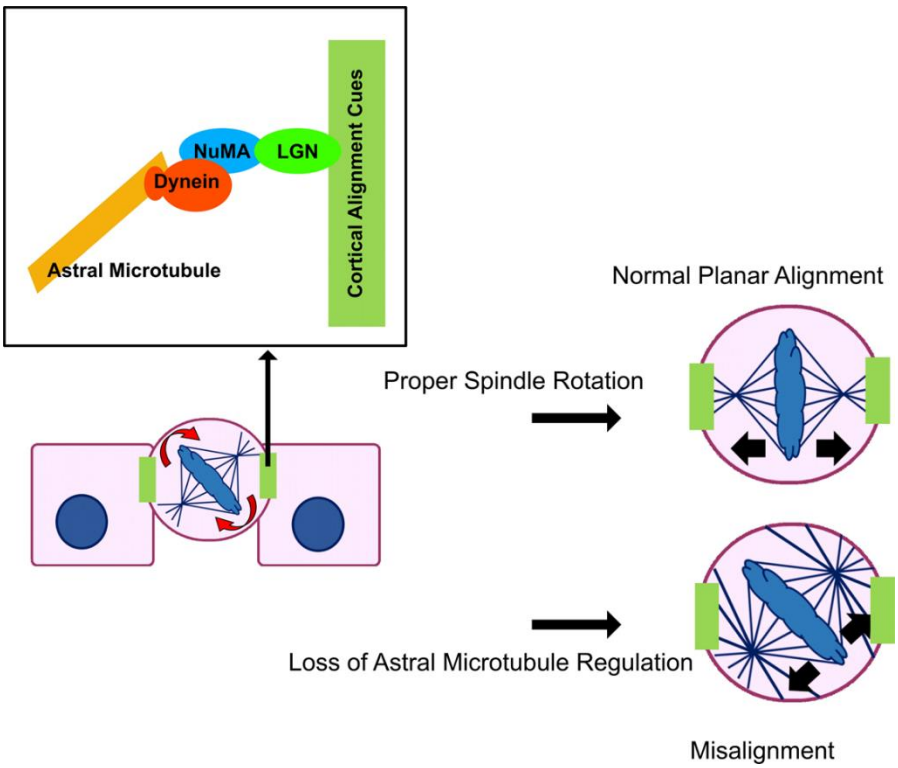


**Figure 1.2 Mitotic Spindle Alignment**

The proteins involved in aligning the mitotic spindle are highly conserved, but these critical players may have several different interacting partners, even in different tissues of the same organism, to have the desired outcome on spindle alignment and OCD. A tripartite complex of Gai, LGN, and NuMA are the main components controlling mitotic spindle orientation (Fig. 2). As the spindle is forming, NuMA is highly enriched at the spindle poles and binds the motor protein Dynein. NuMA and LGN meet at the tips of astral microtubules which get stabilized to the cell cortex. At these tip ends, LGN associates with Gai, which is associated with the cortex through its myristylation. LGN was observed to be the critical linking protein between astral microtubules and the cell cortex that promotes alignment of the mitotic spindle [51, 52]. This binding of Gai to LGN to NuMA to Dynein, stabilizes astral microtubules at the cortex, and it is thought that failure to form a complex at the cortex may result in microtubules being subject to instability [53-55]. While this process explains the stable localization of spindle anchoring machinery, it does not help to explain the planar alignment observed in simple epithelia. To this end, the polarity machinery and junctions become critical.

Experiments involving loss of Par3 or other apical polarity components show disrupted spindle orientation in monolayer epithelia [56-59] although aPKC activity is not critical for orientation in all cases, such as chick neuroepithelia [60]. The spindle orientation-promoting activity of aPKC was shown to be through phosphorylation of LGN, which led to LGN dissociation from Gai and sequestration by 14-3-3 protein [56]. The basal polarity complex Scribble, DLG, and LGL also help to control spindle orientation. DLG was shown to interact directly with LGN and induced cortical localization [61, 62]. Asymmetric division and perpendicular spindle orientation is required in some epithelia, for example in the skin which is stratified or during neuroepithelial development. Again, the polarity machinery plays a critical role in regulating the spindle alignment process in these instances. One protein that was shown to mediate this asymmetric spindle orientation is Inscuteable. Inscuteable was shown to bind to LGN and promote perpendicular spindle orientation with respect to the tissue plane [63, 64]. The recruitment of a spindle pole to the apical domain of basal stem cells allows for perpendicular, stratifying divisions to support the thickness of the other skin layers. Development and replenishment of this outer epidermal layer is critical for protection from abrasion and maintaining moisture within the body. Inscuteable localization to the apical domain is supported through interaction with Par3 and this complex in turn recruits the LGN, NuMA, Dynein complex to attach the astral microtubule of one spindle pole to the apical cortex [65].

Of interest in this field is how astral microtubules are stabilized or degraded and how the mitotic spindle can adopt the proper orientation. Molecular motor proteins play a critical role in this dilemma. The turning force provided to the mitotic spindle is thought to be delivered largely by the minus-end directed Dynein [66-69]. Dynein here refers to the multimeric protein structure consisting of Dynactin and all other associated proteins that allows this motor to move along microtubules and bind cargo. Kinesin motor proteins move toward the microtubule plus-end and primarily support trafficking of cargo along microtubules during interphase but also regulate the process of chromatin segregation during mitosis [70, 71]. One Kinesin8 family protein that has emerged as a critical regulator of mitotic spindle orientation is Kif18b. Through its interactions with MCAK and EB1, Kif18b regulates the depolymerization of astral microtubules [69, 72,

73]. It is most highly expressed in a small window during mitosis or has its localization restricted to the nucleus during interphase [73, 74]. Loss of Kif18b was later shown to disrupt the orientation of the mitotic spindle in HeLa cells with respect to the basal substrate [75]. Interestingly this result showed little detriment to the cell besides a delay in timing from prophase to anaphase, and chromatin segregation still occurred with high fidelity. These results showed Kif18b expression and activity are mainly associated with its role in astral spindle microtubule regulation and may present an approach to study the consequences of misorientation of cell division in epithelia without affecting other critical processes (Fig. 2). A Kif18b conditional knockout mouse revealed that loss of spindle orientation in early hair placode morphogenesis results in a defect in progenitor cell fate commitment [76]. The necessity for asymmetric division in this system is most likely contributing to failure to differentiate into hair placode as the asymmetric distribution of fate determinants is required for this process [77]. Within the rest of the developing epidermis, cell divisions may either occur in perpendicular (stratifying) or parallel (planar) fashion to expand the tissue as required. When Kif18b is lost in the interfollicular epidermis, there is no significant change in the average spindle angle, but his may be due to the bi-distributional nature of spindle alignment in this tissue [31, 76]. With this in mind, loss of oriented division itself may be of little consequence in most stratified epithelial tissues, if differentiation is unaffected.

These studies underline a potentially critical role for spindle orientation in maintaining epithelial homeostasis through tissue organization; however, the results from studies at the tissue level in model organisms suggest there is more to the story. In *Drosophila*, follicular epithelial cells dividing in misoriented fashion tend to reintegrate back into the monolayer [78], while in the wing imaginal disc, misoriented divisions result in cell death of the displaced cell [79]. Interestingly, when cell death is inhibited after misoriented division in the wing disc, cells undergo transformation through an epithelial to mesenchymal-like state [79]. During mammalian kidney development, cells will tend to move into the apical luminal space and divide, then both daughter cells reintegrate [80]. This demonstrates the orientation of cell division is unnecessary in some developing tissues due to their divisions occurring independently of epithelial plane constraints, and also demonstrates misoriented divisions in other tissues or

mature tissues at homeostasis, may simply correct daughter cell displacement by supporting their reintegration. In the mammary gland, 30% of cell divisions in the luminal monolayer were observed to have perpendicular alignment relative to the epithelium, yet no accumulation of cells in the lumen has been observed under normal circumstances [81]. However, when Scrib is deleted from these cells, the incidence of perpendicular divisions increases and cells are seen in an aberrant multilayered state [81]. It may satisfy to contribute the multilayering phenotype to the increased incidence of misoriented divisions, however Scrib also acts in other pathways in mammary epithelium including MAPK (mitogen associated protein kinase) signaling to promote proliferation, survival, and lineage fidelity [81]. In a similar vein, Par3 loss alone or combined with oncogene-driven tumorigenesis, in the mammary gland or prostate, promotes tissue dysplasia and more severe tumors but whether this is related to loss of mitotic alignment is unknown [82, 83]. If mammary epithelial cells divide along the wrong axis, they may be displaced into the luminal space where they will then have to be cleared through cell death or reintegration, or they may continue to survive and divide cause disruption to monolayer organization (Fig. 3)

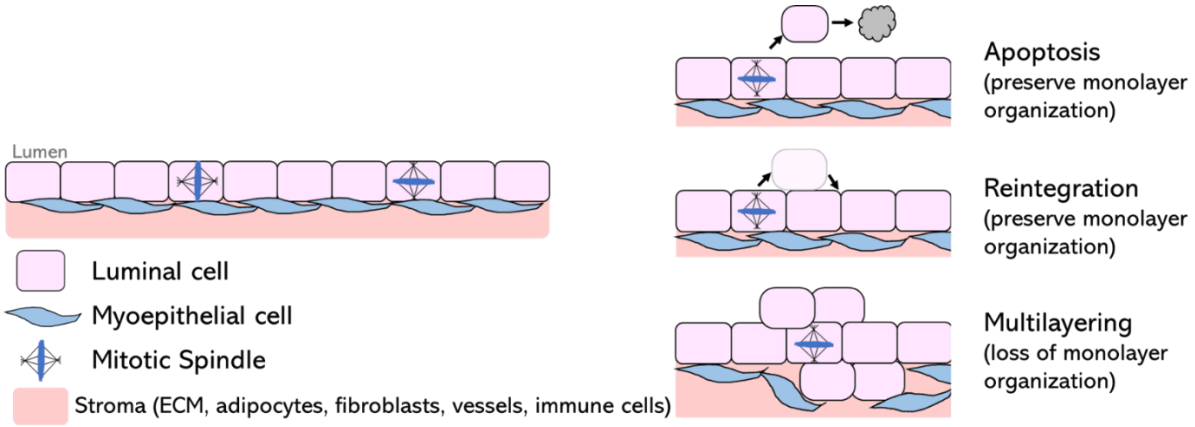


**Figure 1.3 Potential Consequences of Misoriented Division in Epithelial Monolayers**

## 1.2 The Mammary Gland

The mammary gland is a uniquely mammalian organ that nourishes newborns through secretion of milk, although perhaps has developmental origins rooted in other functions. Before the divergence of monotremes and therian mammals (eutherians and marsupials), primordial mammary gland secretions may have primarily been utilized to wet the soft-shelled eggs of early mammals or for preventing infection [84-86]. The mammary gland is still a critical axis of immunity, providing resistance to pathogens to the next generations by secretion of protective immunoglobulins in milk [87]. The major cells that make up the mammary gland are: a luminal epithelial layer that make up the ducts and alveoli that produce milk; a basal/myoepithelial cell layer that contract to induce outflow of milk; and the supporting fibroblasts, endothelial cells, leukocytes, and adipocytes. The mammary gland is a dynamic organ, capable of undergoing several rounds of expansion and contraction in growth with every pregnancy cycle, and it also responds in a cyclic way to hormones and growth factors present during the estrous cycle that have proliferative effects. In section 1.2, the development and function of the mammary gland will be discussed as well as how cancer arises in the mammary gland. For the purposes of this introduction, I will focus mainly on the mouse mammary gland as it shares many similarities with human mammary gland development, structure, and cell types, and I will be using murine mammary glands as a model in the experiments detailed in later sections.

### 1.2.1 Morphogenesis of the Ductal Tree

The mammary gland undergoes several distinct rounds of development at the embryonic, pubertal, and adult stages of life. For the purposes of this introduction, we will focus mainly on the pubertal stages of development where branching morphogenesis occurs and the epithelia organize in such a manner that supports the possibility of future alveologenesis and milk production. But briefly, the mammary gland develops as an invagination from the ectoderm or developing skin of the embryo at embryonic day 10 in mice – observable as a ‘mammary’ or ‘milk’ line on the surface which develops into a placode. FGF and Wnt signaling are critical for this process and

the transcription factor Tbx3 is essential for specification at this stage [88-90]. Once the placode is defined, the cluster of cells burrows deeper into the surrounding mesenchyme and eventually forms a basic tree through several splits of the early end buds. The duct nearest the nipple at this point (E18) is hollow but how this cavitation happens is still not fully understood [91]. One popular theory based on 3D cell culture observations is that apoptosis of the interior cell mass produces the hollow lumen observed at this early stage in embryonic development as well as later on during pubertal development [92]. In male mice, the invaginated rudimentary duct is severed from the nipple through constriction of the mesenchyme, while in humans, hormones regulate the size of the mammary gland expansion during puberty [93, 94].

For the mammary gland to produce a branched network of ducts that produce milk for mammalian offspring, a ductal monolayer system must first form during pubertal morphogenesis. While the luminal epithelium is organized into a cellular monolayer, it originates from multilayered structures present during development called terminal end buds (TEB). TEBs generate ducts as they invade the fat pad, but little is known about underlying mechanisms that control this process. As mentioned previously, apoptosis of the inner body cells of the TEB provides a plausible mechanism for lumen formation and apoptotic cells have been observed in the TEB [95]. This is supported by the observation that inhibiting apoptosis delays the formation of hollow ducts [96]. While this theory is plausible, other studies have seen extensive cell motility in TEB-like cultures of mammary organoids [15, 97]. Furthermore, stratifying divisions can be seen in the exterior luminal TEB cells which would supply more daughter cells to the interior multilayered regions – a process that seems wasteful in attempting to form a ductal monolayer [98]. This leaves the possibility that the cells in the interior body TEB may contribute to some extent to the elongation of the ductal monolayer behind the TEB.

The stroma supporting the epithelium also plays a critical role in development and shaping the mammary gland. One way this occurs is through regulation of TEB branching and constriction of the TEB neck where the mature duct forms. Recent studies provide clues into how this might occur. Modeling suggests that a buildup of extracellular matrix and cells at the tip of the TEB help determine the bifurcation point and the angle at which the new daughter TEBs point into the stroma [36, 99].

Interestingly, extracellular matrix alignment is also predictive of worse breast tumor outcome, lending credence to the idea of the extracellular matrix shaping a motile developing mammary gland [37].

Several upstream growth factor and hormone signaling pathways are required for branching morphogenesis. Insulin-like growth factor 1 (IGF1), estrogen, and progesterone are essential for proliferation of the epithelium [100-102]. Estrogen and progesterone are steroid hormones produced in the ovaries while IGF1 is produced primarily by the fibroblasts in the mammary stroma. This paradigm of incorporating signaling components from near and distant sources is apparent in the mammary gland as it must be able to respond to changes in reproductive cycling through estrogen and progesterone from the ovaries, and cues to generate milk through prolactin from the pituitary gland (reviewed in [93]). Interestingly, only a portion of luminal cells express the estrogen receptor Esr1, indicating the effects of estrogen signaling are mediated through a second paracrine factor. This factor is thought to be the Epidermal growth factor receptor (EGFR) ligand Amphiregulin, which is needed for proper mammary tree growth [103]. Other essential growth factors contributing to mammary gland development include Fibroblast Growth Factor 2 (FGF2) which is critical for supporting TEB growth [94, 104]. Transforming Growth Factor Beta (TGF$\beta$) negatively regulates epithelial growth and is thought to control the spacing of the branching ductal system such that they are evenly distributed in the epithelium [105, 106]. These factors help to control the proliferation and pubertal development of the mammary gland epithelium.

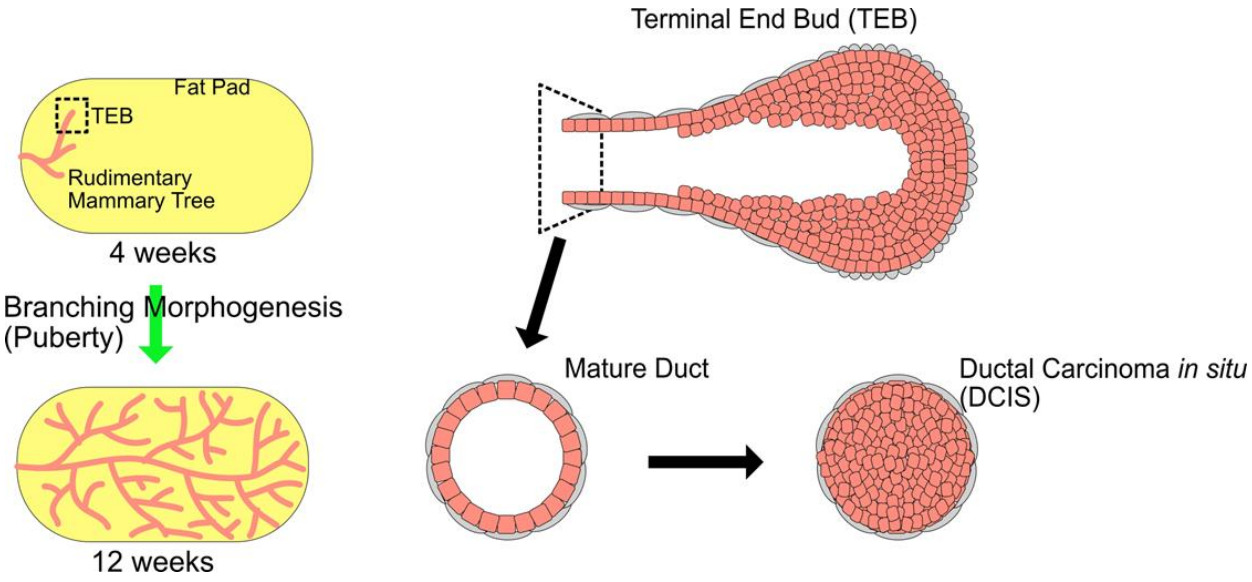


**Figure 1.4 Mouse Mammary Gland Development at Puberty, Multilayered TEB to Monolayer Duct Transition, And Early Breast Cancer Formation Resembling Multilayered TEB**

### 1.2.2 Breast Cancer and Tumorigenesis

Breast cancer is still a leading cause of cancer death and is the most prevalent cancer type in women [107]. While decent therapies exist for hormone receptor or HER2-expressing cancers, understanding how these tumors form and progress may provide insight into treatment or preventative approaches. Generally, early breast lesions are characterized by hyperproliferation and some degree of epithelial dysplasia (such as in DCIS) and may progress into invasive disease from this state although this progression is not guaranteed [108-110]. Most approaches to mimic breast cancer in the lab to study its progression utilize mutational and expression data from patient cancers. Of the most commonly mutated pathways in breast cancer, PI3K/Akt signaling stands out. Several genes within this pathway (PIK3CA, PTEN, AKT1) have been shown to be altered in breast cancers [111]. In choosing a model for breast cancer, it will be critical to incorporate this signaling pathway. PI3K/Akt signaling is also implicated in regulation of mitotic spindle orientation, suggesting a potential mechanism for initiating multilayering in cancer cells [112, 113].

Mouse models that recapitulate aspects of human breast cancers are critical tools for studying the formation and progression of tumors. The most common model is the expression of the viral-derived oncogene middle T antigen from mouse polyomavirus (PyMT) [114]. It was first expressed in mouse mammary gland by use of the mouse mammary tumor virus LTR promoter (MMTV-PyMT) and produced primary tumors weeks after mammary development, while also producing metastasis to secondary metastatic sites, commonly the lung [115]. These cancers also resemble common human subtypes (Luminal-B) and share common expression of key prognostic signaling factors with human cancers such as estrogen receptor, progesterone receptor, and HER2 early in disease [116]. While this model has many positive aspects, one caveat is that disease progression is rapid and many pathways such as Src, PI3K/Akt, MAPK, and PLC-gamma are activated by PyMT [114], of which Src is essential for tumor formation [117]. It has recently been shown that misorientation of cell division occurs in conjunction with the early stages of tissue dysplasia seen in MMTV-PyMT mice, indicating spindle misorientation as a potential first step in tumorigenesis [118]. As the tumors develop rapidly, this model presents challenges with determining if misoriented division is important for the progression of this model. Other models also exist such as loss of Pten, the phosphatidyl-inositol-3,4,5-trisphosphate 3-phosphatase, which regulates PI3K/Akt signaling, although loss of Pten alone causes mild hyperproliferation and dysplasia that is cleared within weeks from the mammary gland, but also results in misoriented cell division [119]. These data from these 2 models point to division misorientation being a key first step in tumor formation.

Besides misoriented division, there are many other potential mechanisms by which epithelial cells could begin to multilayer. Extrusion of oncogenic-Ras-expressing cells clears them from the epithelial layer to promote their disposal, but additional mutations may allow for their survival and proliferation within the lumen, and may be common to other transformed cells [120]. It is possible as well that cancer cells downregulate or internalize junctional proteins in order to break the confines of the epithelial layer and migrate out to the basal or luminal side.

### 1.3 Perspective and open questions

Many systems and processes help to control the organization of epithelium including cell polarity, cell-cell junctions, cell-ECM junctions, the cytoskeleton, cell motility, and the orientation of cell division. Much of the deep knowledge in these fields is developed and tested using immortalized cell lines and invertebrate model organisms such as yeast, fly, and worm. Mice present an approach to study mammalian development; however, there exists many hurdles such as long generation time, limited genetic models, and imaging of live cells. Advances in CRISPR technology, viral delivery, transplantation procedures, and live imaging techniques *in vivo* or *ex vivo*, have shed more light on how these processes regulate epithelial development and organization in mammals. These studies are particularly useful for gaining insight on normal development, homeostasis, and disease progression in humans, a close mouse relative.

The mammary gland is a particularly interesting organ to study epithelial development and organization. While specified during embryogenesis, most of the gland develops and expands during the adolescent/adult stage of life from a multilayered TEB structure. It is also highly plastic, capable of undergoing several rounds of expansion and reduction in response to estrous (or menstrual) cycle, and in response to pregnancy. These circumstances present many challenges at the epithelial cell level in maintaining order. It is thought that most cells withing the multilayered TEB are cleared by apoptosis in order to generate an unobstructed lumen lined by a monolayer of ductal epithelium [91, 92, 121]. This has been challenged recently by the observation that cells in mammary organoids are highly motile and could theoretically contribute to duct expansion [15]. One question in the field of mammary gland development and epithelial biology is: to what extent do cells within the interior TEB contribute to duct elongation and by what mechanisms? Another possibility is that the exterior TEB, ductal-aligned luminal cells proliferate much higher than interior cells and orient their divisions in a planar manner that promotes elongation.

Defects with mitotic spindle and division alignment are also thought to affect mammary gland development as well as development of other tissues [58, 98, 122-

126]. One issue in this field is the difficulty in deciphering direct consequences of loss of division orientation with mutations that perturb other cellular systems. Another difficulty is the challenge of studying loss of OCD in developing tissues and tracking cells in real time. The interpretations from model systems, such as MDCKII 3D cyst culture, may be challenging to translate to whole organs and tissues and follow-up studies will be needed to confirm many phenotypes in primary tissue. It is also proposed that misorientation of division promotes the multilayering of transformed cells and supports growth of multilayered tumors in the mammary gland [118, 119]. However, it is possible that normal or transformed cells dividing with misoriented division correct their position through reintegration into the epithelium or are eliminated through cell death, as seen in other models [79, 80, 127]. These observations prompt the following questions: Can the effects of misoriented division alone be studied in otherwise normal epithelial cells? How, if at all, is epithelial organization maintained after misoriented division? Do transformed cells rely on misoriented division to multilayer?

In the following work presented, I address these questions concerning if and how the ductal mammary gland develops through intercalation, the necessity for TJs during intercalation, the maintenance of epithelial architecture after aberrantly aligned divisions, and the dispensability of misoriented division in promoting transformed cell multilayering.

## Chapter 2: A Junction-Dependent Mechanism Drives Mammary Cell Intercalation for Ductal Elongation

This chapter of my thesis is published in Developmental Cell

https://doi.org/10.1016/j.devcel.2023.04.009

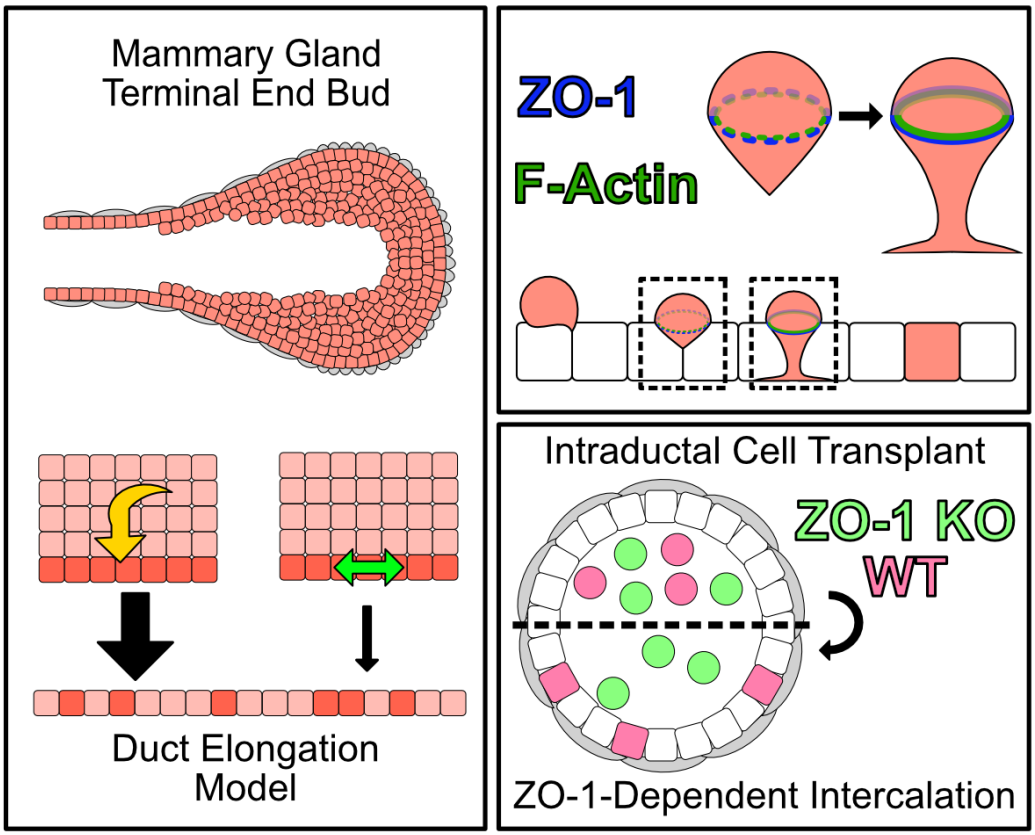


**Figure 2.0 Graphical Abstract**

### 2.1 Abstract

The luminal epithelium of the mammary gland is organized into a monolayer; however, it originates from multilayered terminal end buds (TEBs) during development. While apoptosis provides a plausible mechanism for cavitation of the ductal lumen, it does not account for elongation of ducts behind TEBs. Spatial calculations suggest that most cells in TEBs integrate into the outermost luminal layer to generate elongation. To study this process, we developed a quantitative cell culture assay that determines

efficiency of intercalation into an epithelial monolayer. We found that tight junction (TJ) proteins play a key role in this process. ZO-1 puncta form at the new cellular interface and resolve into a new intercellular boundary as intercalation proceeds. Deleting ZO-1 suppresses intercalation in culture and when cells are transplanted into the mammary gland via intraductal injection. Cytoskeletal rearrangements at the interface are also critical for intercalation. These data identify luminal cell rearrangements necessary for mammary gland development and suggest a molecular mechanism for integration of cells into an existing monolayer.

## 2.2 Introduction

Epithelial cells constitute the building blocks for many of the organs that comprise the animal body, and during development, epithelial tissues need to grow, remodel, and adapt to changing environments [17, 128, 129]. The density and stratification of epithelial cells can be modified by proliferation and extrusion, and tissue morphogenesis can be manipulated by altering cell shape. Convergent extension, which involves the exchange of cell boundaries, alters the aspect ratio of growing embryos [130]. Intercalation of individual cells into a pre-existing epithelial layer has been described in epiboly and keel formation during zebrafish development, the developing murine ureteric bud, multiciliated cell development in *Xenopus* embryo, and in the extending branches of mammary organoids in 3D culture [15, 123, 131-134]. Moreover, re-integration of extruded cells has been observed in the *Drosophila* follicular epithelium [127]. However, models of epithelial cell intercalation remain rare, and the underlying mechanisms are still mostly obscure.

The murine mammary gland represents a powerful model for the investigation of various aspects of epithelial tissue morphogenesis and is particularly relevant for intercalation studies [135]. The gland arises from anlagen near the nipples, and at puberty ducts begin to elongate from swollen cell clusters at their tips, called terminal end buds (TEBs). These TEBs consist of an outer layer of cap cells, which are progenitors of the myoepithelial cells that enclose the mature ducts, plus a mass of epithelial body cells, which provide the luminal cells that form the inner ductal layer

[136, 137]. Body cells are not fully polarized but form micro-lumens between cells, bordered by tight junctions, and adhere to one another through E-cadherin [97]. Somehow, the multiple layers of body cells must resolve into a single luminal layer, surrounded by myoepithelial cells, as the TEBs invade the surrounding fat pad of the mammary gland and the ducts behind them extend. The body cells are proliferative, but also undergo apoptosis, and a plausible model is that cell death removes excess body cells to generate the ductal lumen [95]. Consistent with this idea, inhibition of apoptosis delays the formation of hollow ducts [96]. However, quantitative analysis suggests that apoptotic rates are insufficient to create a single layer of luminal epithelial cells from the mass of body cells in the TEBs [138]. Careful imaging studies of cultured mammary organoids showed that body cells are migratory and can intercalate into the outermost luminal layer adjacent to the basal cells, providing an alternative possible mechanism to elongate ducts [15].

We used published data on proliferation and apoptosis rates in TEBs and ductal elongation rates, plus experimental data on proliferation and cell division orientation in the outermost luminal layer, to model contributions to ductal elongation, and discovered that intercalation is essential and accounts for about 70% of elongation, while cell division orientation and proliferation in the outer regions of TEBs cannot account for observed elongation rates. Intraductal injection of primary mammary epithelial cells demonstrated that intercalation into a preexisting luminal monolayer can occur *in vivo*. To probe mechanism, we developed a new *in vitro* intercalation assay using the murine Eph4 cell line and primary mammary epithelial cells. Cells in suspension when added to a confluent monolayer attach to the monolayer surface, then insert a protrusion between the monolayer cells. Spot junctions marked by ZO-1 appear around the edges of the incoming cell, which ultimately fuse with the junctions of the neighboring monolayer cells to complete the intercalation. Knockout of ZO-1 in the incoming cell blocked intercalation, but surprisingly, ZO-1 knockout in the monolayer cells promoted intercalation. Actin contractility was also found to be required for efficient insertion of cells into the monolayer, but increased contractility in the monolayer inhibited intercalation. Together, these data provide a model for mammary epithelial cell

intercalation that is likely applicable to many other developmental situations and may be relevant to cancer cell invasion.

## 2.3 Results

### 2.3.1 Analysis of TEBs and ductal elongation demonstrates a necessity for cell intercalation

A key question in the morphogenesis of the murine mammary gland is how the mass of body cells within the TEB self-organizes into a single layer of luminal epithelial cells to create an elongating duct. A small fraction of the body cells undergoes apoptosis, which will have a negative effect on elongation, while other cells proliferate, which will have a positive effect. Radial intercalation of body cells into the outermost layer of luminal cells has been observed in mammary organoid formation but this process is challenging to visualize in intact mammary glands [15]. While organoids are a valuable *in vitro* model, they do not fully reiterate the structure of the terminal end bud.

To determine if intercalation is necessary to account for the observed elongation of the mammary ductal tree, we developed a simple geometric model, based on prior work by Paine and colleagues [138]. This earlier model examined the proliferation and apoptotic rates of both the body cells (herein referred to as luminal cells) and cap/myoepithelial cells within different segments of a TEB and mature duct and measured cell sizes, to determine if the observed proliferation/apoptosis rates could account for the experimentally determined rate of elongation. Our model uses the same segmentation into regions as described by Paine et al [138], but to model the processes regulating maturation of the duct from the TEB, we focused only on the luminal cells in these regions (Fig. 2.1 A, S2.1 A,B). We segregated the TEB luminal cells into two compartments: an outermost layer that will generate the single luminal layer of the mature duct, and inner cells that form the body of the TEB (Fig. 2.1 A, Table S2.1). The

exterior layer of luminal cells in the TEB is continuous with the mature duct in that luminal cells in both populations contact cap and myoepithelial cells.

Both intercalation of cells outwardly, as well as planar-oriented division in the exterior layer, may contribute to elongation of the mammary duct. Oriented cell division is thought to be important for development of some epithelial tissues and presents a possible mechanism for elongation of the outermost luminal layer [122, 139]. This scheme is presented as model 1 in Fig. 2.1B where the apoptosis of cells in the interior clears the luminal space of multilayered cells. Another hypothesis is that most of the cells contributing to elongation of the mature duct are derived from the interior sub-compartment in the TEB, necessitating intercalation. In this model (model 2 – Fig. 2.1 B), oriented cell division in the outermost layer may contribute a small fraction of the

overall elongation.

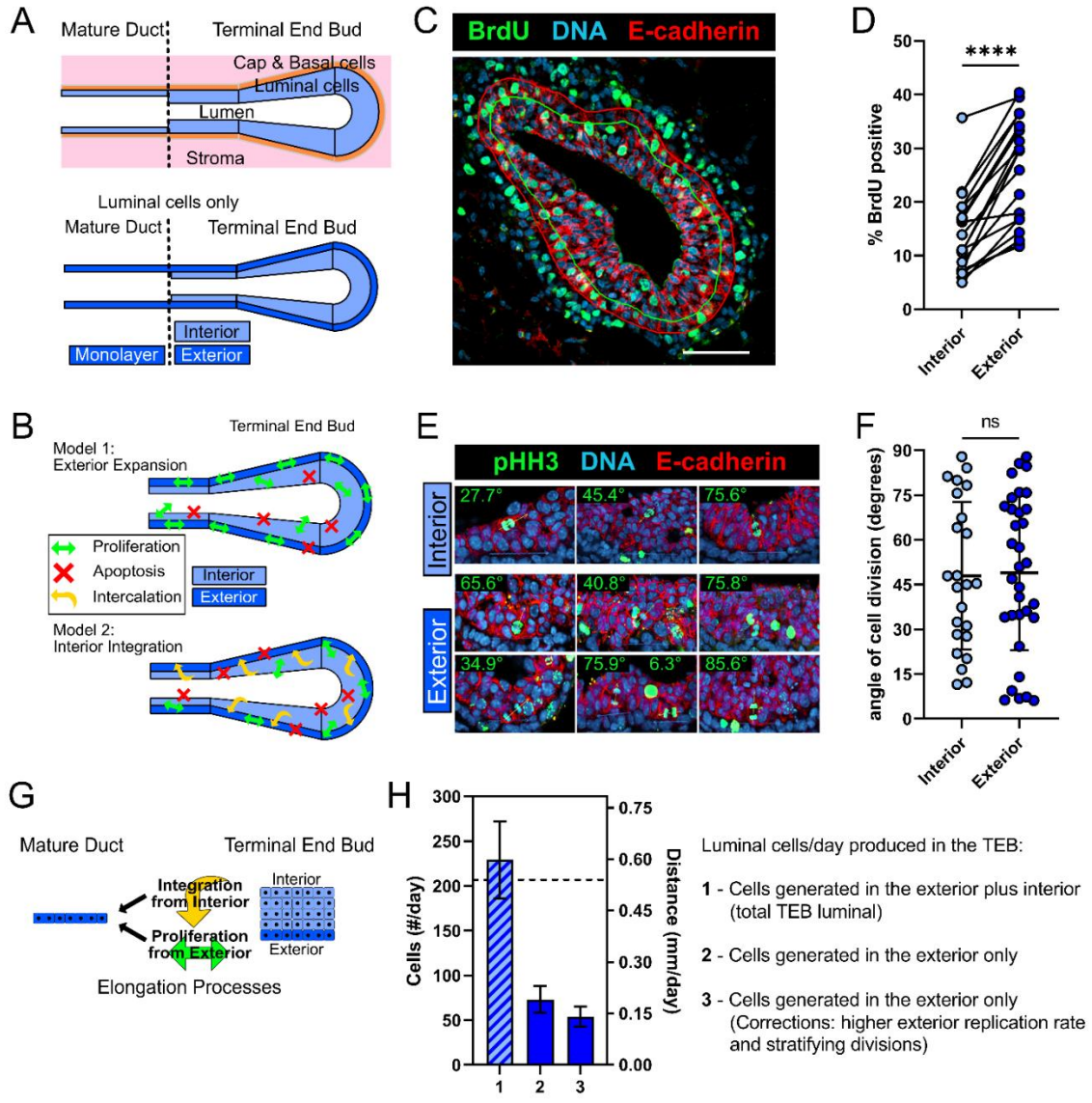


**Figure 2.1 Luminal cell layer proliferation is insufficient for ductal elongation behind the TEB**
**A**. Top: Schematic of the terminal end bud showing luminal and other cell types present, and segregated into distinct regions characterized by Paine et al [138] (see also Fig. S1 A,B). Bottom: Luminal cells in the TEB with marked interior and exterior (outermost) luminal cell compartments. **B**. Models of luminal cell processes that might regulate elongation of the mature duct. Model 1: exterior expansion, highlights planar-oriented division of the exterior luminal cells contiguous with the ductal luminal layer to produce ductal extension behind the TEB. Proliferation and apoptosis in interior luminal cells in model 1 may be at equilibrium and interior cells contribute little to elongation. In model 2: interior integration, neither planar cell division orientation, nor location of luminal cell proliferation and apoptosis in the TEB contribute significantly to elongation. Rearrangement by intercalation of interior body cells to the outermost layer and mature duct could provide most of the cells for elongation in this model. **C**. Female 6 wk-old FVB mice were administered BrdU in PBS at 100 mg/kg for 2 hrs prior to harvesting, fixing, cryo-sectioning, and staining the mammary glands. Example immunofluorescence staining of TEB for indicated markers. Regions of interest are outlined. Within red ROI: all luminal (E-cadherin+) cells in the TEB. Within green ROI: Luminal TEB cells in the interior. Exterior (outermost) TEB luminal cells are located between red and

green ROI borders. Scale bar = 50μm. **D**. Percent BrdU-positive cells in the exterior versus interior luminal TEB regions. Paired t-test, n= 19 TEBs compiled from 3 mice; $p < 0.0001$. **E**. Example TEBs stained for DNA, phosphorylated(S10)-Histone H3, and E-cadherin to highlight dividing luminal cells, used to determine the angle of division orientation with respect to the orientation of the outside surface of the TEB, as reported in F. **F**. Quantification of division orientations in interior and exterior TEB luminal compartments. Unpaired t-test, n= 24, 33 divisions; Mean +/- SD, $p = 0.8812$. **G**. Schematic of how each luminal cell compartment in the TEB could contribute to the mature elongating duct. Interior cells could integrate into the exterior, or cells already in the exterior (outermost) layer could proliferate and give rise to daughter cells in that layer. Both these processes would support elongation. **H**. Quantification of new cells produced in the TEB per day (based on the geometric model with data from Paine et al., 2016 and from this study). Calculations are shown in Tables S1 and S2. Values are also represented as ductal elongation rate (mm/day) based on the average width of a mature duct cell. The dashed line at 0.54mm/day marks the average elongation of ducts per day as determined by Paine et al [138]. Column 1 is the net total cells produced in the TEB per day in both interior and exterior luminal compartments extrapolated from the replication rate, death rate, and TEB size (Table S1). Columns 2 shows cells produced per day within the outermost (exterior) layer only, assuming the replication rate is the same in both the interior and exterior cells (Table S2). The propagated uncertainty in this prediction is also shown (error bars – derivation shown at bottom of Table S2). Column 3 shows cells produced per day within the exterior layer only, with proliferation rate calculated from BrdU staining (Table S3). This accounts for differences observed between interior and exterior replication rates (as seen in Fig. 1 D). Also added in this calculation is a replication correction factor of -50% for misoriented cell division (as seen in Fig. 1 F).

To determine the extent to which cell division contributes to elongation, the ratio of luminal interior and exterior proliferation in the TEB were determined from sections of pubertal murine mammary glands by BrdU incorporation. Relative exterior proliferation is nearly double that of the interior layers (Fig. 2.1 C,D). This result might suggest that the outermost layer of luminal cells, contacting the basement membrane and continuous with the mature duct, is the primary contributor to ductal elongation. However, these cells must divide in the plane of the outermost layer to efficiently expand this layer, but stratifying, non-planar divisions have been observed previously during mammary development [98]. To determine the proportion of cells contributing to exterior elongation after division, the orientations of dividing cells in the outermost layer were measured from stained sections of mammary gland. The plane of division was found to be random (Fig. 2.1 E,F), indicating on average, 50% of daughter cells will be positioned in the interior after division, and in the absence of intercalation will not contribute to elongation.

To determine the extent to which TEB luminal exterior divisions contribute to elongation, we applied the geometric model, where the dimensions of the TEB remain relatively unchanged throughout development and all excess cells generated in the TEB must contribute to the mature duct or die [138]. Given these constraints, the only plausible mechanisms for elongating the duct by addition of cells are through

intercalation for the interior sub-compartment plus planar proliferation for the outermost layer (Fig. 2.1 G). For each TEB compartment, we segregated the exterior and interior portions of luminal cells to first determined the extent each layer contributes to elongation, assuming the replication and death rates of cells in each compartment are the same. While the number of cells produced by the luminal cells in the entire TEB is sufficient to match the observed elongation distance (Fig. 2.1 H – column 1, Fig. S2.1 D), the exterior layer only provides about 30% of these cells (Fig. 2.1 H – column 2), suggesting most of the cells contributing to elongation must have intercalated from the interior region (Table S2.2). However, these results for elongation driven by the outermost layer do not take into account division orientation or replication rate differences between the interior and exterior luminal TEB compartments observed earlier (Fig. 2.1 D,F). To determine how these factors alter elongation, the exterior replication rate was derived from the percent of cells with BrdU incorporation (Fig. S2.1 B,C, Sup.Table 2.2), and applied to the model. In addition, the replication rate was corrected (multiplied by 0.5) to account for random division orientations. Similar to the results of the previous model (Fig. 2.1 H – column 2), the exterior layer only provides approximately one quarter of the cells needed for elongation of the mammary duct when the exterior proliferation correction factors are applied (Fig. 2.1 H – column 3, Table S2.3). This analysis, in which only the outermost layer contributes to elongation, cannot support the extent of elongation seen during mammary gland development. Analysis of cycling cells in the interior versus the exterior of each TEB also revealed that the interior produces most of the cells that will contribute to elongation, relative to each TEB we measured (Fig. S2.1 C, Table S2.3,2.4). Data generated in this study and extrapolated from that of Paine et al [138] also show similar contributions to mature duct elongation from interior cells (Fig. S2.1 D). Thus, our calculations show that proliferation in the exterior layer of TEB luminal cells is insufficient to drive mammary duct elongation. The integration of the majority of the interior TEB cells into the outermost layer suggests intercalation is the primary driver of ductal elongation.

### 2.3.2 An *in vitro* assay for epithelial cell intercalation

Very little is known about the molecular mechanisms of intercalation in any system and particularly in mammalian epithelia. To address this issue, we developed an *in vitro* method, initially using Eph4 murine mammary epithelial cells (Fig. 2.2 A). Fully confluent monolayers of mApple-labeled Eph4 cells were grown on Labtek coverglass chambers, to which unlabeled Eph4 cells in suspension were then added to simulate the multilayered state of the developing TEB. The monolayers were imaged for 72 hrs, and integration was detected as the appearance of unlabeled cells within the mApple+ monolayer. The area of unlabeled cells provides a quantitative measure of successful intercalation over time (Fig. 2.2 B,C).

Intercalation was reproducibly detectable within 5 -10 hrs and peaked by approximately 20 hrs (Fig. 2.2 D,E). Of the cells or clusters observed above the monolayer, approximately 60% of these exhibited full or at least partial integration (Fig. 2.2 E). A majority of intercalation events initiated within 25h but the area in the monolayer displaced by intercalating cells continued to rise until approximately 60 hrs after plating, potentially due to intercalating clusters or intercalated cell division (Fig. 2.2 F,G). We noted that cells in suspension frequently intercalated as small clusters rather than as single cells and appeared to penetrate preferentially into the confluent monolayer at multi-cellular junctions. Total integration correlated positively with the number of cells in suspension added to the monolayer and correlated negatively with monolayer cell density (Fig. S2.2 A-D). However, if cell proliferation was inhibited using the CDK2 inhibitor Roscovitine, there was no significant effect on intercalation over 24 hrs (Fig. S2.2 E-H).

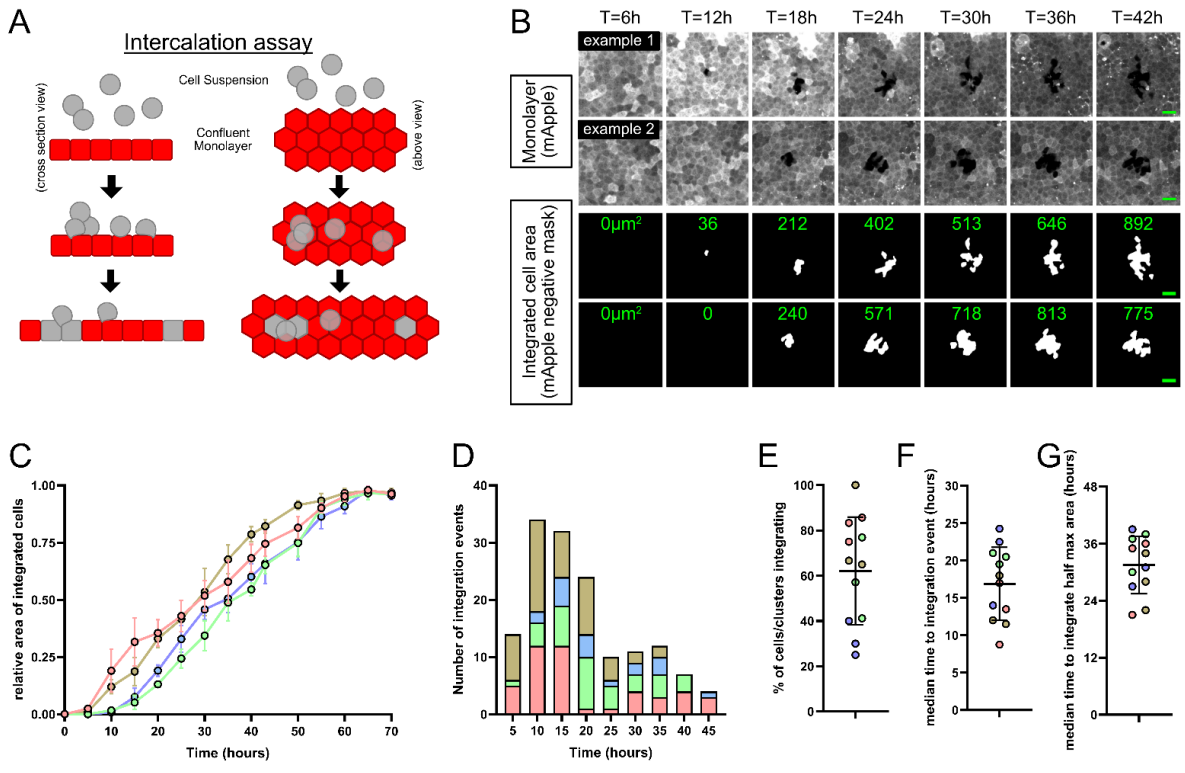


**Figure 2.2 Establishment of a quantitative cell culture assay to study intercalation**
**A**. Diagram of intercalation assay where unlabeled Eph4 cells in suspension (grey) are added to a confluent monolayer of labeled Eph4 cells (red) to simulate multilayered conditions reflective of the TEB. **B**. Time-lapse imaging of intercalation assay where unlabeled cells are added to a confluent monolayer of cells expressing mApple (mApple+). Area of intercalation is determined by the displacement of the mApple+ cells (and lack of fluorescence). Images are confocal projections. Lower panels show negative binary masking of the mApple+ areas, and the computed areas (in $\mu m^2$) of integrated cells (green text). Scale: 20μm. **C**. Measurement of mApple-negative area over time normalized to maximum area. Values are per field of view, 4 replicates. **D**. Number of integration events over the timelapse experiments. Each integration event is determined by the moment an mApple+ area begins to be displaced. Each color represents data from a different experimental replicate. Replicates are summed in the histogram at 5 hr increments. **E**. Mean percentage of cell clusters observed above the monolayer that have integrated by 70 hr. **F**. Median time until intercalation begins. Determined from Fig. 1 D. **G**. Median time until half of the integration area maximum is reached. Determined from Fig.1 C.

To determine whether primary mammary epithelial cells are capable of *in vitro* intercalation, we isolated cells from adult mouse mammary glands, which were grown initially as mammospheres. To select for the luminal population, cells were cultured in the absence of ROCK inhibitor, since ROCK inhibition expands the basal cell population [140]. These cells were then plated on coverglass chambers to create monolayers, stained with the cell dye CFSE to label the monolayer population, and unlabeled mammary epithelial cells were added (Fig. 2.3 A,B). The added cells incorporated successfully into the monolayers, with an efficiency comparable to or exceeding that of

Eph4 cells at a similar monolayer density (Fig. S2.3 A,B). Therefore, both mammary primary cells and cell lines have the capacity for intercalation.

A key step in intercalation must be the integration of the existing junctions with newly formed ones in incoming cells. To observe how these junctions form, intercalating primary luminal cells were fixed and stained for the adherens junction marker E-cadherin and tight junction marker ZO-1. In early stages of intercalation, a discontinuous circular junction forms on the apical surface between an intercalating cell and a monolayer cell, which is positive for both ZO-1 and E-cadherin (Fig. 2.3 C); another example appears to be at a later stage of intercalation where the incoming cell has formed more complete junctions that have attached to existing monolayer junctions (Fig. 2.3 D). After complete integration, continuous junctions have formed between the intercalated and monolayer cells (Fig. S2.3 C).

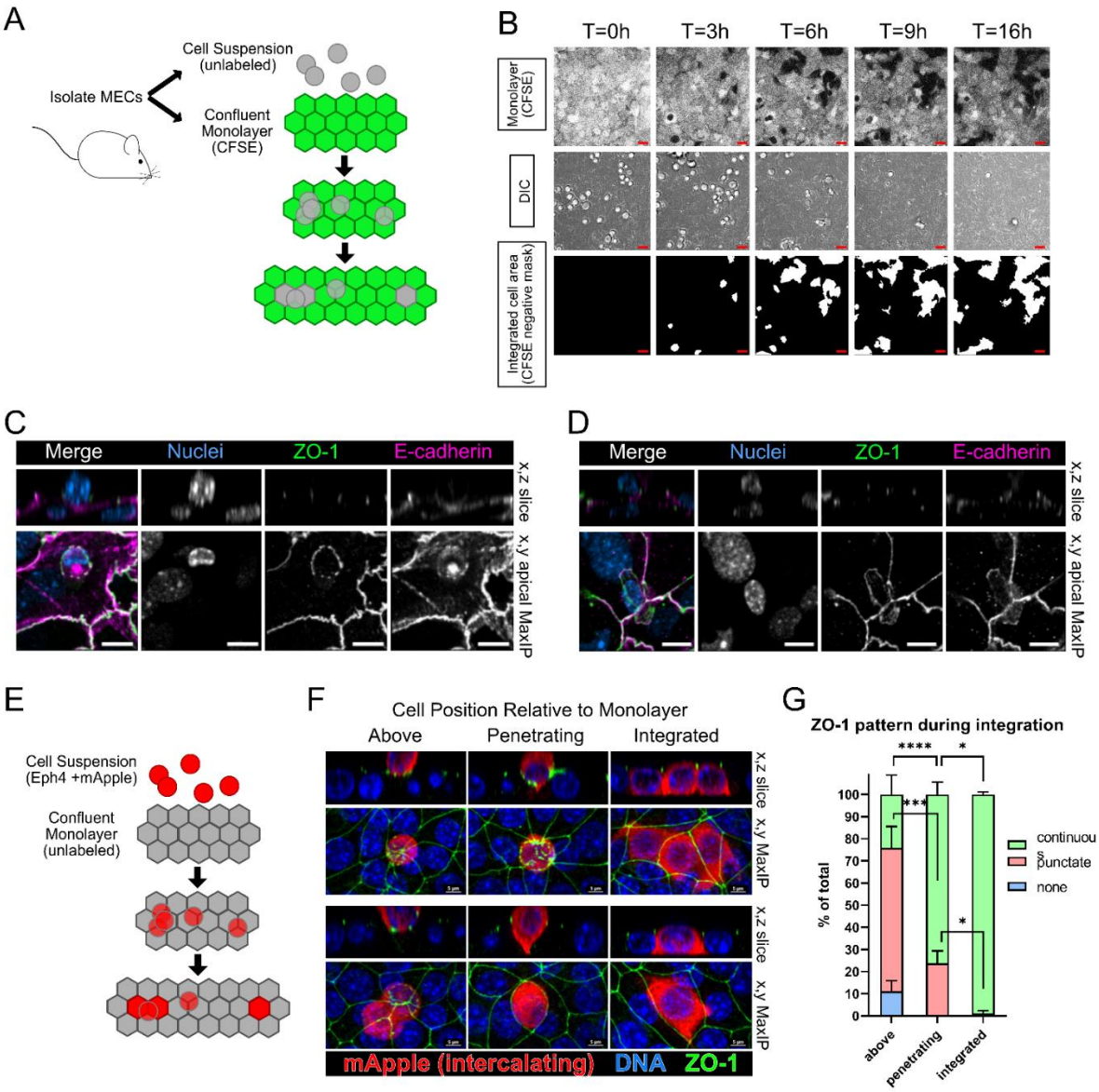


**Figure 2.3 Primary mouse mammary epithelial cells intercalate through formation of junctional plaques**

**A**. Schematic of primary mouse mammary epithelial cell (MEC) isolation, labeling and plating for intercalation assay. **B**. Timelapse imaging of intercalation by unlabeled MECs into confluent MEC monolayer stained with CFSE. Scale: 20μm. **C - D**. Immunofluorescence imaging of primary MECs undergoing intercalation, with staining for ZO-1 and E-cadherin. Cells were fixed at 24 hrs after addition of the unlabeled cells in suspension. Puncta of ZO-1 are visible at cell interface between monolayer and intercalating cells (C). D shows a cell with continuous ZO-1 staining that has moved over a multi-cellular junction. Scale: 10μm. **E**. Schematic of intercalation assay for F: Eph4 cell monolayer (unlabeled) and intercalating cells (mApple+). **F**. Eph4 cells were fixed during intercalation and stained for ZO-1, then imaged as confocal z-stacks for mApple (in the intercalating cells), DNA, and ZO-1. Examples of cells displayed along the x-z and x-y axes, in 3 different states are shown: above, penetrating, or integrated into monolayer. Scale: 5μm. **G**. Quantification of intercalating cells in each state (above, penetrating, integrated into monolayer) with ZO-1 staining being absent, punctate, or continuous. Mean +/- SD. Comparisons shown: *p < 0.05, ***p<0.001, ****p<0.0001.

### 2.3.3 A role for adherens and tight junctions in epithelial cell intercalation

To further investigate the process of intercalation, Eph4 cell integration experiments were fixed 18 hrs after addition of cells to the monolayer, then immuno-stained for ZO-1 (Fig. 2.3 E). As with the primary cells, the Eph4 ZO-1 localization pattern is initially punctate in most incoming cells that contact the monolayer. The surface of the monolayer becomes depressed, and the ZO-1 forms a continuous junction with neighboring monolayer cells. A protrusion then penetrates between adjacent monolayer cells until it contacts the basal substrate and expands to complete the integration (Fig. 2.3 F). The maturation from a punctate to continuous pattern of ZO-1 (Fig. 2.3 G), suggests that TJ dynamics might be a critical first step before cells intercalate. A punctate to continuous pattern of E-cadherin that colocalizes with ZO-1 is also visible at the interface between the intercalating and monolayer cells (Fig. S2.3 D). Interestingly, the polarity protein Par3 partially co-localizes to areas where ZO-1 is enriched at the intercalation interface (Fig. S2.3 E), suggesting that the cell polarity machinery may be involved in these junction rearrangements.

To test the necessity for tight and adherens junction formation during intercalation, we generated cells null for either ZO-1 or E-cadherin using CRISPR/Cas9 gene editing (Fig. S2.4 A-C). The formation of intercellular adherens junctions is a universal feature of epithelial tissues, characterized by the formation of trans-interacting E-cadherin molecules on the lateral membranes. Loss of E-cadherin can result in cell extrusion from a monolayer *in vitro* and from mammary ducts *in vivo* [10, 19]. We predicted, therefore, that knockout of E-cadherin in Eph4 cells added in suspension to a monolayer of WT cells would block their intercalation. To ensure a homogenous ablation, several single cell clones for control (NT), ZO-1 loss, and E-cadherin loss were isolated, and knockout was verified by immunofluorescence cell staining (Fig. S2.4 A-C).

We first grew cells plated sparsely and allowed them to proliferate to confluence, to determine if there were defects in monolayer formation. Loss of E-cadherin resulted in poor monolayer formation with cells lacking both tight junctions and adherens

junctions (Fig. S2.4 A), while the absence of ZO-1 had no impact on TJ formation as determined by Claudin-4 staining, which remained junctional and at similar levels to control cells (Fig. S2.4 A,B). This result is consistent with previous data that ZO-1 is not essential for TJ organization [141]. E-cadherin localization was also unaffected by loss of ZO-1 (Fig. S2.4 A,B). There was also no significant increase in multilayering of cells in these confluent monolayers, which can be caused by extrusion or over-proliferation (Fig. S2.4 A,D).

When the E-cadherin-negative cells were added to WT confluent monolayers, their ability to integrate was severely impaired, demonstrating that adherens junction formation is essential for intercalation. Interestingly, the deletion of ZO-1 also impaired intercalation into a WT monolayer (Fig. 2.4 A-C), suggesting that it plays a key role in assembling new TJs between the incoming cell and the monolayer cells. To further probe the role of ZO-1 during intercalation, we reversed the experiment, plating ZO-1 null cells in the monolayer and adding WT cells in suspension. Remarkably, these cells intercalated more efficiently into the monolayer lacking ZO-1 than into a WT monolayer (Fig. 2.4 D-F). This unexpected result suggests that although ZO-1 is needed by intercalating cells to establish junctions with the monolayer, the tight junctions in ZO-1-null monolayer cells are less stable and more easily re-organized to incorporate intercalating cells.

Mammary organoids provide an established *in vitro* model that bears some similarities to TEBs, including luminal cell intercalation during organoid morphogenesis [15]. To investigate whether luminal cells lacking ZO-1 are able to organize into monolayers within organoids, we sparsely transduced mouse mammary tissue fragments with a CRISPR-GFP lentivirus to knock out either ZO-1 or E-cadherin (as a positive control) [142] (Fig. S2.4E-G). Shamir et al. showed that luminal cells lacking E-cadherin do not efficiently incorporate into organoids [10], but the effect of loss of ZO-1 is unknown. Organoids were cultured for 14 days. GFP+ ZO-1 ablated cells become less frequent in monolayer-organized areas of the organoid compared to control (NT) GFP+ cells. As a positive control, E-cadherin ablation also prevented incorporation into monolayer regions as expected, to a higher degree than did ZO-1 loss (Fig. S2.4 E,F). These data are consistent with a role for ZO-1 in the organization of mammary ducts.

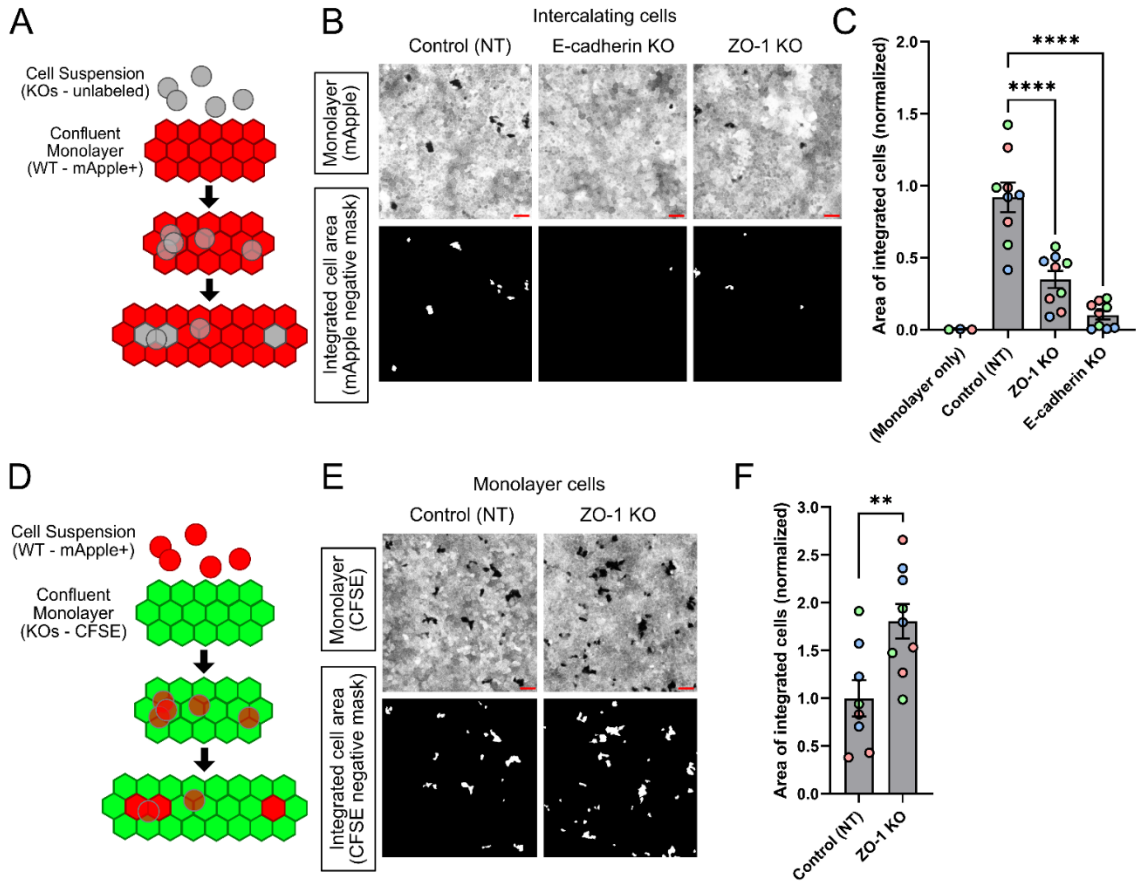


**Figure 2.4 ZO-1 regulates intercalation**
**A**. Schematic of intercalation assay. **B**. Example images of intercalation for control (NT, non-targeting gRNA), E-cadherin KO or ZO-1 KO clones. Example region shown. Scale: 50μm. **C**. Quantification by area of intercalated cells for control, E-cadherin and ZO-1 KO. Each clone shown in one color; n = 3 experiments. Mean +/- SEM; One-way ANOVA, ****p < 0.0001. **D**. Schematic of intercalation assay for ZO-1 KO monolayers and control (WT) intercalating cells.
**E**. Example images of intercalations for control (WT) and ZO-1 KO cells into the confluent ZO-1 KO monolayer labeled with GFP. WT cells added in suspension, labeled with mApple. Scale bar: 50μm. **F**. Quantification by area of intercalated WT cells. Each clone shown in one color. N = 3 experiments, clones grouped by color, Mean +/- SEM; unpaired t-test, **p = 0.0080.

### 2.3.4 Intraductally injected cells can intercalate into the luminal layer of mature ducts *in vivo*

We next sought to determine if intercalation into the luminal cell layer of mammary ducts can be observed *in vivo*, and if ZO-1 is a key regulator of this intercalation. To test this, a competitive transplantation assay was used where cells were introduced into murine adult mammary glands via intraductal injection, which has

been used previously. First, mammary cells were isolated from adult mice and transduced with lentivirus to knock out ZO-1 using CRISPR (sgRNA Tjp1) and to introduce GFP as a cell marker. Other cells were transduced with lentivirus containing a control non-targeting sgRNA and expressing mCherry. Transduced cells were then cultured as mammospheres, dissociated, and combined 1:1 (GFP+: mCherry+) (Fig. 2.5 A). Some transduced cells were plated on coverslips and stained for ZO-1 to confirm knockout as well as to determine transduction efficiency (Fig. 2.5 B). The 1:1 cell mixtures were transplanted into isogenic recipient mice via injection through the nipple, and examined for GFP+ and mCherry+ cell intercalation into existing ductal monolayers. Early after injection (18 hrs), an approximately 1:1 ratio of control and ZO-1 knockout cells was detected within the ductal lumen (Fig. 2.5 C,E). At 5 days post-injection, however, multiple mCherry+ control cells had integrated into the ductal luminal layer, but GFP+ ZO-1 knockout cell integration was much less apparent (Fig. 2.5 D,E). Intercalated cell distributions for all mice are shown in Fig. S2.5. This competitive transplantation assay demonstrates that intercalation can occur within mammary gland ducts *in vivo* and is dependent on the major tight junction organizing protein ZO-1 to integrate cells into the mature duct.

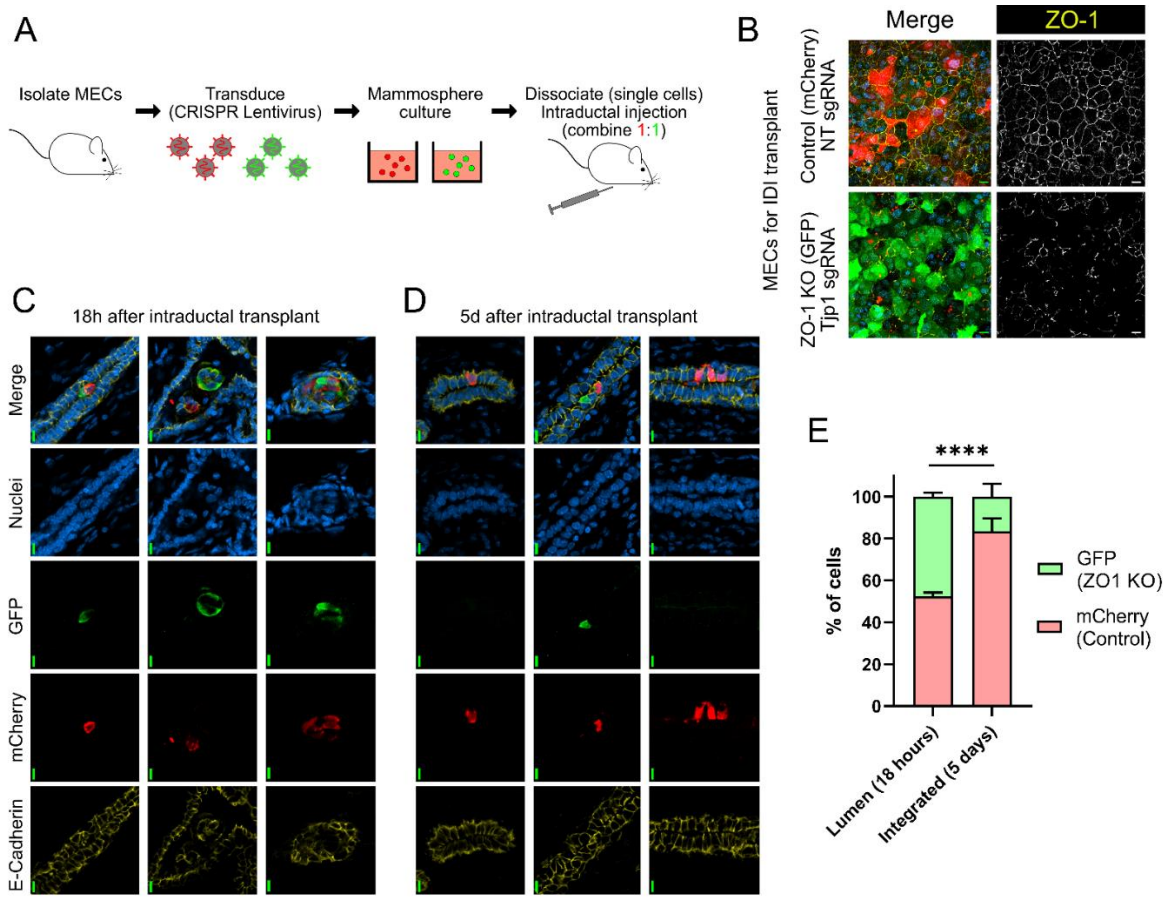


**Figure 2.5 ZO-1 loss impairs intercalation of mammary epithelial cells *in vivo***
**A**. Schematic of workflow for intraductal competitive intercalation assay. Primary mammary epithelial cells (MECs) were isolated and transduced with a LentiCRISPRv2-GFP lentivirus to target ZO-1 for deletion and label cells green. Non-targeting sgRNA in LentiCRISPRv2-mCherry was used as a negative control to label WT cells red. Cells were expanded as mammospheres, then digested to single cells, mixed, and transplanted intraductally at a 1:1 ratio. **B**. Cells infected with control (mCherry) or ZO-1 targeting (green) CRISPR lentivirus, were plated, fixed, and stained for ZO-1 to assess knockout efficiency. Scale: 10μm. **C**. Examples of cells present 18 hrs after injection in the mammary glands of recipient mice. Scale: 10μm. **D**. Examples of cells integrated into the existing ductal epithelium 5 days after transplantation. Scale: 10μm. **E**. Comparison of the distribution of cells found in the lumens at 18 hrs or 5 days post-transplantation. Per experiment: 18 hrs: 2 mice, 5 days: 5 mice. 2 experiments grouped. Fisher's exact test, n= 413 total cells. Mean +/- SD, ****p < 0.0001

### 2.3.5 Actomyosin dynamics regulate the reorganization of cells during intercalation

Actomyosin assemblies play a critical role in many cellular processes, and are likely to be involved in mammary cell intercalation as they are in other systems such as multiciliated cell development in the *Xenopus* epidermis [143-145]. In epithelia, the

apical perijunctional actin ring supports the integrity of the connected cells in the epithelium and Myosin II also acts at this level to control contraction and rearrangement of the cells [146]. To investigate the role of the actin network during intercalation, we used live imaging of cells expressing LifeAct-GFP intercalating into monolayer cells expressing mApple (Fig. 2.6 A,B). Initially, an actin-rich protrusion attaches to the apical surface of a monolayer cell. This attachment expands into a circle centered between monolayer cells, as we had observed for ZO-1. The circle enlarges and eventually takes on a more polygonal shape as the cell fully integrates into the monolayer. A protrusion is often seen penetrating between the cells to reach the substratum and has begun to spread actin-rich pseudopods beneath neighboring cells. We quantified the basal area occupied by incoming cells, which shows that the mean time for 50% expansion of this area is about 2 hrs (Fig. S 2.6A). LifeAct intensity at the apical interface between the intercalating cell and monolayer (normalized to total LifeAct intensity) remained relatively constant throughout the intercalation process even through establishment of new perijunctional F-actin rings after full integration (Fig. S 2.6B). At the basal side, F-actin levels increase sharply after contact with the substratum and remain at this level, while the areas occupied by integrating cells grow more slowly (Fig. S2.6 C).

To further probe the role of the actomyosin network in this process, we tested the effects of Arp2/3 inhibitor CK-666 and Myosin II inhibitor Blebbistatin. Arp2/3 promotes branched actin formation, while the motor protein Myosin II allows for contraction along actin filaments and both of these components are involved in cell motility as well as junction assembly and rearrangement. When either Arp2/3 or Myosin II was inhibited, there was a reduction in intercalation (Fig. 2.6 C-E). This result shows the importance of actomyosin during intercalation; however, it is not possible to determine from these experiments if the effect of the drug is on the intercalating cells, monolayer cells, or both populations.

Migrating cells in mammary organoid cultures accumulate phosphatidylinositol (3,4,5)-trisphosphate ($PIP_3$) at the leading edge, with recruitment of downstream signaling and cytoskeletal components to promote exterior-directed motility [15]. To investigate if a similar pathway promotes monolayer intercalation, we used a biosensor

containing the $PIP_3$-binding domain of Akt fused to Venus fluorescent protein [147]. We detected $PIP_3$ enrichment at the protruding tip of intercalating cells and at lateral junctions after intercalation was complete (Fig. S2.6 D,E). Surprisingly, however, when PI3K activity was inhibited with LY-2940002 the area of cells integrated into the monolayer was not significantly reduced (Fig. S2.6 F-H). A blot for phospho-Akt confirmed the activity of the inhibitor, suggesting that PI3K signaling is not essential for cellular intercalation (Fig. S2.6 I).

While inhibiting the actomyosin network might hamper intercalation at several stages, we first looked at the early junction rearrangement seen with ZO-1 during intercalation to determine if the formation of this nascent connection was affected. Perturbations to the actomyosin network can disrupt formation of apical junctions, and the resulting organization is often more punctate than linear [148-150]. The intercalation assay was performed with inhibitors of either branched actin formation or myosin activity and cells were fixed at 16hrs to observe early stages of intercalation. ZO-1 staining at this time was mostly punctate at cells sitting atop the monolayer, with some displaying a continuous ZO-1 pattern, as seen in Fig. 2.3 C-G (Fig. 2.6 F,G). When branched actin formation or myosin activity were inhibited, a significant increase was detected in cells that have no ZO-1 at the interface with the monolayer. In congruence with this result, fewer cells were seen with continuous ZO-1 staining at the interface; however, there was a small or no change in the number of cells with punctate staining (Fig. 2.6 F,G). Together, these observations suggest that inhibiting acto-myosin dynamics impairs formation of puncta and maturation to continuous junctions, which blocks intercalation (Fig. 2.6 H).

**Figure 2.6 Actomyosin dynamics regulate intercalation**
**A**. Outline of live imaging experiment in B.: cells expressing LifeAct-GFP were added to WT monolayers expressing mApple for visualization. Live imaging with confocal microscopy. **B**. Stills of intercalation event with LifeAct-GFP-labeled intercalating Eph4 cell and mApple-labeled monolayer. First row: maximum intensity (MI) projection of both channels overlaid. Second row: interface of intercalating cell and monolayer, LifeAct-GFP only. Third row: basal surface, LifeAct-GFP only. Time normalized to initial detection of intercalation at the base of the monolayer. **C**. Schematic of intercalation assay for D, F: control (wildtype) mCherry+ monolayer and (wildtype unlabeled) intercalating cells added with inhibitors. **D**. Example images of cell intercalation and effects of CK-666 (300uM) to inhibit the ARP2/3 complex or Blebbistatin (50μM) to inhibit myosin activity. Scale bar = 50μm. **E**. Quantification of areas of intercalated cells. 3

experiments. One-way ANOVA, Mean +/-SD, $p < 0.0001$ for all comparisons shown. **F**. Immunofluorescence imaging of cells prior to intercalation, with staining for ZO-1, F-actin, and mApple (monolayer). Cells were fixed at 16 hrs after addition of the unlabeled cells in suspension. ZO-1 pattern at the interface, excluding areas of existing monolayer junctions, was then scored. Examples are shown for each treatment with orthogonal slice (Y, X) and MI projection of the interface region (X, Y). Scale: 10μm. **G**. Quantification of intercalating cells with ZO-1 staining being absent (none), punctate, or continuous for each of the treatments shown. Mean +/- SD. comparisons to DMSO control shown: *$p < 0.05$, **$p<0.01$, ****$p<0.0001$. **H**. Model of intercalation. Cells begin to form nascent junction at the cell-cell interface. The actomyosin network then forms and regulates cell movement at the nascent junction interfaces. Probing structures are seen in cell culture and similar elongated luminal cell bodies are seen in the TEB. Intercalation proceeds as the cell pushes inward and anchors itself to the substrate. Cell shape is then resolved as the monolayer accommodates the integrated cell.

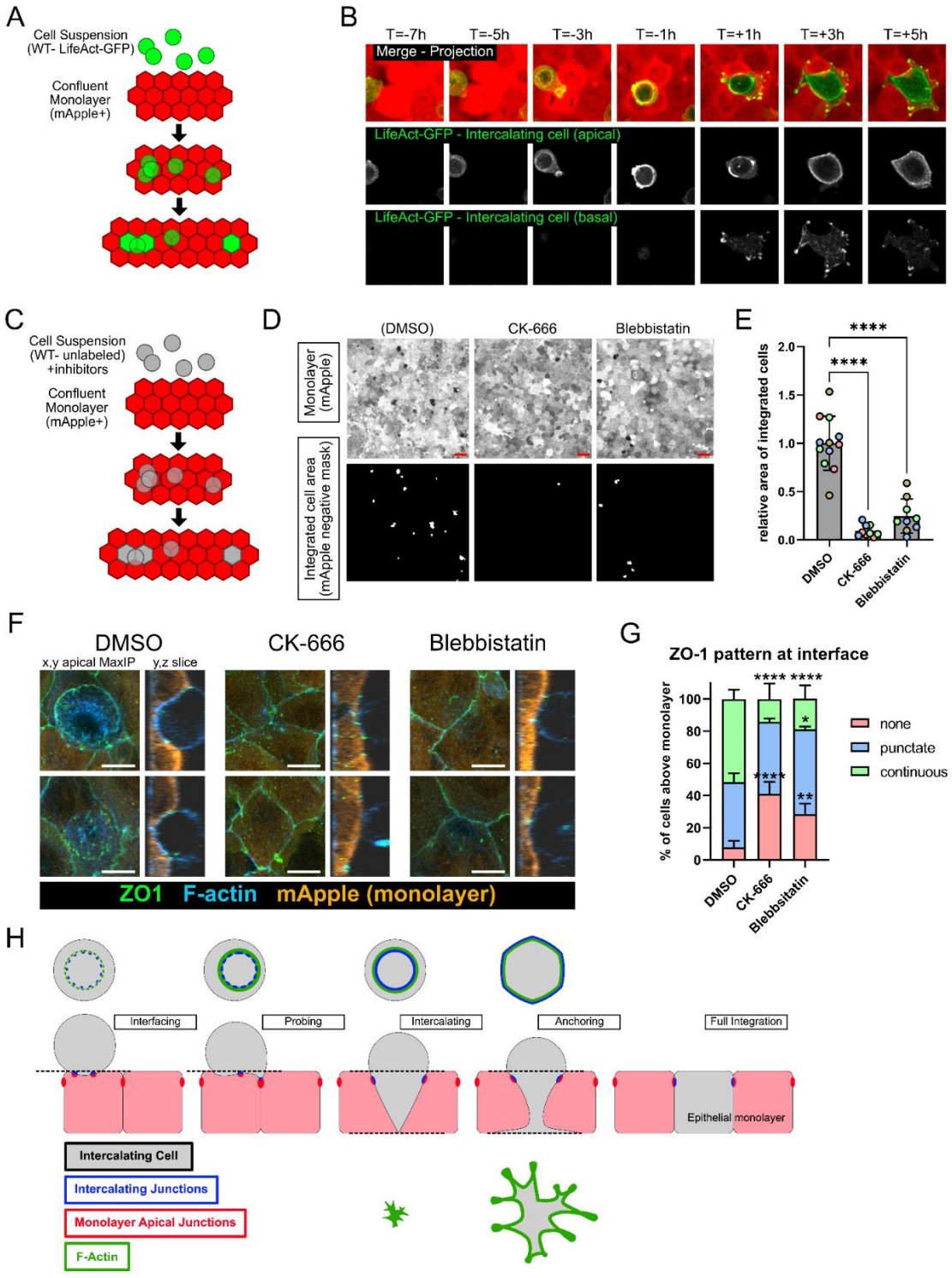


## 2.4 Discussion

A question of fundamental importance to developmental biology is how ductal structures self-organize. The murine mammary gland provides a valuable model by which to investigate this question. The ductal tree of the gland develops over several weeks at puberty, from primordial buds attached to the nipples, and invades into the surrounding fat pad. Large terminal end buds (TEBs) at the tips of the ducts generate most of the cells that contribute to the ductal structure. A longstanding mystery, however, has been the mechanism by which the mass of body cells within the TEBs resolves into a single layer of luminal cells in the mature ducts behind the TEBs. A similar process occurs in other budded ductal organs such as the salivary glands [35]. Proposed mechanisms in the mammary gland have implicated apoptosis of body cells to create the ductal lumen, selective proliferation, and division orientation of luminal cells adjacent to the basal cell layer, and cell intercalation. However, apoptosis rates were estimated to be too small to contribute significantly to ductal organization (Paine et al 2016). Here we calculate contributions to ductal elongation of proliferation, the orientation of cell divisions within the outermost layer of body cells, and intercalation of interior cells into this outermost layer. Notably, intercalation can account for most of the ductal elongation rate, and neither exterior proliferation nor division orientation contribute substantially to this rate. An important consideration, however, is that intercalation alone would produce an isotropic expansion of the ductal surface area, so ducts would expand in diameter as well as in length. Convergent extension movements might constrain the diameter and promote elongation, but a plausible alternative mechanism is that contractility of myoepithelial cells around the neck enforces anisotropic extension, which is consistent with the structure of our organoid cultures, in which the myoepithelial cells are more numerous in the narrow neck regions (Fig S2.4 E-G).

To further understand the mechanism of intercalation we developed an *in vitro* assay to quantify intercalation by Eph4 murine mammary epithelial cells, or by primary mammary cells. This assay also allows for live imaging and tracking of intercalating vs. monolayer populations with high resolution. We discovered that while ZO-1 is not required for normal tight junction assembly and monolayer formation in culture, it is necessary in the added cells in suspension for efficient intercalation into the monolayer.

Surprisingly, however, deletion of ZO-1 from monolayer cells substantially increased rather than decreased intercalation by WT cells. We interpret this asymmetric requirement for ZO-1 as a reflection of its role in stabilizing junctions: de novo formation of spot junctions will be impaired by loss of ZO-1, but the stability of pre-existing junctions in the monolayer will likely hinder the re-organization necessary to integrate them with those of the incoming cell, so loss of ZO-1 in monolayer cells might promote intercalation by destabilizing the tight junctions. Interestingly, blocking contractility or branched actin formation in all the cells, using a Myosin or Arp2/3 inhibitor, respectively, strongly reduces intercalation and prevents maturation of early junctional puncta at the intercalation interface. We note that while ZO-1 is a key regulator of tight junction formation, we cannot rule out other roles in processes that might indirectly affect intercalation. For example, ZO-1 null endothelial cells display changes in cell tension, although in a junction-dependent manner [151]. ZO-1 also can regulate gene expression through interaction with transcription factor ZONAB or by regulating Hippo signaling [152, 153].

We also showed that loss of E-cadherin blocks intercalation, but since it disrupts both adherence and tight junctions this was an expected outcome. Indeed, adherence junctions have long been recognized as essential for maintenance of TEB structure. Disruption of E-cadherin by blocking antibodies, loss of p120, or genetic ablation all destroy epithelial integrity in mammary gland as luminal cells disassociate [10, 12, 13]. Adherence to the basal/cap cell layer is also disrupted when P-cadherin, which is expressed in basal and cap cells, is inhibited by introducing a specific blocking antibody *in vivo* [12].

Finally, a key question for our study was whether the phenomenon of Eph4 cell intercalation is applicable to actual mammary epithelia. Notably, primary murine mammary epithelial cells in culture were able to intercalate even more efficiently than the Eph4 cells; and intraductal injection of isolated mammary cells revealed *in vivo* intercalation into the luminal cell layer of intact ducts. Moreover, deletion of ZO-1 in the isolated mammary cells significantly inhibited *in vivo* intercalation, just as was seen *in vitro*. Intraductal injection provides, therefore, a powerful new approach to investigate the process of intercalation in an *in vivo* setting.

## 2.5 Methods

Experimental models and subject details

Animals

The Vanderbilt Division of Animal Care (DAC) ensures that all mice within the Vanderbilt facility are monitored daily for health status. DAC also ensures the overall welfare of the mice, and provides daily husbandry that includes environmental enrichment, clinical care, protocol record keeping, building operations, and security. The Vanderbilt mouse facility has three experienced Animal Care Technicians who attend to the daily needs of the animals. DAC ensures that all federal, state, and university guidelines for the care and use of animals are understood and maintained. Mice were housed with a standard 12 hrs light/12 hrs dark cycle. Mice were provided normal laboratory chow and water. All mouse experiments were performed with approval from the Vanderbilt Institutional Animal Care and Use Committee.

Female FVB/NJ mice aged 6-8 weeks were used for proliferation studies related to modeling. BrdU was administered in PBS at 100mg/kg via intraperitoneal injection and mammary glands were harvested after 2 hrs. Female C3H/HeJ mice aged 8 wks or older were used as donor and recipient for intraductal transplantation experiments. All mice were acquired from The Jackson Laboratory.

Isolation and culture of primary cells

The $4^{th}$ pair mammary glands were isolated from adult female mice, minced with scissors, and digested in DMEM/F12, 2mg/mL collagenase, 100U/mL Penicillin and Streptomyocin, 600U/mL Nystatin, and 5μg/mL insulin for 1 hr shaking at $37^{O}$C. The resulting pellet was then treated with 2U/mL DNase for 5 min, washed 5x with DMEM/F12, then digested to single cells with 0.25% Trypsin for 12 min shaking at $37^{O}$C. Single cells were then strained through 40μm pore strainer. Single cells were transduced and grown in low-attachment plates in DMEM/F12, 5ng/mL EGF, and 1x ITS. Aliquots of cells were plated onto cover-glasses and allowed to adhere and form monolayers before fixing and immunostaining to determine the percentage of cells in

each condition that were transduced and the efficiency of the CRISPR knockout. The mammospheres (low-attachment culture) were digested using Trypsin at 37$^{O}$C to obtain single cells before being combined 1:1 (control:knockout) to be transplanted into the mammary duct. For primary cell *in vitro* intercalation assays, 150x10^3 single cells were plated onto 8-well chambered coverglasses and allowed to proliferate to confluence for 1-3 days. Monolayer cells were then stained for 10 min at 37$^{O}$C with CFSE (2.5ug/mL in DMEM/F12), washed 3 times for 5 min each with DMEM/F12 plus 5% FBS. Unlabeled primary cells were then added, and live imaging was started within 30 min to observe intercalation.

Cell lines

Mouse mammary EpH4 cells were provided by Dr. Jürgen Knoblich (Institute of Molecular Biotechnology, Vienna, Austria). EpH4 cells were cultured in Dulbecco's Modified Eagle Medium (DMEM) (ThermoFisher Scientific, Waltham, MA) supplemented with 10% Fetal Bovine Serum (FBS) (R&D Systems, Minneapolis, MN), and incubated at 37$^{O}$C and 5% CO2.

METHOD DETAILS

TEB luminal elongation model and calculations

A geometric two-dimensional model of murine mammary TEBs was based on that described by Paine et al [138], in which the TEB was subdivided into several regions. For the purposes of our analysis, however, we ignored the basal layer of cap cells, and segmented the luminal body cells into two compartments, an outermost (exterior) layer of luminal cells that is adjacent to the basal cap cells, and an interior compartment that comprises all other body cells in the TEB. The area of each luminal compartment was then calculated from measured parameters (Paine et al 2016). See Table S1,2 for all formulas and calculations

Area of the exterior layer = $A_E$ = TEB perimeter x cell height

Interior area $A_I$ = total TEB area – exterior TEB area = $A_T - A_E$

We then determined the ratios $A_I/A_T$ and $A_E/A_T$. These ratios were multiplied by the total luminal cells per region (TEB luminal region 1-3) and summed to calculate the numbers of exterior and interior cells:

$$N_E = \sum_{r1}^{r3} N_T * \frac{A_E}{A_T}$$

$$N_I = \sum_{r1}^{r3} N_T * \frac{A_I}{A_T}$$

To determine the contribution of just the outermost cells to ductal elongation, previously reported rates of proliferation and death[138] were applied to the number of cells determined per area (Fig 1H – column 2, Table S1,2). Final corrections to the model of elongation driven by interior/exterior are reflected in Fig 1H – column 3. Corrections to the replication rate, r, were determined using data from Fig 1. Correction 1 was for the higher observed replication rate, $r_E$, of the exterior cells relative to interior cells. Correction 2 was for the random orientation of cell division in the outermost layer. (Corrected $r_E = 0.5*r_E$). Both corrections are reflected in Fig 1H – column 3, and in Fig S1 C,D.

*Determining the proliferation rate of the outermost luminal layer in the TEB*. We empirically determined the rate of division in the exterior and interior luminal TEB by BrdU incorporation. BrdU was administered to 6wk-old mice and the percent of BrdU+ luminal cells was determined. The replication rate was then extrapolated from this data as described previously in Paine et al [138], based on the duration of S-phase, when cells are receptive to BrdU labeling, being approximately 6 hrs.

Plasmid construction and lentivirus production

The sgRNAs used in this study are listed in the Resources Table. gRNAs were designed using CHOPCHOP. sgRNAs were cloned into lentiCRISPR v1 or v2 vector at the BsmBI restriction site using Zhang lab protocol (Shalem et al., 2014; Sanjana et al.,

2014). pLVTHM-mApple was generated as described in Ahmed et al., 2017. pLVTHM-Venus was generated as described in McCaffrey et al. [154].
293T cells were cultured in DMEM, 10% FBS, and 100U/mL Penicillin and Streptomyocin. To produce lentivirus, 293T cells were transfected with packaging plasmids psPax2 and pMDG2-VSVG along with the desired plasmid to be packaged in the lentiviral genome. This was done using calcium phosphate transfection. Medium was changed after 18 hrs and virus-containing media was collected after 36 hrs. In some cases, virus-medium was concentrated using Amicon 100k centrifugal filters.

In vitro intercalation assay

Eph4 cells were cultured in DMEM, 10% FBS (fetal bovine serum), and 100U/mL Penicillin & Streptomyocin. For intercalation assay, 150x10^3 single cells were plated onto 8-well chambered coverglasses. After 24 hrs, other cells were then dissociated to single cells with Trypsin and washed before being added to the previously plated monolayers. Integration of the intercalated cells into the monolayer was then determined by imaging the area displaced in the monolayer after 24 hrs. In all assays where area was determined, monolayer cells expressed a fluorescent marker. Thresholding was used to determine the area where monolayer signal was displaced, and the total area of integration was summed. Figures include example images of the monolayer fluorescence, masks of the determined area of integration, and normalized area of integration quantifications. For many experiments, co-stain with either Hoechst or differentially labeled cell populations were used to ensure areas where monolayer cells were displaced were indeed intercalated cells.

In vivo intercalation assay

Single mammary epithelial cells were transplanted into mammary ducts via the nipple of anesthetized mice. Cells either expressed: CRISPR-mCherry-non-targeting-sgRNA or CRISPR-GFP-Tjp1-sgRNA. Labeled cells were combined in a 1:1 ratio and 5-10 x10^3 labeled cells in 10μL of DMEM/F12 (basal media – no growth factors) were injected with a custom Hamilton syringe (blunt end style: 3, gauge: 30, needle length: 15mm). Transduction efficiency was less than 100% and as a result approximately 5-10 x10^3

unlabeled wildtype cells were also injected. Mice were harvested 18 hrs or 5 days after transplantation and the composition of cells present in the lumen or integrated in the duct, respectively, was quantified.

Organoid formation assay

Organoids were formed as described previously [142]. Briefly, inguinal mouse mammary glands (4th pair) were isolated from 12 wk old C3H mice, then minced and digested in collagenase for 1 hour shaking at 37 $^{O}$C. Enrichment for epithelial tissue pieces was performed by serial centrifugation pulses, and plated in Matrigel (extracellular matrix) with media consisting of DMEM/F12 (1:1), 3ng/mL FGF2, 5ng/mL EGF, and 1x ITS – replenished daily. Organoids were fixed in 4% PFA at day 6, 9, and 14.

Immunostaining

Cells and organoids were fixed with 4% paraformaldehyde (PFA) for 10 min, or overnight for tissue. Tissue was then placed in 30% sucrose solution for at least 24 hrs until embedding and cryo-sectioning. Samples (cells and tissue) were blocked and permeabilized with 5% normal goat serum in PBS with 0.2% TritonX-100. Primary or secondary antibodies were incubated for 1 hr with cells or overnight at 4$^{O}$C for tissue sections and organoids. Hoechst or phalloidin stains were added during secondary antibody incubation. Slides were mounted with Fluoromount-G.

Confocal microscopy and image processing

All imaging was performed using a Nikon A1R scanning confocal microscope and analysis was done with Nikon Elements software. Live cell imaging was performed in a TOCRIS chamber at 37 $^{O}$C with 5% $CO_2$. Imaging was performed at intervals as specified per experiment. Generally, intervals for long term intercalation experiments were 30 min, and were 15-20 min for shorter intercalation experiments. Confocal images were collected with z-steps ranging from 1.5$\mu$m for intercalation assay field analysis or 0.0 - 1$\mu$m step for higher magnification analysis of cell junction staining. Objectives used: 20x, 40x, 60x. Maximum intensity projections (IP) were created for

display of intercalation assay field analysis and for other staining experiments. TEB images are individual sections and not maximum intensity projections.

Statistical analysis

Statistical tests performed are described in the figure legends for each graph with comparisons. In general, unpaired t-test, paired t-test, one-way ANOVA, and Fisher's exact test were performed in GraphPad Prism. Graphs shown also indicate error bar definitions in figure legends (SD, SEM, etc.). p values are listed in figure legends for all comparisons shown on each graph.

## 2.6 Supplemental Data

| | TEB Luminal 1 | TEB Luminal 2 | TEB Luminal 3 | Duct Luminal 4 |
|---|---|---|---|---|
| Corresponding region (Paine et al., Plos Comp Biol, 2016) | Region 5 | Region 6 | Region 7 | Region 8 |
| Cell Width (μm) *w* | 11.1 (±0.2) | 10.8 (±0.1) | 11.3 (±0.2) | 9.8 (±0.1) |
| Cell Length (μm) *l* | 7.1 (±0.1) | 6.7 (±0.1) | 7.3 (±0.1) | 6.84 (±0.07) |
| Total Region Area ($\mu m^2$) $A_T$ | 8949.66 | 11935.78 | 12414.75 | - |
| Exterior Area ($\mu m^2$) $A_E$ = perimeter * *w* | 2327.68 | 3481.27 | 4892.90 | - |
| Interior Area ($\mu m^2$) $A_I = A_T - A_E$ | 6621.98 | 8454.51 | 7521.85 | - |
| Cell number (#) $N_T$ | 113.56 | 164.95 | 150.5 | - |
| Cell number (#) $\Delta N_T$ | 6.29 | 9.24 | 14.56 | - |
| Proliferation rate ($day^{-1}$) r | 0.6976 | 0.5746 | 0.6124 | - |
| Proliferation rate ($day^{-1}$) Δr | 0.073 | 0.0609 | 0.0695 | - |
| Apoptotic rate ($day^{-1}$) d | 0.0797 | 0.1064 | 0.0694 | - |
| Apoptotic rate ($day^{-1}$) Δd | 0.0132 | 0.0137 | 0.0115 | $M_T$ --> Duct Luminal |
| Total New cells/day $M_T$ | 70.17 | 77.23 | 81.72 | **229.12** |
| Total New cells/day $\Delta M_T$ | 13.75 | 12.88 | 16.41 | 43.04 |

**Table S2.1 TEB dimensions and luminal cell turnover.**
Values used for modeling luminal cells produced in interior or exterior of TEB. All values were determined by or using data reported by Paine et al.

| | | | TEB Luminal 1 | TEB Luminal 2 | TEB Luminal 3 | | |
|---|---|---|---|---|---|---|---|
| Cell number calculation | $N_E$ Exterior cells (#) | $N_E = N_T * (A_E/A_T)$ | 29.54 | 48.11 | 59.32 | | |
| | $N_I$ Interior cells (#) | $N_I = N_T - N_E$ | 84.02 | 116.84 | 91.18 | Total cells | % of Elongation |
| | $M_E$ New Exterior cells/day | $M_E = N_E * (r_E - d_E)$ | 18.25 | 22.53 | 32.21 | 72.98 | 31.9% |
| | $M_I$ New Interior cells/day | $M_I = M_T - M_E$ | 51.92 | 54.70 | 49.51 | 156.14 | 68.1% |
| Uncertainty in calculation | $\Delta N_E$ Exterior cells (#) | $\Delta N_E = \Delta N_T * (A_E/A_T)$ | 1.64 | 2.70 | 5.74 | | |
| | $\Delta N_I$ Interior cells (#) | $\Delta N_I = \Delta N_T + \Delta N_E$ | 7.93 | 11.94 | 20.30 | Total ΔM | % (ΔM/M) |
| | $\Delta M_E$ New Exterior cells/day | $\Delta M_E = M_E * \text{sqrt}( (\Delta r^2) + (\Delta d^2) + (\Delta N_E^2) )$ | 3.72 | 3.96 | 7.18 | 14.86 | 20.4% |
| | $\Delta M_I$ New Interior cells/day | $\Delta M_I = \Delta M_T + \Delta M_E$ | 17.46 | 16.84 | 23.59 | 57.90 | 37.1% |

**Table S2.2 Number of cells expected to contribute to elongation from interior or exterior TEB regions, Related to Figure 2.1 & S2.1.**
Calculations used to determine relative exterior and interior TEB luminal cell contribution to mature duct based on data in Table S1. Derivation of the uncertainty in our model is also shown in the bottom half of table and is also presented as % (ΔM/M).

| | | | | | | | $M_E$ New Exterior cells/day | | | |
|---|---|---|---|---|---|---|---|---|---|---|
| Mouse | TEB | BrdU positive (%) | Proliferation rate ($day^{-1}$) $r_E$ | Mature Duct Cell Length (μm) *l* | Luminal cells ($N_E$) | Apoptotic rate ($day^{-1}$) (Luminal Average) $d_E$ | $M_E = N_E * ((r_E * 0.5) - d_E)$ | average $M_E$ (mouse) | Duct Elongation Length (mm) $L = M_E * (l / 2)$ | % of total elongation |
| 1 | 1 | 12.0% | 0.480 | 6.840 | 137.0 | 0.085 | 21.2 | 60.7 | 0.0725 | 9.3% |
| 1 | 2 | 17.9% | 0.718 | 6.840 | 137.0 | 0.085 | 37.5 | | 0.1283 | 16.4% |
| 1 | 3 | 39.5% | 1.581 | 6.840 | 137.0 | 0.085 | 96.6 | | 0.3305 | 42.2% |
| 1 | 4 | 11.7% | 0.467 | 6.840 | 137.0 | 0.085 | 20.3 | | 0.0694 | 8.9% |
| 1 | 5 | 21.4% | 0.854 | 6.840 | 137.0 | 0.085 | 46.9 | | 0.1602 | 20.4% |
| 1 | 6 | 36.4% | 1.455 | 6.840 | 137.0 | 0.085 | 88.0 | | 0.3008 | 38.4% |
| 1 | 7 | 40.4% | 1.615 | 6.840 | 137.0 | 0.085 | 99.0 | | 0.3385 | 43.2% |
| 1 | 8 | 25.9% | 1.035 | 6.840 | 137.0 | 0.085 | 59.2 | | 0.2026 | 25.9% |
| 1 | 9 | 29.5% | 1.182 | 6.840 | 137.0 | 0.085 | 69.3 | | 0.2369 | 30.2% |
| 1 | 10 | 29.5% | 1.180 | 6.840 | 137.0 | 0.085 | 69.2 | | 0.2366 | 30.2% |
| 2 | 12 | 33.3% | 1.333 | 6.840 | 137.0 | 0.085 | 79.7 | 69.5 | 0.2724 | 34.8% |
| 2 | 13 | 29.8% | 1.191 | 6.840 | 137.0 | 0.085 | 69.9 | | 0.2392 | 30.5% |
| 2 | 14 | 34.1% | 1.366 | 6.840 | 137.0 | 0.085 | 81.9 | | 0.2800 | 35.7% |
| 2 | 15 | 36.5% | 1.459 | 6.840 | 137.0 | 0.085 | 88.3 | | 0.3020 | 38.5% |
| 2 | 16 | 12.8% | 0.512 | 6.840 | 137.0 | 0.085 | 23.4 | | 0.0799 | 10.2% |
| 2 | 17 | 31.3% | 1.250 | 6.840 | 137.0 | 0.085 | 73.9 | | 0.2529 | 32.3% |
| 3 | 19 | 14.3% | 0.571 | 6.840 | 137.0 | 0.085 | 27.5 | 32.1 | 0.0940 | 12.0% |
| 3 | 20 | 16.9% | 0.677 | 6.840 | 137.0 | 0.085 | 34.7 | | 0.1187 | 15.1% |
| 3 | 21 | 16.7% | 0.667 | 6.840 | 137.0 | 0.085 | 34.0 | | 0.1163 | 14.8% |
| | | | | | | Average | 59.0 | 54.1 | 0.2017 | 25.7% |
| | | | | | | SD | 27.11 | | 0.0927 | 11.8% |
| | | | | | | SEM | | 11.31 | | |

**Table S2.3 Exterior cell generation and estimated contribution to elongation, Related to Figure 2.1 & S2.1**

Data showing %BrdU positive exterior cells converted into replication rate for exterior cells. These values along with the correction factor for random division orientation were then used to determine the cells generated in the exterior layer per day.

| | | | | | | | $M_I$ New Interior cells/day | | | |
|---|---|---|---|---|---|---|---|---|---|---|
| Mouse | TEB | BrdU positive (%) | Proliferation rate ($day^{-1}$) $r_I$ | Mature Duct Cell Length (μm) *l* | Luminal cells ($N_I$) | Apoptotic rate ($day^{-1}$) (Luminal Average) $d_I$ | $M_I = N_I * (r_I - d_I) + (0.5 * M_E)$ | average $M_I$ (mouse) | Duct Elongation Length (mm) $L = M_I * (l / 2)$ | % of total elongation |
| 1 | 1 | 7.1% | 0.283 | 6.840 | 292.0 | 0.085 | 87.3 | 180.7 | 0.2987 | 38.1% |
| 1 | 2 | 16.3% | 0.653 | 6.840 | 292.0 | 0.085 | 195.4 | | 0.6681 | 85.3% |
| 1 | 3 | 35.7% | 1.429 | 6.840 | 292.0 | 0.085 | 421.8 | | 1.4427 | 184.1% |
| 1 | 4 | 7.4% | 0.295 | 6.840 | 292.0 | 0.085 | 90.9 | | 0.3109 | 39.7% |
| 1 | 5 | 8.8% | 0.353 | 6.840 | 292.0 | 0.085 | 107.6 | | 0.3679 | 47.0% |
| 1 | 6 | 21.9% | 0.877 | 6.840 | 292.0 | 0.085 | 260.7 | | 0.8915 | 113.8% |
| 1 | 7 | 21.6% | 0.863 | 6.840 | 292.0 | 0.085 | 256.8 | | 0.8781 | 112.1% |
| 1 | 8 | 13.9% | 0.557 | 6.840 | 292.0 | 0.085 | 167.4 | | 0.5727 | 73.1% |
| 1 | 9 | 10.8% | 0.430 | 6.840 | 292.0 | 0.085 | 130.2 | | 0.4454 | 56.8% |
| 1 | 10 | 7.2% | 0.289 | 6.840 | 292.0 | 0.085 | 89.0 | | 0.3044 | 38.8% |
| 2 | 12 | 16.7% | 0.667 | 6.840 | 292.0 | 0.085 | 199.3 | 176.8 | 0.6817 | 87.0% |
| 2 | 13 | 19.0% | 0.762 | 6.840 | 292.0 | 0.085 | 227.1 | | 0.7768 | 99.1% |
| 2 | 14 | 17.1% | 0.684 | 6.840 | 292.0 | 0.085 | 204.5 | | 0.6995 | 89.3% |
| 2 | 15 | 19.1% | 0.765 | 6.840 | 292.0 | 0.085 | 228.0 | | 0.7796 | 99.5% |
| 2 | 16 | 5.9% | 0.237 | 6.840 | 292.0 | 0.085 | 73.8 | | 0.2524 | 32.2% |
| 2 | 17 | 10.6% | 0.424 | 6.840 | 292.0 | 0.085 | 128.3 | | 0.4388 | 56.0% |
| 3 | 19 | 6.7% | 0.269 | 6.840 | 292.0 | 0.085 | 83.3 | 93.7 | 0.2847 | 36.3% |
| 3 | 20 | 5.0% | 0.202 | 6.840 | 292.0 | 0.085 | 63.5 | | 0.2173 | 27.7% |
| 3 | 21 | 11.1% | 0.444 | 6.840 | 292.0 | 0.085 | 134.4 | | 0.4597 | 58.7% |
| | | | | | | Average | 165.8 | 150.4 | 0.5669 | 72.3% |
| | | | | | | SD | 89.56 | | 0.3063 | 39.1% |
| | | | | | | SEM | | 28.36 | | |

**Table S2.4. Interior cell generation and estimated contribution to elongation, Related to Figure 2.1 & S2.1**

Data showing %BrdU positive interior cells converted into replication rate for interior cells. These values along with the correction factor for contribution from the exterior (due to stratifying divisions) were then used to determine the cells generated in the interior per day.

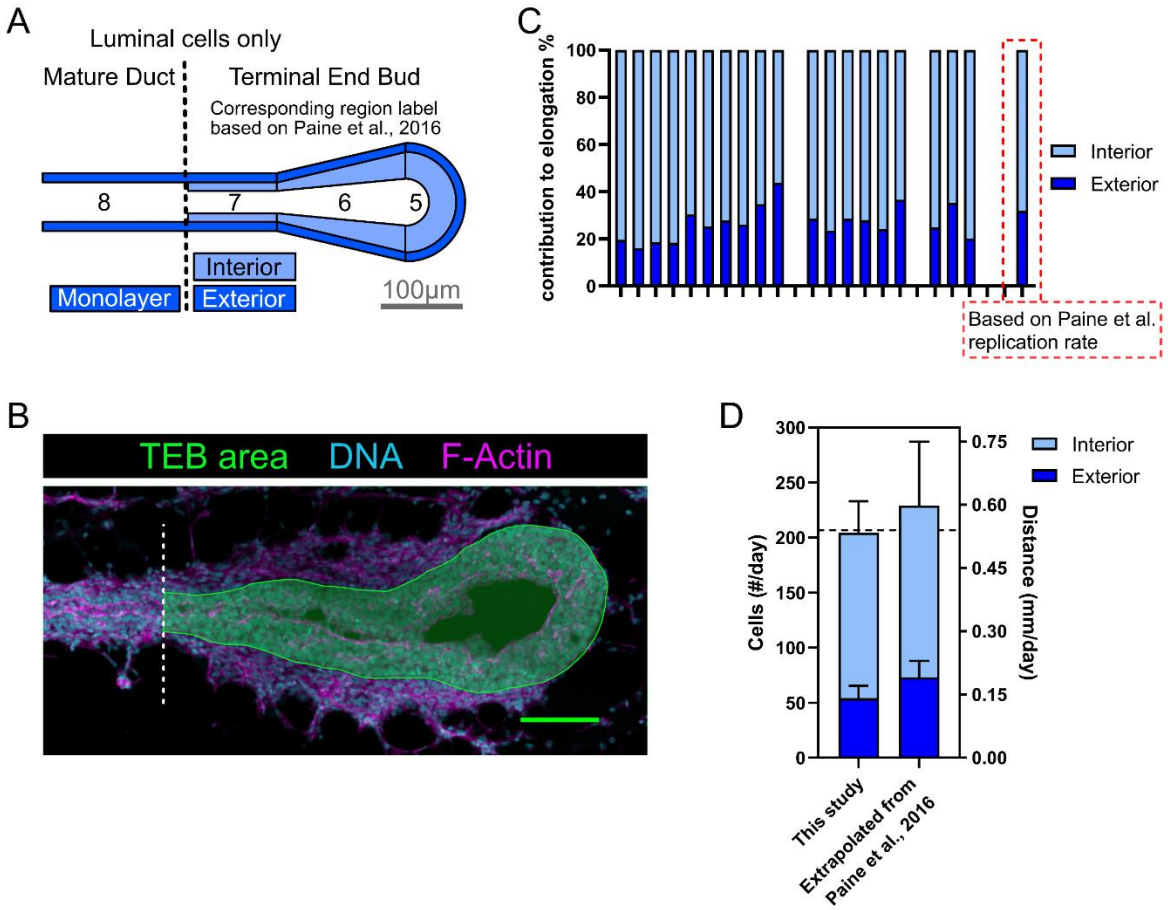


**Figure S2.1 Models of the TEB and mechanisms contributing to elongation. Related to Figure 2.1** **A**. Schematic of TEB showing luminal cells only (TEB and mature duct), segregated into distinct regions (including section numbering as used by Paine et al., 2016). Colors represent interior and exterior (outermost) luminal cell compartments. **B**. Example TEB section from a 6-week-old FVB mouse stained to indicate nuclei (DNA) and F-actin. Multilayered TEB region highlighted in green. Scale bar = 100µm. **C**. Contribution of interior or exterior (outermost) luminal cells to ductal elongation for each TEB, based on total numbers of cells produced in each TEB that contribute to the mature duct. Proliferation rates for interior and exterior luminal TEB regions were measured (Fig. 1C) and calculations are shown for each TEB. 3 mice, 19 TEBs (sets from different mice spaced apart). Also shown is the contribution to elongation derived from replication rate reported in Paine et al., 2016 (data outlined in red). **D**. TEB elongation per day driven by interior or exterior luminal cells, reported as cell number and distance. Comparison of data collected in this study and that of Paine et al., 2016

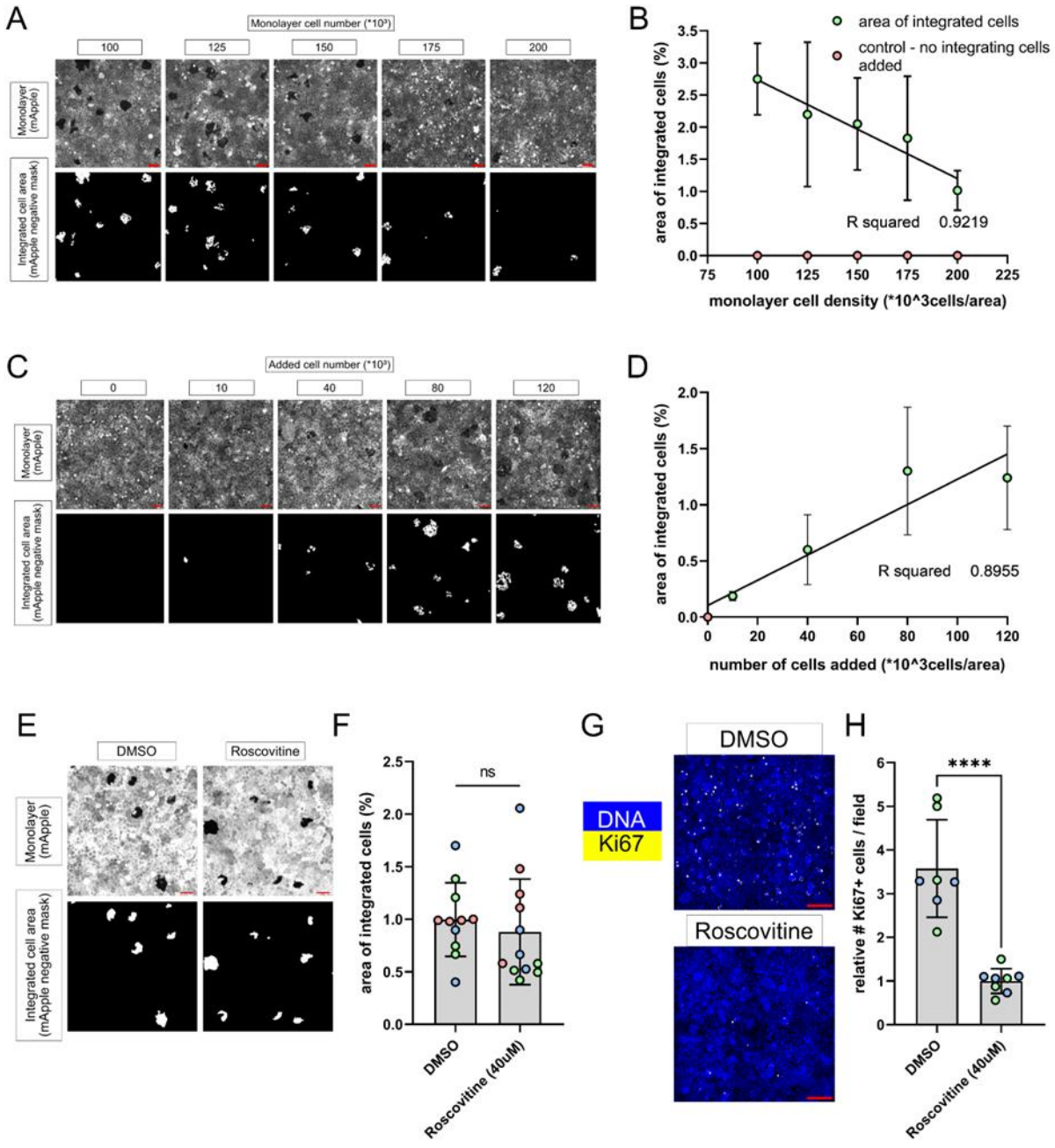


**Figure S2.2 Cell density but not cell division alters intercalation dynamics. Related to Figure 2.2** **A**. Intercalation assay with variable monolayer cell densities at plating. Scale: 50μm. **B**. Plot of integrated cell area (as percent of total monolayer area) versus monolayer density. 1 example experiment shown. Mean +/- SD. **C**. Intercalation assay with variable added (intercalating) cell number and fixed monolayer density. Scale: 50μm. **D**. Plot of integrated cell area (as percent of total monolayer area) versus number of added cells. 1 example experiment shown. Mean +/- SD. **E**. Intercalation assay performed after treatment of cells with 40 μM Roscovitine, to inhibit cell division, or vehicle (DMSO). Example field of mApple+ monolayers (top) with areas displaced by unlabeled intercalating cells shown below as inverse binary masks. Scale: 50μm. **F**. Areas of integration from Fig S2 E. Unpaired t-test. Mean +/- SD, n = 3 experiments, p = 0.5303. **G**. Field of Eph4 cells from intercalation assay in Fig. S2 E stained for DNA and

Ki67 as a proliferation marker. Scale: 200μm. **H**. Normalized number of Ki67-positive cells per field. 2 experiments. Unpaired t-test. Mean +/- SD; $p < 0.0001$.

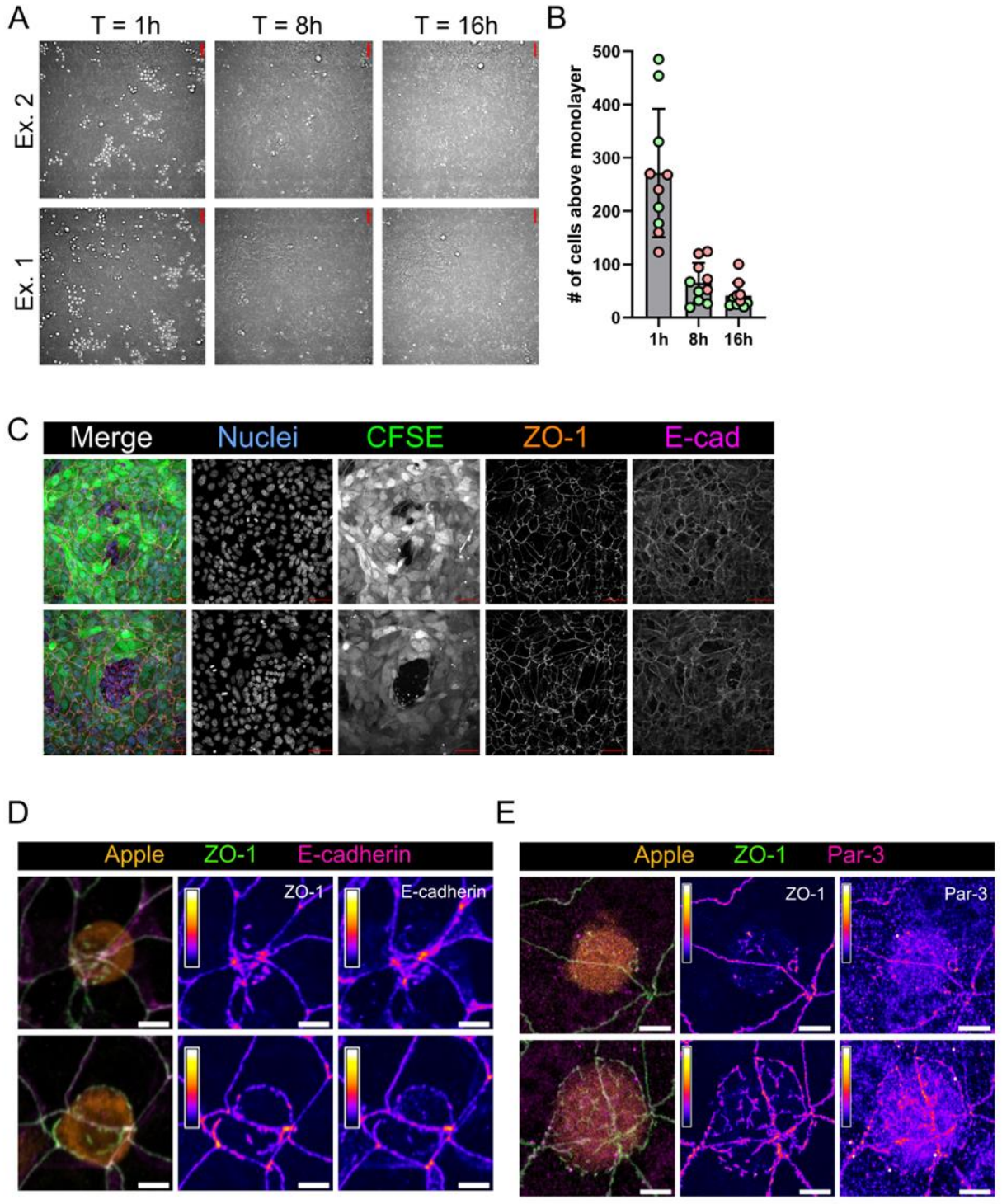


**Figure S2.3 Primary luminal cell intercalation and junction rearrangements. Related to Figure 2.3** **A**. Timelapse imaging of DIC channel only. Cell clusters sitting atop monolayer are apparent. 2 example fields. Scale: 50μm. **B**. Total number of cell clusters located above the monolayer. 2 experiments graphed. Each data point represents one field of view; colors represent different biological replicates. **C**. Intercalation assay with primary MECs (as in Fig. 3 A-D) fixed after 24hrs and stained for junctional markers, showing full integration of intercalating cells into the monolayer. Maximum-intensity projection of monolayer. Scale: 20μm. **D**. Immunofluorescent staining of ZO-1 and E-cadherin during intercalation.

Maximum-intensity projection of interface between monolayer and intercalating cells (Apple+). Scale: 5μm. Fluorescence intensities mapped to a Fire LUT. **E**. Immunofluorescent staining of ZO-1 and Par-3 during intercalation. Max-intensity projection of intercalation interface between monolayer and intercalating cells (Apple+). Scale: 5μm. Fluorescence intensities mapped to a Fire LUT.

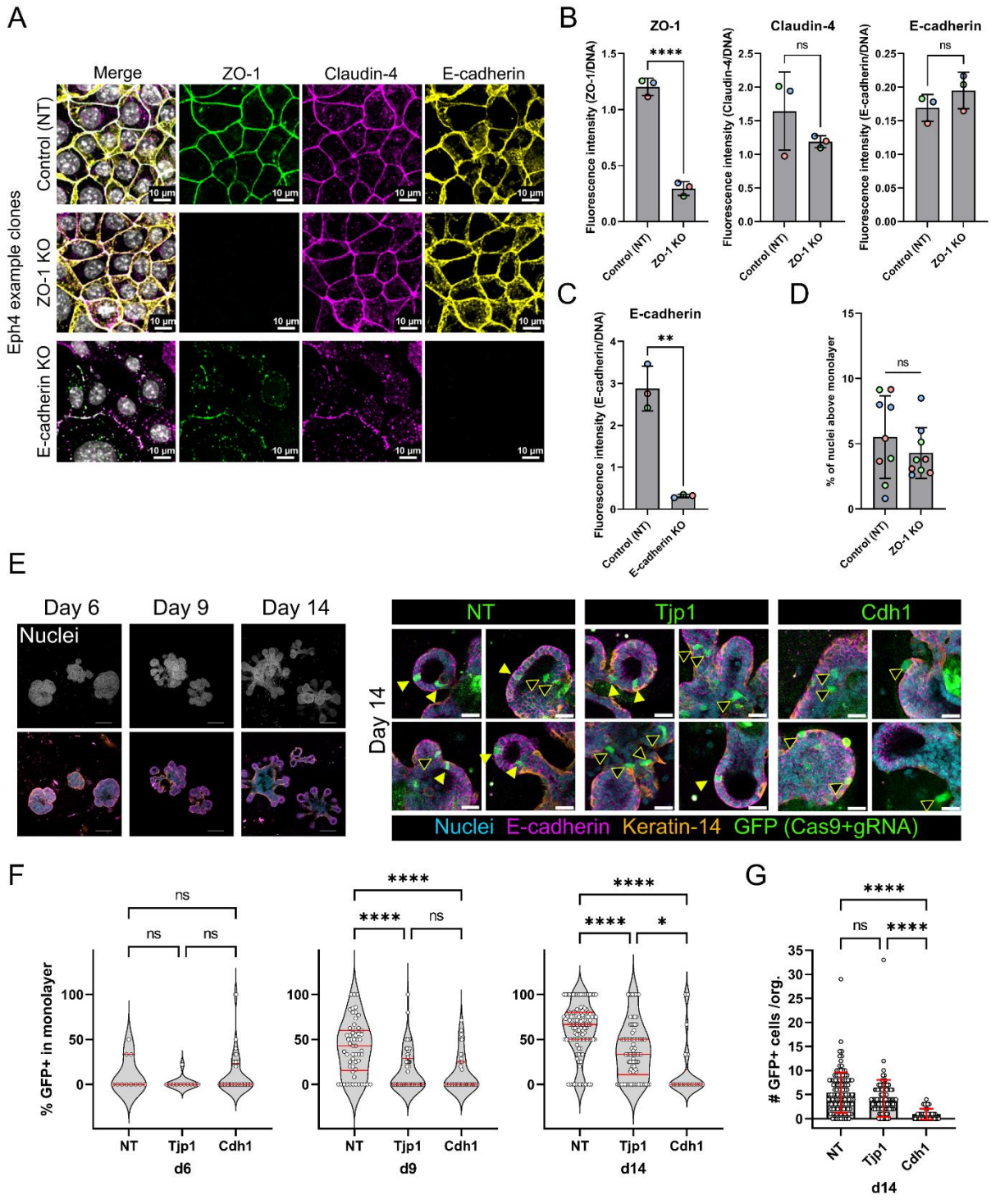


**Figure S2.4 ZO-1 loss does not impair monolayer organization in 2D but reduces cell incorporation into monolayered regions of mammary organoids. Related to Figure 2.4**
**A**. The same number of cells were plated for each clone and fixed at confluent density. Cells were then immunostained for ZO-1, Claudin-4, E-cadherin, and DNA. Deletion of ZO-1 does not alter the location of either Claudin-4 or E-cadherin to intercellular junctions, but deletion of E-cadherin disrupts tight junctions. Immunofluorescence of knockout clones after expansion to confluent monolayer. One example clone for

each knockout (ZO-1 and E-cadherin) is shown. Scale: 10μm. **B**. Quantification of knockout efficiencies. Fluorescence intensities for total ZO-1, Claudin-4, and E-cadherin in control (non-targeting sgRNA) and ZO-1 knockout (Tjp1 sgRNA) clones. Intensity for each channel was determined for a random field of view for each clone. Intensities for each marker were normalized to DNA intensity in the same field to account for cell number differences. Mean +/-SD. unpaired t-test. $p < 0.0001$, $p = 0.2514$, $p = 0.2519$. **C**. Comparison of E-cadherin staining of control (non-targeting sgRNA) clones and E-cadherin knockout (Cdh1 sgRNA) clones. Mean +/-SD. unpaired t-test. $p = 0.0011$. **D**. Multilayering analysis of control and ZO-1 knockout clones as measured by percent of nuclei above the monolayer compared to total nuclei. Mean +/-SD. unpaired t-test. $p = 0.3384$. **E**. Left: Progression of mouse mammary organoid morphology at 6, 9, and 14 d in culture. Top row: maximum-intensity projections of nuclear staining. Bottom row: Single confocal sections of organoids stained for luminal (Cdh1) and basal (Krt14) markers. Right: d14 organoids from tissue fragments transduced sparsely with CRISPR-GFP lentivirus. Guide RNA target NT: non-targeting control, Tjp1: ZO-1 gene, Cdh1: E-cadherin gene). Example images of GFP+ cell locations within organoids after 14 d in culture. Yellow arrowheads: GFP+ luminal cell located in monolayer region of organoid. Black arrowheads: GFP+ luminal cell not incorporated into a monolayer region of organoid. F. Quantification of GFP+ luminal cell location within organoids. Plots show % GFP+ cells within a monolayer region per organoid. Median and quartiles shown in red, d6, n = 79, d9, n = 186, d14, n = 252 total organoids. One-way ANOVA. d6: ns, d9 and d14: $p < 0.0001$. Individual comparisons shown. **G**. Quantification of total GFP+ cell number per organoid. One-way ANOVA, d14: $p < 0.0001$. Individual comparisons shown. Mean+/-SD.

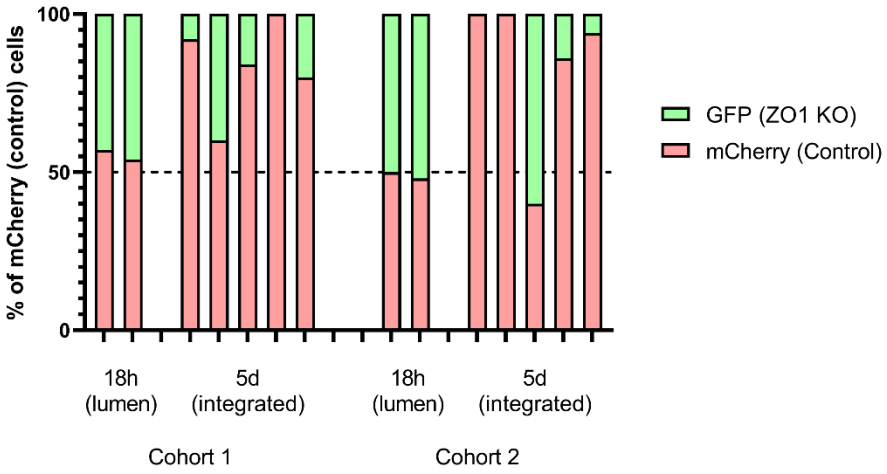


**Figure S2.5 Individual mice from transplants. Related to Figure 2.5**
Distribution of cells found in each mouse after intraductal injection. The first 2 columns of each cohort are mice taken soon after injections to verify 1:1 distribution in the lumen. Next columns are mice taken after 5 days to allow cells in lumen to intercalate (5 per cohort). Dotted line drawn at 50%.

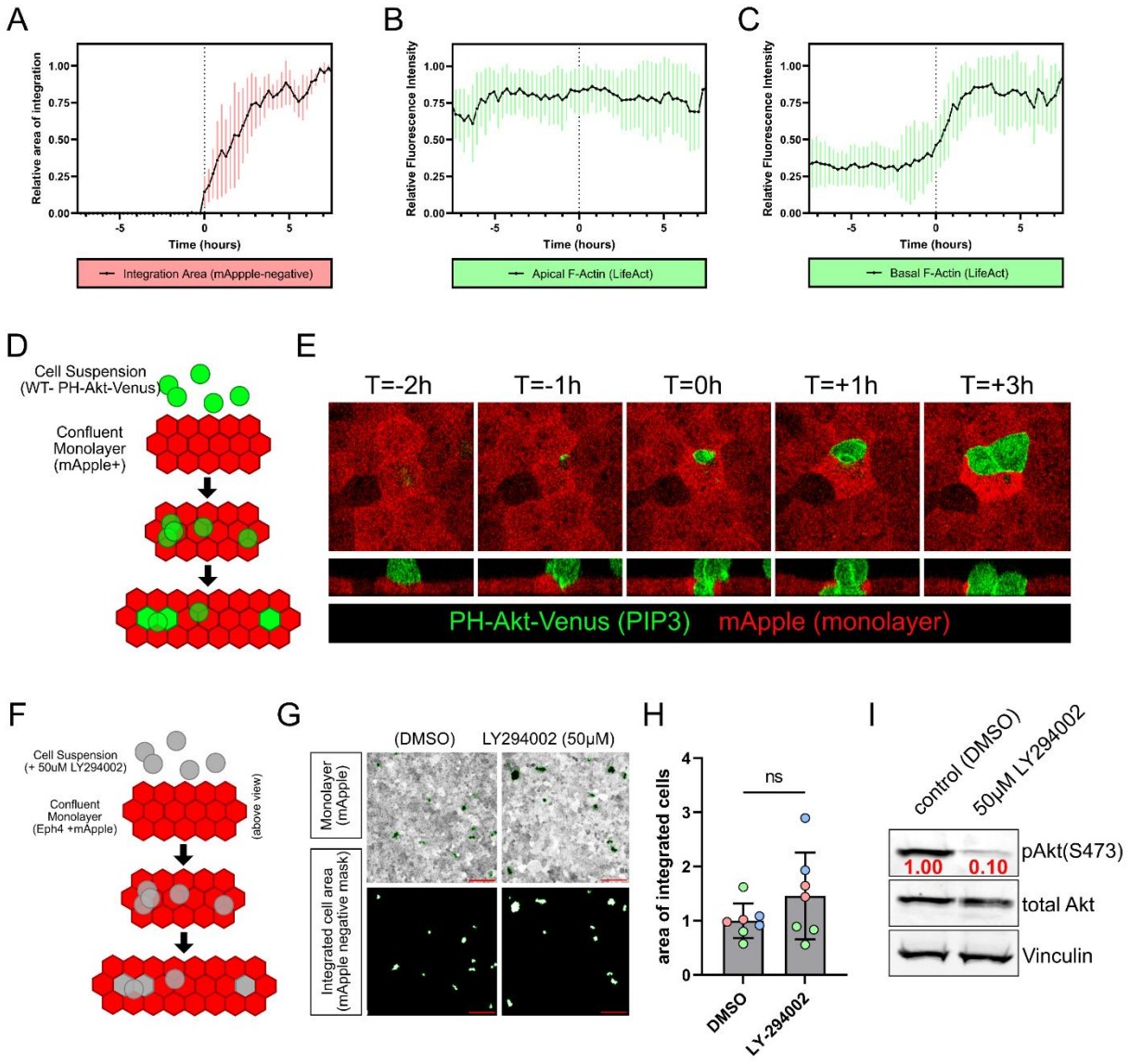


**Figure S2.6 Live imaging of F-actin rearrangement associated with intercalation. Related to Figure 2.6**

**A.-C**. Quantification of integration area and F-actin intensity at apical interface and basal surface from live imaging analysis of intercalation events. Example shown in Fig. 6 B. Time normalized to initial intercalation denoted at time = 0h. n = 8 cells, Mean +/- 1SD. Fluorescence intensity, area, and time are normalized.

**A**. Area displaced in the monolayer by intercalating cell. **B**. F-Actin (LifeAct) intensity at apical region (interface) of intercalating cell relative to total LifeAct intensity. **C**. F-Actin (LifeAct) intensity at basal/bottom surface of intercalating cell relative to total LifeAct intensity. **D**. Schematic of intercalation assay with mApple+ monolayer plus intercalating cells (green) that express the $PIP_3$ biosensor (PH-Akt-Venus). **E**. Example intercalation event. Time is expressed relative to cell touching basal substrate. Top frames shown from X,Y plane, bottom frames show X,Z plane. **F**. Schematic of intercalation assay with mApple+ monolayer and unlabeled intercalating cells added plus PI3K inhibitor LY-2940002. **G**. Example images of intercalations for control (+DMSO) and +PI3K inhibitor treated cells, Scale bar: 50μm. **H**. Quantification of G. showing normalized areas of intercalated cells. Colored data points represent biological replicates. N = 3 experiments, Mean +/- 1 SD; unpaired t-test, p = 0.1865. **I**. Inhibitor control.

Immunoblot of cells treated with DMSO (vehicle control) or LY294002 (50μM) after 18hrs. Quantification of phosphorylated Akt (S473) relative to total Akt signal shown in red on p-Akt blot.

## Chapter 3: Control of Cell Division Orientation is Dispensable for Mammary Gland Organization and Misorientation is not Required for Tumor Initiation

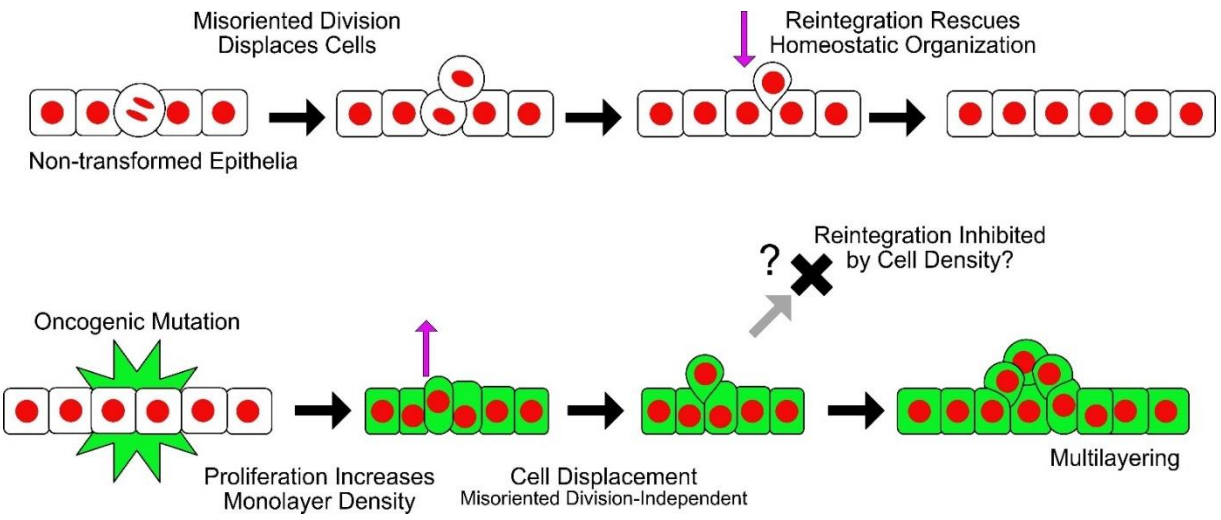


**Figure 3.0 Graphical Abstract**

### 3.1 Abstract

Most human cancers arise in epithelial tissues. Mis-orientation of epithelial cell division has been postulated to play a role in the initial stages of tumorigenesis by disrupting tissue organization however the results of division misorientation independent of other transforming perturbations is unknown. Here we perturb normal planar-aligned division orientation in mammary cells by ablating the astral microtubule binding protein Kif18b. Kif18b loss caused random division orientation in Eph4 and MDCKII cells in 2D and disrupted MDCKII cyst morphogenesis in 3D. Remarkably, cells correct daughter cell displacement after division misorientation through cellular re-integration into the monolayer. This result was also seen in primary mammary luminal cells grown in (3D) acinar culture. Live imaging reveals transformed cell monolayers do not require misorientation of cell division to induce multilayering and instead multilayer in a misoriented-division-independent manner. Overall, we show misoriented divisions tend

to be corrected by re-integration and transformed cells may favor other mechanisms to disrupt the normal architecture of the epithelium.

### 3.2 Introduction

Most human cancers arise in epithelial tissues. Mis-orientation of epithelial cell division has been postulated to play a role in the initial stages of tumorigenesis by disrupting tissue organization, but to date there have been virtually no experimental tests of this hypothesis [118, 119, 124, 155-158]. Mis-orientation of division has been observed in several mouse models of mammary tumorigenesis, such as polyomavirus middle T antigen (PyMT) expression or loss of the tumor suppressor Pten [118, 119], but the consequences of this mis-orientation have not been examined. If misoriented divisions do result in tissue dysplasia, then the mechanisms of normal orientation may provide insight into how tissues protect from aberrant organization. Displacement of transformed cells may be due to either misoriented cell division, extrusion by neighboring cells, or migration [159]. Regardless of their mechanism of displacement, primary dysplasia in the mammary gland in most cases is typically characterized by accumulation of cells in the luminal space of the gland [160-162].

How different epithelial tissues respond to aberrant cell division orientation is unclear. Mitotic spindle orientation dictates the plane of cytokinesis and placement of daughter cells within a tissue [42, 163]. Experiments in MDCKII epithelial cells show that loss of spindle anchoring proteins causes disruption of mitotic spindle orientation, leading to defects in normal lumen formation[164]. Disruption of polarity by loss of Par3 or Scrib also results in random spindle orientation and defects in morphogenesis [56, 82, 165, 166]. However, whether spindle misorientation *itself* is causal to these defects in morphogenesis and epithelial dysplasia in mammalian tissues has not been explored.

A cell dividing out of the epithelial plane may undergo cell death, reintegration, or continue to proliferate after it is initially displaced. Studies in *Drosophila* show the remarkable ability of different epithelial tissues to maintain their structure after

misoriented division, through diverse methods [127, 167]. For example, in the developing *Drosophila* wing disc epithelium, loss of planar spindle orientation caused basal displacement after cell division and apoptosis of displaced cells. Inhibition of apoptosis in displaced cells resulted in hyperplasia and epithelial to mesenchymal transition, as well as expression of matrix metalloproteinase [167]. These results indicate that in certain epithelial contexts, misoriented cell division, if not corrected, can lead to tissue disorganization and tumor formation. *Drosophila* oocytes are surrounded by follicular epithelium, which is a monolayer of polarized epithelial cells. Surprisingly, when spindle anchoring proteins are ablated, and the division axis is altered, the normal structure of the follicular epithelium is maintained. Time-lapse imaging revealed that daughter cells outside the epithelial plane were able to reintegrate into the monolayer [127], a very different outcome to the wing disc epithelium. Reintegration occurs normally in the developing mammalian kidney, where dividing cells displace into the lumen; one daughter cell maintains a thin basal process and retracts into its original position in the epithelium while the other cell reintegrates in a different position and other similar integration events have been show in epithelial development [123, 168].

The mammary gland is a dynamic epithelial tissue, that undergoes structural rearrangements from development through reproductive life in mammals. Mammary epithelium is bilayered containing luminal epithelial cells and basal cells, together composing the majority of the branched ductal gland, surrounded by the stroma of the fat pad [169, 170]. In adult mouse mammary gland, cell divisions occur periodically during estrous cycles and in pregnancy, and it is an excellent model for studying epithelial morphogenesis as well as tumorigenesis. It is unknown currently whether the mammary gland at homeostasis can correct cell displacement after aberrant division, and studying these processes may have broad impact on epithelial biology and the understanding of tumor initiation. Determining how cell division misorientation affects epithelial tissue and how this is corrected will aid in the understanding of epithelial tissue maintenance in homeostasis, and early key stages in tumorigenesis.

## 3.3 Results

### 3.3.1 Kif18b loss in mammary epithelial cells results in division misorientation but not loss of epithelial organization

A major hurdle to studying the effects of misoriented division in epithelia is the off-target effects that alter cell junctions and polarity with other approaches [157]. Recently, the ablation of the kinesin-8 protein Kif18b has been shown to alter mitotic spindle orientation in mouse epidermal epithelia [76]. Kif18b promotes astral microtubule depolymerization to regulate proper mitotic spindle rotation [171-173], and we hypothesized this would cause misoriented cell division in Eph4, a mammary epithelial cell line. To elucidate the role of cell division orientation in maintaining epithelial organization, we tested the approach of deleting Kif18b with a lentiviral CRISPR/Cas9 system [174]. Targeting of the Kif18b locus with 2 sgRNA was confirmed by PCR of genomic DNA and sequencing, which revealed an excised 5' region of the Kif18b gene (Fig. S3.1A,B). No significant defects in chromatin segregation fidelity, proliferation rate, apical-basal polarity, or junctional integrity were observed, in accordance with studies in HeLa cells (data not shown) [175]. To determine division axis and fate of displaced cells, we performed live cell imaging of Eph4 monolayers expressing Histone2B fused to mScarlet (Fig. 3.1A). Loss of Kif18b resulted in randomized division axis relative to the plane of the monolayer, while control (WT – non-targeting gRNA) cells divided parallel to the monolayer plane (Fig. 3.1B). After perpendicular divisions, a daughter cell could be seen displaced from the monolayer (Fig. 3.1A), but remarkably, the majority of these cells reintegrated into the monolayer (determined by nuclei height – Fig. 3.1C). This reintegration appears to rescue and maintain normal monolayer architecture.

To determine the effect of cell division misorientation on primary epithelial cells, mouse mammary luminal cells were isolated from dissociated mammary glands (as described in [142]). To facilitate luminal cell tracking and division orientation, we utilized mice expressing a Keratin-8-dependent H2B-GFP (more details in the methods, Fig.

3.1D). Isolated luminal cells were transduced with lentivirus to express Cas9/gRNA, cultured in suspension to select with puromycin, and plated in extracellular matrix suspension (Matrigel) to form mammary acini/cyst structures (similar to those described in [176]). Luminal cultures where Kif18b is ablated divided with random orientation to the epithelial plane and underwent reintegration (Fig. 3.1E,F), supporting our findings that a secondary mechanism is present to ensure proper daughter cell placement in the epithelial layer. Kif18b-ablated luminal cysts also formed polarized hollow lumens at the same rate as the control, as determined by apical Muc1 localization (Fig. 3.1G,H).

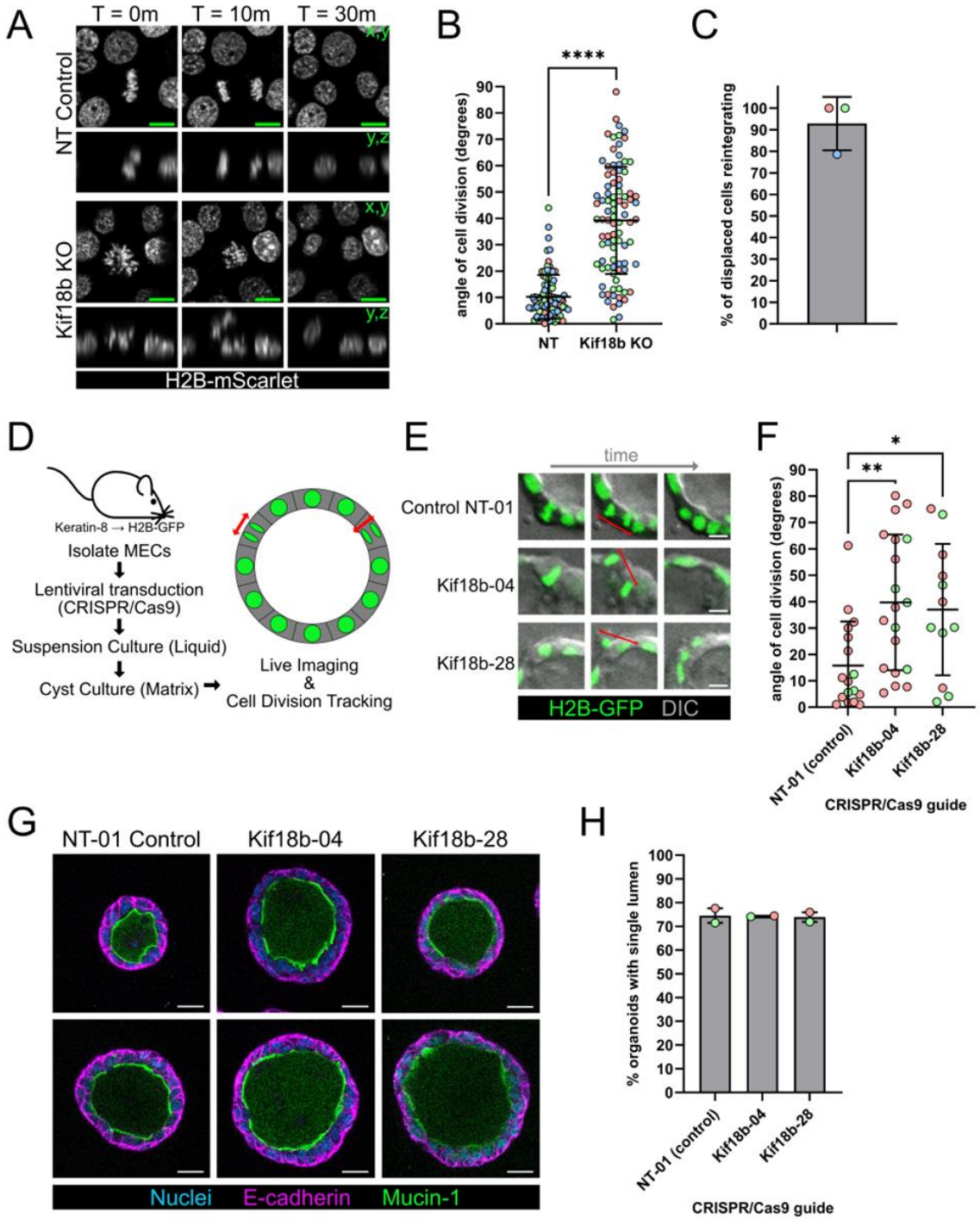


**Figure 3.1 Kif18b loss in mammary epithelial cells results in spindle misorientation**
**A.** Eph4 cell divisions in control or Kif18b knockout cells. Histone H2B-mScarlet. Scale: 10um. **B.** Quantification of division angle. 3 Kif18b knockout, 3 control (NT) clonal cell lines. Angle of chromatin segregation relative to basal substrate. Unpaired T-test. $p<0.0001$. **C.** Percentage of cells with division angle greater than 45deg reintegrating into the monolayer as determined by nuclei height. 3 Kif18b KO clones. **D.** Isolation of mouse primary mammary epithelial cells, transduction with lentivirus containing Cas9 &gRNA to delete Kif18b, and 3D cyst culture & live imaging workflow. Mice express Histone H2B-

GFP dependent on Keratin-8-driven CreER activity. Tamoxifen added in culture. Lentivirus also expresses puromycin resistance gene. Puromycin added in liquid culture at 4ug/mL for 7 days before plating in matrix to promote cyst growth. **E.** Example cell divisions in mammary cysts expressing Keratin8-driven Histone H2B-GFP. Cysts with Kif18b gRNA divide in random orientation with respect to basal axis compared to NT control gRNA cells. **F.** Quantification of division orientation in mammary cysts. Control (NT) or Kif18b gRNA and Cas9. **G.** Examples images of mammary cysts grown for 13 days. No significant difference between NT control and Kif18b gRNA (+Cas9). Experimental setup described in D. **H.** Quantification of percentage of mammary cysts with single hollow lumens after 13 days in culture.

### 3.3.2 MDCKII epithelial architecture disruption after misoriented division is prevented by slowing of division rate, allowing reintegration

While our previous experiments show oriented cell division is dispensable for maintaining a single lumen in a 3D culture model with primary mammary epithelial cells, data from MDCKII cyst morphogenesis experiments suggest otherwise. The MDCKII cyst formation assay is a well characterized 3D model for epithelial morphogenesis in which cell division misorientation coincides with defects in formation of a single lumen [41, 56, 164]. To test whether loss of division orientation by Kif28b ablation caused aberrant MDCKII cystogenesis, Kif18b was again targeted for ablation using a lentiviral CRISPR system. Several knockout and control clones were generated, and Kif18b loss again resulted in misoriented cell division and displaced cell reintegration in 2D, as with Eph4 cells (Fig. S3.2A-C). Interestingly, MDCKII cyst morphogenesis revealed a significant increase in defective lumen formation compared to control non-targeting cells (Fig. 3.2 A,B). Misoriented cell divisions have been reported to cause defects in cystogenesis [164, 177-179], and our data support these claims; however, this observation is contrary to the lack of observed defects when these cells are grown in 2D, where cell reintegration is observed (Fig. S3.2C). To decipher this result, we used live cell imaging to track cell divisions and cell fate after division in MDCKII cysts. Cells dividing out of the plane of the epithelium did not always result in cyst defects and usually resulted in reintegration (Fig. 3.2C-E). We hypothesized that MDCKII cells undergoing cystogenesis are dividing at a rate that prevents possible reintegration of displaced cells and promotes lumen formation defects. To test this, MDCKII cystogenesis was performed in reduced serum media (1% vs 5%), slowing the rate of division. The slowing of cell division has been proposed to support relaxation of cells

after misoriented division and preserve lumen formation although this has not been formally tested [58]. This rescued lumen formation in Kif18b null MDCKII cysts, suggesting planar cell divisions are not essential for MDCKII cyst formation, given cells divide infrequently enough to allow displaced cells to reintegrate into the monolayer (Fig. 3.2 F,G). While other perturbations, besides Kif18b loss, reported in the literature cause misoriented cell division in MDCKII cyst formation, they may also inhibit cell reintegration, resulting in more lumen defects.

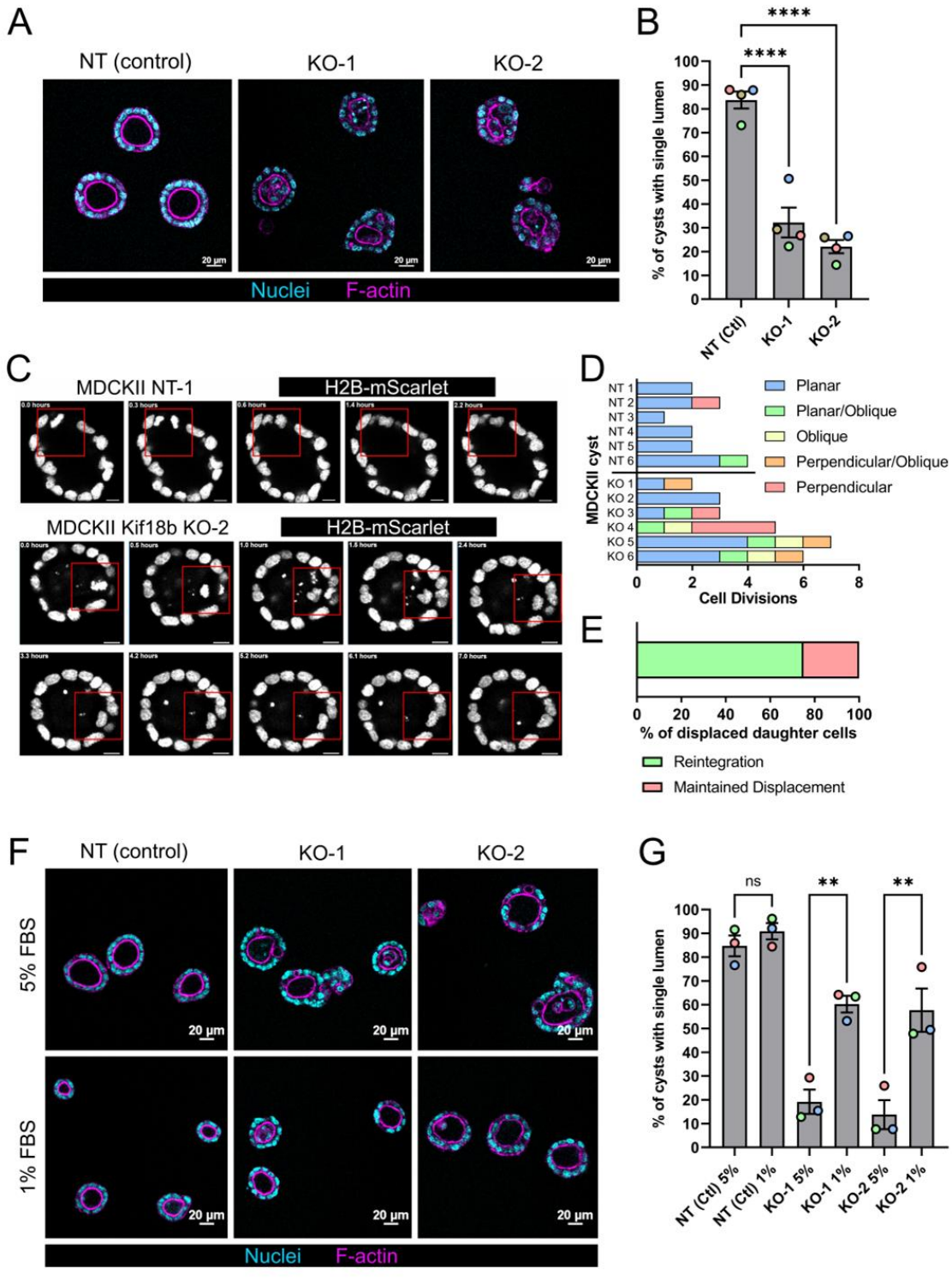


**Figure 3.2 MDCKII epithelial architecture disruption after misoriented division is prevented by slowing of division rate, allowing reintegration**

**A.** MDCKII NT control or Kif18b KO cells grown as cysts for 7 days and stained for F-actin (phalloidin) and DNA (Hoechst). Scale = 20um. **B.** Quantification of single lumen formation in cysts with Kif18b knockout or control (NT). Lumen is defined by apical F-actin staining. N=4 experiments,

>40cysts/sample/exp. One-way ANOVA. (****)p< 0.0001. **C.** Live imaging of MDCKII cysts expressing H2B-mScarlet with Kif18b KO or control (NT) showing division orientation. **D.** Quantification of division orientation in MDCKII cysts based on H2B-mScarlet chromatin segregation axis relative to the basal cell surface. 6 control and 6 KO cysts shown. **E.** Outcome of displaced daughter cells after misoriented division.
**F.** Kif18b knockout or control MDCKII cyst examples in 5% or 1% FBS at 7 days. Scale = 20um. **G.** Quantification of lumen formation in MDCKII NT control or Kif18b KO cysts at 7 days in 5% FBS or 1% FBS. N=3 experiments, >40cysts/sample/exp. One-way ANOVA. (ns)p= 0.798, (**)p< 0.01.

### 3.3.3 Misoriented cell division through Kif18b loss does not affect mammary epithelial organization during development or maintenance

To test if misoriented division affects the morphogenesis or homeostasis of primary epithelia *in vivo*, we sought to ablate Kif18b in the mouse mammary gland. Cells were isolated from adult mammary fat pads, transduced them with lentivirus to introduce Cas9, mCherry, and non-targeting control or Kif18b gRNA, and transplanted them into pre-pubertal recipient mice. This assay allows for the effects of misoriented division to be studied in the mammary gland since primary cells with loss of Kif18b divide with random orientation relative to the plane of the luminal layer. The cell isolation and transplant procedure is outlined in Fig. 3.3 A,B. The glandular outgrowths were examined after 8 weeks to determine if cells in the Kif18b knockout gland were still present and incorporated into normal mammary organization. Although only a few of the transplanted mice had outgrowth and the cells were interspersed with unlabeled cells, there were no observable differences between non-targeted control and Kif18b in the gross structural organization or relative frequency of transduced cells in the mammary glands (Fig. 3.3 C,D). Although inefficient, the proportion of mammary glands regenerated was not different between control and Kif18b gRNA transplanted cells. While these data are promising, further experiments are needed to verify this result in more mice and whole mount analysis of the outgrown glands should be performed to assess the degree of branching in these mutant mammary glands.

To overcome the inefficiencies of transplantation and regrowth, and to study the endogenous mammary gland, we adopted the use of a conditional Kif18b knockout mouse crossed with a Kerartin-8-promoter-driven CreER (Tamoxifen-dependent Cre recombinase activity) to ablate Kif18b in luminal cells in the mammary gland. We first used adult mice with intact mammary glands and administered Tamoxifen to induce

knockout of Kif18b and activate a Cre-dependent H2B-GFP to track knockout or control cells (homozygous or heterozygous Kif18b knockout mice, respectively; Fig. 3.3 E,F). Ten days after the last dose of Tamoxifen the mammary glands were analyzed, revealing a similar level of activation of H2B-GFP in both control and knockout Kif18b mice. The organization of the ductal/tubule monolayers was also intact in both samples, indicating that Kif18b is not required for normal mammary gland homeostasis at adulthood. This data suggests that any cell divisions that may have resulted in displaced daughter cells in the lumen may have been corrected by reintegration as seen previously in cultured luminal cells (Fig. 3.1 D-H). Further studies will be required to more clearly elucidate the role of oriented cell divisions on normal mammary gland development, although the data suggests that oriented cell division is dispensable for mammary gland development due to reintegration. This conclusion is supported by the observation that almost 30% of cells in the normal mammary gland monolayer divide with non-planar orientation, yet hardly any cells can be observed within the ducts [81].

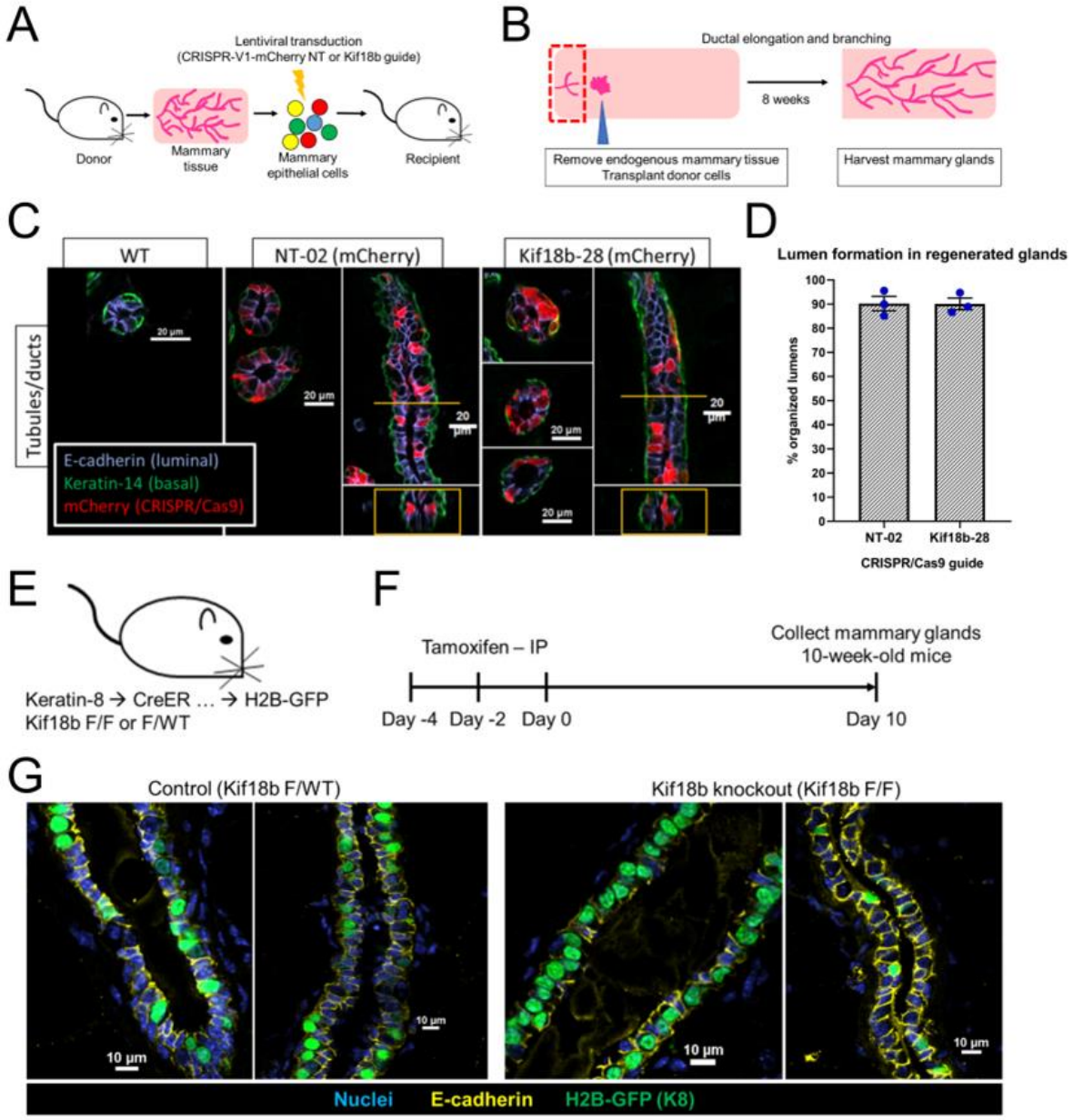


**Figure 3.3 Misoriented cell division through Kif18b loss does not affect mammary epithelial organization during development or maintenance**

**A.** Approach to ablate Kif18b in primary mammary epithelial cells. Isolated cells from WT tissue were transduced with lentivirus to introduce Cas9 and gRNA (NT or Kif18b), before being transplanted into recipient mice. **B.** Outline of transplantation procedure. Endogenous mammary tissue fills only a fraction of the fat pad at onset of puberty in mice (3-4 weeks old). This portion of the mammary gland is removed, and donor cells are engrafted into the remaining fat pad. Through pubertal development, branching morphogenesis occurs in the transplanted mammary epithelial cells. **C.** Analysis of regenerated glands with Kif18b ablation vs. control (NT). Sections are stained with E-cadherin (luminal cells), Keratin-14 (basal cells), and express mCherry along with the Cas9 &gRNA. **D.** Mammary tubules formed from cells with Kif18b ablation contain hollow lumens at similar levels compared to NT control tubules. N=1 regenerated mouse, 3 different regions analyzed. **E.** Mouse model with conditional knockout of Kif18b locus dependent on Keratin-8-driven Cre recombinase with modified estrogen receptor (CreER) that

activates Cre only in the presence of Tamoxifen (estrogen analog). This mouse also expresses a Cre-dependent Histone H2B-GFP so cells with active Cre and Kif28b ablation can be tracked. (Kif18b F/F = 2 Kif18b loci with flanking loxp sites to excise a portion of the Kif18b gene resulting in null expression). **F.** Tamoxifen injection scheme for determining if Kif18 loss alters epithelial cell organization in adult mammary glands. 8 week old mice were subject to intraperitoneal (IP) injection of Tamoxifen then analyzed 10 days after last injection by tissue sectioning and immunofluorescence staining. **G.** Mammary glands from Kif18b-ablated or control (heterozygous) mice showing normal duct and tubule architectures.

### 3.3.4 Transformed cells do not require division misorientation to multilayer

The extent to which misoriented cell division drives the process of multilayering seen in most early tumors, is unknown. Other factors may also contribute to the progressive loss of epithelial organization. To determine if misoriented division in transformed cells induces multilayering we used 2 transformed cell models – Pten knockout or polyomavirus middle T antigen expression (PyMT) – as well as Kif18b knockout which we have demonstrated results in misoriented divisions in epithelia. We confirmed both models induced expression of the downstream signal transducer Akt as determined by phosphorylation of S473 (Fig. S3.4A,B). In agreement with previous studies, Pten loss or PyMT expression induces multilayering [119, 180]. This is in contrast with loss of Kif18b, which does not induce multilayering (Fig. 3.4A,B). It is possible that as the monolayer becomes dense, reintegration may become unfavorable to cells that have been displaced after division and therefore, contribute to multilayering. We next performed live imaging to determine if division is occurring in a misoriented fashion in Pten KO or PyMT Eph4 cells. Interestingly, we find no significant difference in the mean division angle with respect to the substrate in Pten KO or PyMT-expressing cells, while Kif18b KO cells display misoriented division. This is suggestive of a different mechanism than misoriented division at play for multilayering, but we cannot rule out the possibility that infrequent oblique or perpendicular divisions sometimes seen in transformed cells do induce the multilayering seen.

To determine how cells multilayer, we again used live imaging to track nuclei as they rise above the height of the monolayer. Because of the greatest degree of multilayering seen, we chose to look at monolayers of cells expressing PyMT as they initiate multilayering (Fig. 3.4 E-G). Interestingly, most cells that rise above the

monolayer do so without themselves undergoing division but as a result of neighboring cells dividing or moving into the ejected cell area (Fig. 3.4F,G). This suggests cells may be pushed out of the monolayer. Surrounding cells continue to divide even at a high density as they also express PyMT. This does not rule out that cells actively crawl out of the monolayer but the high density at which multilayering is seen, suggests loss of organization is due to monolayer crowding. This would also explain why cells that are displaced do not reintegrate as opposed to Kif18b KO cells.

To test if transformed cell displacement may be corrected if not for monolayer density, we first sought to determine if transformed cells atop the monolayer are capable of integrating into a wildtype monolayer. We used a previously characterized *in vitro* integration assay we developed to study intercalation of mammary epithelial cells (see Chapter 2, methods for details). We have observed previously that intercalation is inhibited at high densities, which may support multilayering instead of reintegration of transformed cells. Monolayers of mApple-labeled wildtype Eph4 cells were seeded at the same confluent densities, then equal numbers of either NT control, Kif18b KO, Pten KO, GFP control, or GFP PyMT cells were added to the monolayers to facilitate integration (Fig. 3.4H). After 24h, the integration efficiency was determined by quantifying the total area displaced in the monolayer, indicating areas where cells had integrated (Fig. S3.4 C,D). Confocal imaging revealed cells made attachment with the basal substrate and neighboring wildtype cells, and rearranged their actin network such that it resembled non-transformed cell architecture (Fig. 3.4I). Strikingly, the previously multilayering transformed cells were able to integrate into a normal monolayer with similar efficiency to control cells over a short period of time. This brief reversion to relatively normal morphology suggests that the multilayering of these cells is dependent on the state of the epithelial layer and that while divisions are required to reach a critical density where cells multilayer, the orientation of the divisions has little effect on the rate of multilayering.

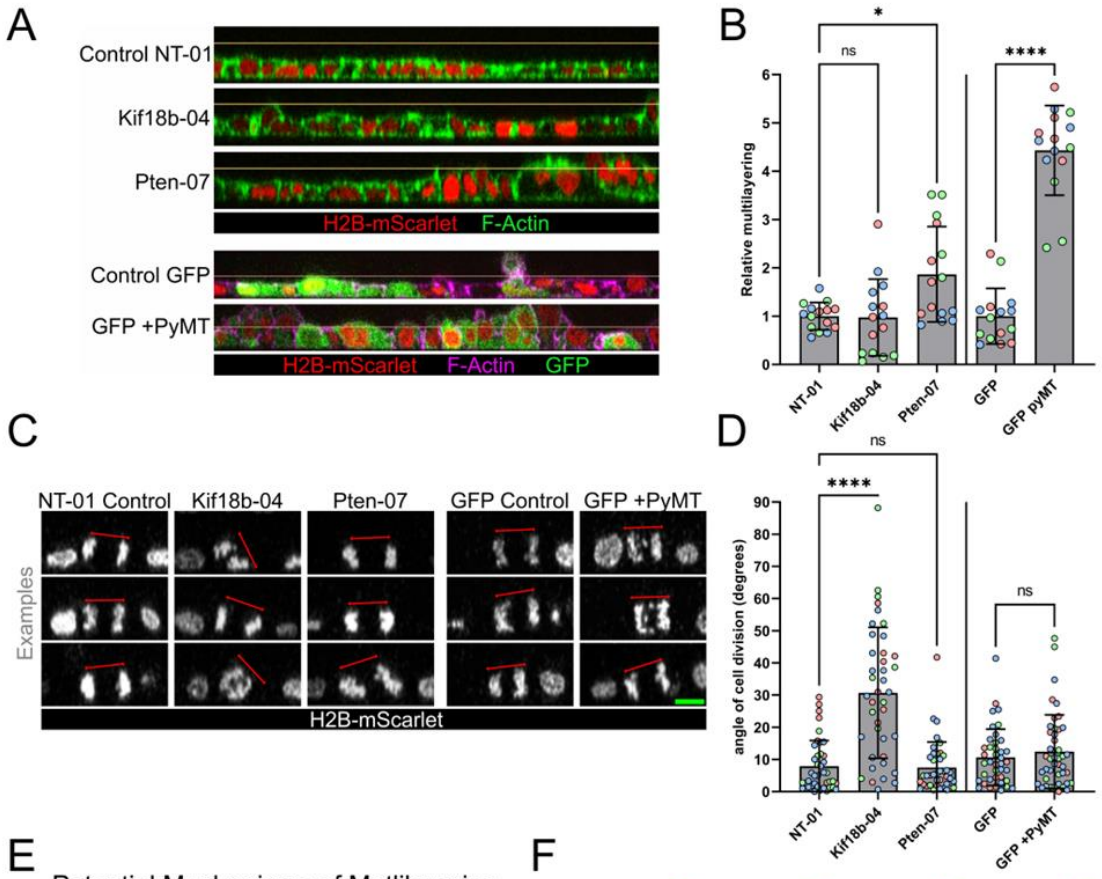
A
Control NT-01
Kif18b-04
Pten-07
H2B-mScarlet F-Actin
Control GFP
GFP +PyMT
H2B-mScarlet F-Actin GFP
B
Relative multilayering
ns
*
****
NT-01
Kif18b-04
Pten-07
GFP
GFP pyMT
C
NT-01 Control
Kif18b-04
Pten-07
GFP Control
GFP +PyMT
Examples
H2B-mScarlet
D
angle of cell division (degrees)
ns
****
ns
NT-01
Kif18b-04
Pten-07
GFP
GFP +PyMT
E
Potential Mechanisms of Mutlilayering
Misoriented Division
Other
(Non-misoriented div.)
F
PyMT
0m
25m
50m
75m
100m
125m
150m
175m
H2B-mScarlet
G
0
20
40
60
80
100
% of multilayering cells
Misoriented division
Other (Non-misoriented division)
H
Cell Suspension
(CFSE/GFP)
Confluent
Monolayer
(mApple)
I
NT-01
Kif18b-04
Pten-07
GFP
GFP +PyMT
Nuclei
mApple (monolayer)
F-actin
GFP (+/-pyMT)

**Figure 3.4 Transformed cells do not require division misorientation to multilayer**
**A.** Multilayering analysis in Eph4 cells with CRISPR/Cas9 ablation of Kif18b (Kif18b-04 gRNA), Pten (Pten-07 gRNA), or control (NT, non-targeting gRNA). As well as, cells expressing GFP control or GFP and Polyomavirus middle T antigen (PyMT). Eph4 cells express H2B-mScarlet to track nuclei multilayering. Orthogonal views of monolayer cultures 3 days after confluency are shown. **B.** Quantification of multilayering seen in A. as a percentage of total cells that are above the monolayer nuclei distance. N=3 experiments. One-way ANOVA. (ns)$p>0.05$, (*)$p<0.05$, (****)$p<0.0001$. **C.** Cell division orientation in monolayers of Eph4 cells expressing H2B-mScarlet. Division orientation in cells at chromatin segregation during mitosis highlighted by red arrow. (3 examples shown for each). **D.** Angle of cell division as seen in C. relative to the basal axis, parallel with the monolayer. N=3 experiments. One-way ANOVA. (****)$p<0.0001$, (ns)$p>0.05$. **E.** Diagram showing misoriented division-dependent, or -independent potential mechanisms which cells may use to multilayer. **F.** Example live imaging of an orthogonal plane of a monolayer of Eph4 cells expressing PyMT and H2B-mScarlet. Cell highlighted (star) can be seen rising above the monolayer over time without dividing. Scale = 10um. **G.** Proportion of sustained multilayering events quantified from monolayers of PyMT cells based on live imaging (as in F.). These events were characterized into either extrusion/compaction or misoriented division. N = 12 multilayering events. **H.** Outline of integration assay. Unlabeled Eph4 cells (NT-01, Kif18b-04, Pten-07, GFP, or GFP +PyMT) were added to confluent monolayers of mApple-labeled Eph4 cells at the same monolayer density. Cells were allowed to integrate into the existing monolayer over the course of 24 hours. **I.** Example images of cells that had integrated after 24h. All cells had similar integration efficiencies as measured by total area within the monolayer (Fig S4). Scale =10um.

## 3.4 Discussion

In this study we used ablation of Kif18b, a regulator of astral microtubule depolymerization, expressed mostly during mitosis, to randomize mitotic spindle orientation and cause misoriented division and displacement of daughter cells from the planar epithelial sheet. Using this approach and live imaging, we found that mammary epithelial cells unexpectedly reintegrate after displacement to preserve epithelial organization. This process of reintegration acts as a buffer against dysplasia, after spindle orientation fails. Reintegration has been observed in the *Drosophila* follicular epithelium and in some mammalian epithelia during development [123, 127, 168].

The role of cell division orientation in epithelial homeostasis has remained shrouded in mystery. Its immediate control over daughter cell location after division, the number of proteins regulating the process, and its misalignment in many patient tumors and mouse models all suggest that it plays a critical role in maintaining epithelial organization [41, 118, 158]. While misoriented division is observed after perturbing many cellular systems such as cell polarity, cell-cell junctions, cell-matrix junctions, the cytoskeleton, and other pathways that may incorporate into the mitotic spindle positioning regulatory network, there may also be confounding effects besides that of misoriented division that contribute to defective epithelial morphogenesis.

Future experiments should incorporate mixed populations as it more accurately describes the environment for a transformed cell soon after mutation. Other studies point to extrusion as a pivotal player in extrusion of the transformed cell, and the necessity for wildtype surrounding cells in this process [120, 181, 182]. Several studies also point to the potential for oriented divisions regulating tissue formation, however other signaling pathways may also be disrupted in these models [126, 183, 184]. Careful delineation of the subtle mutant phenotypes in polycystic kidney disease models has led to a shift away from a hypothesis that loss of oriented cell division as the sole contributor to cyst formation, to one that incorporates perturbations in many signaling pathways such as the primary cilia and planar cell polarity [185-187]. In mammary cell cultures loss of oriented cell division is also seen alongside defects in epithelial

organization, but it is unknown what contribution division misorientation plays in this phenotype [188].

Using two models of transformed cells, Pten KO and PyMT-expression, we show misoriented division is dispensable for forming multilayered regions in epithelium in culture. Live imaging using PyMT cells suggests most multilayering events arise from individual cells protruding out of the monolayer as neighboring cells crowd the area. Interestingly, while normal cells or cells with Kif18b KO alone can reintegrate, these transformed monolayers do not rearrange displaced cells and continue to multilayer. It is possible that the cell monolayer beneath the multilayered cells becomes too dense to allow for reintegration, but future studies will have to directly test this. We tested the capability for Pten KO or PyMT-expressing cell to integrate into an existing monolayer with a set density lower than that at the time of multilayering. As shown previously, both control (wildtype) and Kif18b KO cells are able to integrate into an existing monolayer. Surprisingly, we find the transformed cells are also capable of integration at least for a brief period, further demonstrating it is the local context the cell is in which determines the capacity for the cell to multilayer.

## 3.5 Methods

Animals

The Vanderbilt Division of Animal Care (DAC) ensures that all mice within the Vanderbilt facility are monitored daily for health status. DAC also ensures the overall welfare of the mice, and provides daily husbandry that includes environmental enrichment, clinical care, protocol record keeping, building operations, and security. The Vanderbilt mouse facility has three experienced Animal Care Technicians who attend to the daily needs of the animals. DAC ensures that all federal, state, and university guidelines for the care and use of animals are understood and maintained. Mice were housed with a standard 12 hrs light/12 hrs dark cycle. Mice were provided normal laboratory chow and water. All mouse experiments were performed with approval from the Vanderbilt Institutional Animal Care and Use Committee. Tamoxifen was administered in sunflower seed oil at

mg/kg via intraperitoneal injection every other day for 6 days. Mammary glands were harvested 10days after last dose. Female C3H/HeJ mice aged 8 wks or older were used as donor and recipient for intraductal transplantation experiments. For surgeries, mice were anesthetized using Avertin solution before injecting 50K transduced cells into cleared mammary fat pads.

Plasmid construction and lentivirus production

The sgRNAs used in this study are listed in the Resources Table. gRNAs were designed using CHOPCHOP. sgRNAs were cloned into lentiCRISPR v1 or v2 vector at the BsmBI restriction site using Zhang lab protocol (Shalem et al., 2014; Sanjana et al., 2014). pLVTHM-mApple was generated as described in Ahmed et al., 2017. pLVTHM-Venus was generated as described in McCaffrey et al. [154]. pWPI-H2B-mScarlet was generated through BmgBI and BamHI restriction sites into pWPI-mcs-mScarlet. pCW-GFP-P2A-PyMT was cloned from pCW-GFP (Addgene #162823) by PCR of PyMT fragment and P2A site, then inserted into pCW-GFP using BsrGI and BamHI.

293T cells were cultured in DMEM, 10% FBS, and 100U/mL Penicillin and Streptomyocin. To produce lentivirus, 293T cells were transfected with packaging plasmids psPax2 and pMDG2-VSVG along with the desired plasmid to be packaged in the lentiviral genome. This was done using calcium phosphate transfection. Medium was changed after 18 hrs and virus-containing media was collected after 36 hrs. In some cases, virus-medium was concentrated using Amicon 100k centrifugal filters.

In vitro intercalation assay

Eph4 cells were cultured in DMEM, 10% FBS (fetal bovine serum), and 100U/mL Penicillin & Streptomyocin. For intercalation assay, 150x10^3 single cells were plated onto 8-well chambered coverglasses. After 24 hrs, other cells were then dissociated to single cells with Trypsin and washed before being added to the previously plated monolayers. Integration of the intercalated cells into the monolayer was then determined by imaging the area displaced in the monolayer after 24 hrs. In all assays where area was determined, monolayer cells expressed a fluorescent marker.

Thresholding was used to determine the area where monolayer signal was displaced, and the total area of integration was summed. Figures include example images of the monolayer fluorescence, masks of the determined area of integration, and normalized area of integration quantifications. For many experiments, co-stain with either Hoechst or differentially labeled cell populations were used to ensure areas where monolayer cells were displaced were indeed intercalated cells.

Mammary cyst formation assay

Cells were isolated as described previously [142]. Briefly, inguinal mouse mammary glands (4th pair) were isolated from 12 wk old C3H mice, then minced and digested in collagenase for 1 hour shaking at 37 $^{O}$C. Enrichment for epithelial tissue pieces was performed by serial centrifugation pulses, and then digested in Trypsin 0.25% for 15min at 37 $^{O}$C. MECs were then transduced with lentivirus to introduce Cas9 &gRNA, cultured in mammosphere media for 1 week, selected using 4ug/mL puromycin, then digested in Trypsin 0.25% for 15min at 37 $^{O}$C to isolate single cells. Cells were plated in Matrigel (extracellular matrix) with media consisting of DMEM/F12 (1:1), and 1x ITS – replenished daily. Cysts were fixed in 4% PFA at day 13.

MDCKII cyst formation

MDCKII cells were subcultured in DMEM with 10%FBS and 100U/mL Penicillin and Streptomyocin. To form cysts, MDCKII cells were trypsinized (0.25%) and strained to obtain single cells. Single cells were then plated on thinly Matrigel coated 8well-chambered coverglass at 2500cells per well. Cells were cultured in MEM with 5% or 1% FBS, and 2% Matrigel.

Immunostaining

Cells and cysts were fixed with 4% paraformaldehyde (PFA) for 10 min, or overnight for tissue. Tissue was then placed in 30% sucrose solution for at least 24 hrs until embedding and cryo-sectioning. Samples (cells and tissue) were blocked and permeabilized with 5% normal goat serum in PBS with 0.2% TritonX-100. Primary or secondary antibodies were incubated for 1 hr with cells or overnight at 4$^{O}$C for tissue

sections and organoids. Hoechst or phalloidin stains were added during secondary antibody incubation. Slides were mounted with Fluoromount-G.

Confocal microscopy and image processing

All imaging was performed using a Nikon A1R scanning confocal microscope and analysis was done with Nikon Elements software. Live cell imaging was performed in a TOCRIS chamber at 37 $^{O}$C with 5% $CO_2$. Imaging was performed at intervals as specified per experiment. Generally, intervals for long term experiments were 10-20 min. Confocal images were collected with z-steps ranging from 1.5μm for intercalation assay field analysis or 0.5-1μm step for higher magnification analysis. Objectives used: 20x, 40x, 60x. Maximum intensity projections (IP) were created for display of intercalation assay field analysis and for other staining experiments.

Statistical analysis

Statistical tests performed are described in the figure legends for each graph with comparisons. In general, unpaired t-test, paired t-test, one-way ANOVA, and Fisher's exact test were performed in GraphPad Prism. Graphs shown also indicate error bar definitions in figure legends (SD, SEM, etc.). p values are listed in figure legends for all comparisons shown on each graph.

## 3.6 Supplemental Data

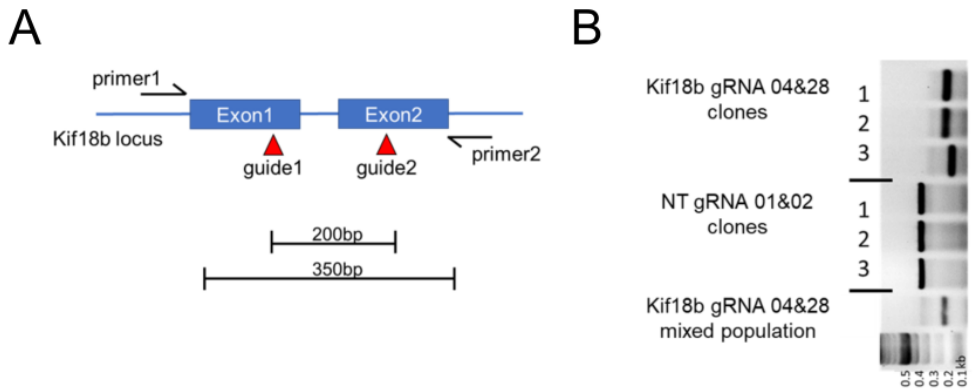


**Figure S3.1 Kif18b ablation in Eph4 cells**
**A.** Strategy for verification of Kif18b locus targeting with gRNA and Cas9. **B.** PCR genotyping of Kif18b locus.

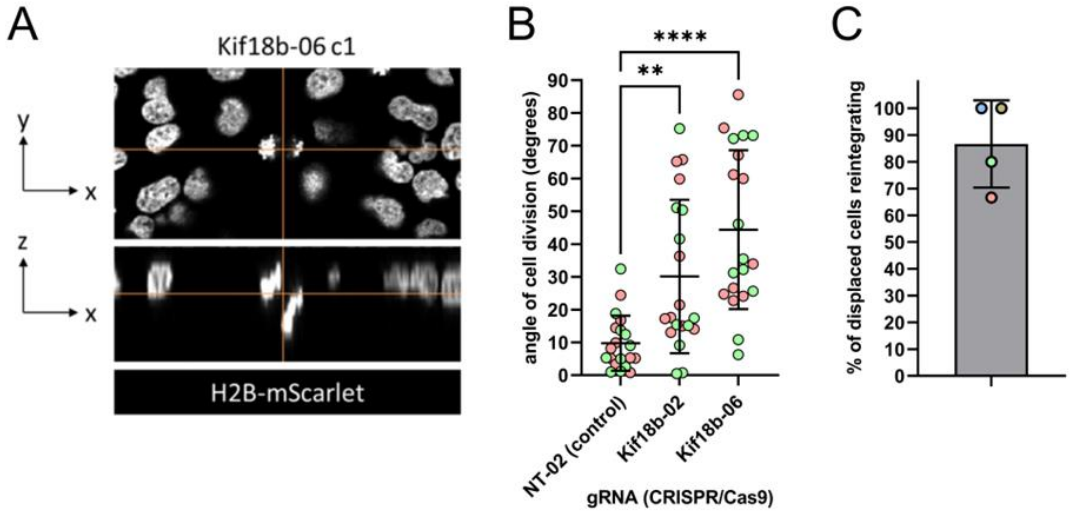


**Figure S3.2 Kif18b loss in MDCKII cells causes misoriented cell divisions**
**A.** Example cell division in Kif18b KO MDCKII cell in 2D. **B.** Quantification of division orientation in MDCKII clones. 2 NT control clones shown (NT-01 gRNA) and 4 Kif18b KO clones (Kif18b-02 or -06 gRNA). **C.** Percentage of cells with division angle greater than 45deg reintegrating into the monolayer as determined by nuclei height. 4 Kif18b KO clones.

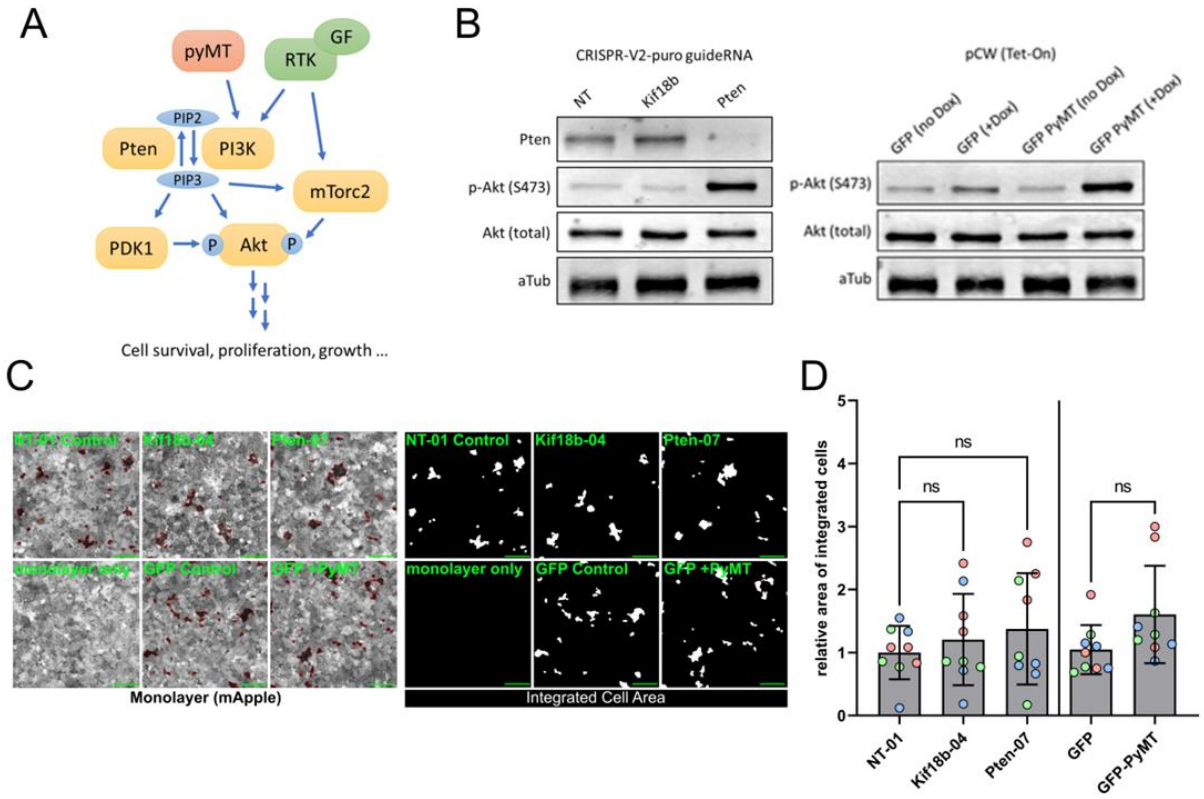


**Figure S3.3 Pten knockout and PyMT-expressing cells hyper-activate Akt but integrate into wildtype monolayers with similar efficiency to control cells**
**A.** Pathways describing activation of Akt by either loss of Pten or PyMT expression. **B.** Western blot for Pten and Akt activation (phosphorylation of S473). No changes seen in Kif18b gRNA sample. **C.** Cellular integration into a wildtype monolayer. Cells were added to monolayers and analyzed after 24h. Example field of mApple+ monolayers (left) with areas displaced by unlabeled intercalating cells shown (right) as inverse binary masks. Scale: 100um. **D.** Relative area of integrated cells from C. One-way ANOVA. Mean +/- SD, n = 3 experiments, (ns)p > 0.05.

# Chapter 4: Discussion and Future Experiments

## 4.1 Epithelial Intercalation in Mammary Gland Formation

The cellular processes that shape epithelial tissues are critical to understand for insight into the formation of organs and to understand how these processes go awry in disease states. In my work studying mammary gland development and early tumor formation, I have explored several processes that help to control the organization of epithelial cells. In chapter 2, I found the cells within the TEB must contribute to the elongating ductal epithelium and that this process requires junction and cytoskeletal contributions to achieve this. Quantitative measurements of a model of intercalation revealed the tight junction organizing protein ZO-1 was required for efficient monolayer integration, and for intercalation of cells *in vivo*, as determined by intraductal transplantation. The actin-myosin cytoskeletal system was also required for intercalation in culture. The mechanisms by which the cells in the TEB rearrange, if at all, were previously under-explored. The prevailing theory in lumen clearance for duct generation was that apoptosis removed interior TEB cells. I have shown using mathematical modeling, the contribution of interior cells to elongation of the duct significantly outweighs the contribution of cells from the exterior TEB. In this model, cells are cleared from the multilayered regions and contribute to the duct, in a concerted effort that converts a disorganized region (TEB) into an extending monolayer (duct). I then developed a quantitative cell culture model to study the process of intercalation. While intercalation had previously been shown using organoid models, this approach is difficult to quantify differential perturbation of the surrounding cells remains challenging [15]. Interestingly, although ZO-1 loss did not impair monolayer growth from sparse subculturing, the loss of ZO-1 in intercalating cells prevented intercalation, suggesting the integration of cells requires the tight junction incorporation first.

I have also shown that impairing either branching actin formation or myosin activity severely inhibits intercalation. This may be mostly through defects in the ability to establish new cell-cell junctions at the interface, a critical step if a cell is to integrate into an existing monolayer. Other studies have also shown that expansion of a new

linear junction requires actin-myosin coordination [146, 148, 149]. It is likely that ZO-1 binding to and stably recruiting F-actin at the interface, as well as the organization of the new junctional plaque, is necessary for intercalation. Future experiments should be designed to investigate the necessity of the F-actin binding domain of ZO-1 in intercalation. ZO-1 is a large protein and many domains may be required for its activity in intercalation [189]. Expressing ZO-1 truncation mutants in ZO-1 null cell and testing their capacity to rescue intercalation would determine which domains and protein interactions are necessary for this process and may expand the understanding of ZO-1-dependent intercalation. Further future experiments probing other cytoskeletal components such as microtubules may be of use. Microtubules have been shown to be important in intercalation in Xenopus ectoderm development, and in supporting proper polarization of mammary epithelial cells [32, 190]. Loss of proper microtubule polarization within multilayered cells may prevent directed migration. The microtubule depolymerizing drug Nocodazole could be used to determine if loss of microtubules prevent intercalation.

One area in need of further elucidation is how the epithelial apical surface that is generated can expand during intercalation. In this process, the incoming cell must push the monolayer cells away to make space within the monolayer. The actin cytoskeleton is likely important in generating the downward force required to insert the intercalating cells, but the initial expansion of the new junctional interface must rely on some expansive process to accommodate a cell into the monolayer. Studies using Xenopus ectoderm development show intercalating multiciliated cells (MCC) expand a newly generated apical surface through formin-dependent expansion at the apical perijunctional ring, and not from pulling forces within the monolayer [191]. Future experiments should delineate if this mechanism also occurs during mammary cell intercalation. Interestingly, MCC intercalation occurs in a basal to apical direction and the intercalation assay described here shows mammary epithelial cells may intercalate in an apical to basal direction. Due to this difference, the mechanisms controlling intercalation in each system may differ.

The forces regulating 3D epithelial rearrangements such as in intercalation are challenging to delineate. I showed that disruption of the actin-myosin network causes defects in intercalation using small molecule inhibitors of either Arp2/3 complex or Myosin contraction. In using pharmacological approaches during the intercalation assay, both the monolayer and integrating cells are affected, making it challenging to draw conclusions on inhibition in intercalating vs. monolayer cells. One approach to begin to further elucidate how contractility affects intercalation is to use genetic tools that are able to be switched on or off. I have performed preliminary experiments using such tools suggesting there may be a cell type-specific effect of contractility during intercalation. Myosin light chain kinase (MLCK) phosphorylates myosin light chain and promotes contraction. Monolayers of cells expressing an inducible constitutively active Myosin light chain kinase (CA-MLCK) were activated with doxycycline for 18 hours and then wildtype cells were added. Monolayers with phosphorylated S19 Myosin control staining can be seen in Fig. 1A. Hypercontractility in the monolayer prevented intercalation of normal cells (Fig. 1B-D). This suggests the monolayer contractility is an important determinant for efficient integration likely due to the inability of cells to displace existing cells in the monolayer and for the intercalating cell protrusions to reach the basal side. If the converse experiment is done where intercalating cells now are hypercontractile, there is a slight decrease in intercalation (Fig. 1E-G). Overall, either inhibition or overactivation of Myosin II reduces intercalation capacity, suggesting properly regulated levels of contractility in both intercalating cells and monolayers is a determining factor for integration. Development of an inducible, constitutively active myosin phosphatase (MYPT) would help determine how loss or reduction in contractility affects intercalation.

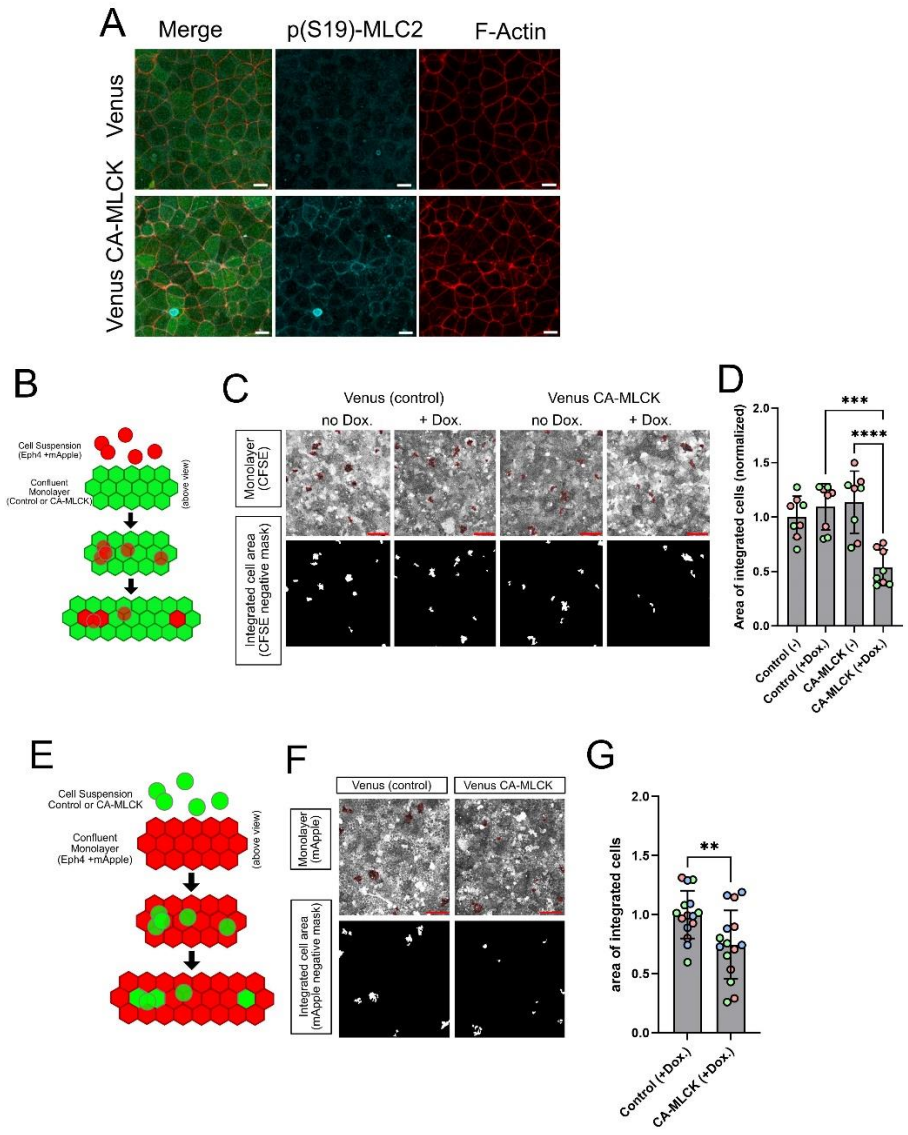


**Figure 4.1 Contractility regulates intercalation**
**A.** Eph4 monolayers expressing Dox-inducible Venus + constitutively active Myosin light chain kinase (CA-MLCK) or Venus alone and treated with Doxycycline (1ug/mL) to induce expression. Staining for F-actin and phosphorylated S19 Myosin light chain 2 after 18 h of Dox. treatment. Scale bar = 10um. **B.** Intercalation assay setup for C.: Control (Venus only) or CA-MLCK (+Venus) monolayer and control (mApple) intercalating cells added. **C.** Examples of intercalated cells and negative binary mask. Scale: 50um. **D.** Quantification of normalized areas of intercalated cells. 2 experiments. Mean +/-SD. One-way ANOVA, ***p = 0.0001, ****p < 0.0001. **E.** Schematic of intercalation assay for F.: control monolayer (mApple+) and added intercalating cells (Venus+). **F.** Examples of intercalated cells and negative binary mask. Scale: 50um. **G.** Quantification of areas of intercalated cells, from 3 experiments. Unpaired T-test, Mean +/-SD, p = 0.0093.

## 4.2 Oriented Cell Division

The role of oriented cell division in epithelial morphogenesis, homeostasis, and tumorigenesis has also been shrouded in mystery [118, 119, 124, 155-158, 192]. Experimental approaches have been limited to test the effects of misorienting the division axis in vertebrate epithelial cells. *Drosophila* as a model system has led the way in determining the effects of loss of OCD on tissue formation, probably due to the ease of targeting essential spindle orienting proteins such as NuMA (mud) without detriment to other cellular processes, whereas NuMA loss in vertebrate cells not only interferes with mitotic spindle dynamics, but also nuclear assembly and is detrimental to cell health [193, 194]. Other components of the spindle machinery may express multiple related proteins that compensate for loss of another. I took the approach of knocking out Kif18b, a microtubule depolymerizing factor present during mitosis. With this approach, I was able to see severe division misorientation and, strikingly, no effect on monolayer organization as the cells displaced by misoriented division reintegrate into the monolayer in a process resembling intercalation as characterized previously. This reintegration or intercalation of vertebrate epithelial cells has been observed previously in developing epithelial tissues such as the lung, kidney, and mammary gland as described in chapter 2 [15, 123, 168]. While the result that cells displaced atop a monolayer integrate into it has been described in chapter 2, it was previously unknown whether mature epithelial cells, particularly in the mammary gland, were capable of this process.

I find that reintegration after misoriented division rescues normal epithelial architecture and lumen formation in several 2D and 3D culture models. One interesting 3D model is MDCKII cyst formation. Several studies have detailed the use of this model to study the role of division axis orientation and lumen formation [41, 56, 164, 177-179]. When grown in high (normal) serum media, I also observed most Kif18b KO cysts displayed multiple lumen, but when switched to low serum media so proliferation was slowed, the rate of single lumen formation was rescued in Kif18b KO cysts. This suggests reintegration, as seen in live imaging of single lumen Kif18b KO cysts, can support proper epithelium maintenance at low enough division rate. What's more

interesting is that primary mammary epithelial cells grown in 3D with loss of Kif18b do not display lumen formation defects because of reintegration. Kif18b KO mammary glands also appear totally normal, suggesting oriented cell division is dispensable for luminal cells during mammary development and maintenance.

A recent study characterized loss of ZO-1 in the mouse intestine and found that misoriented cell divisions contributed to the observed epithelial dysplasia [195]. This ZO-1 KO-dependent misoriented division phenotype was also replicated in MDCKII cyst formation and inhibited lumen formation [196]. Interestingly, I do not find loss of ZO-1 alone promotes multilayering in our Eph4 2D model although loss of ZO-1 does prevent reintegration of displaced cells. One would think we would then see multilayering in this system if misoriented divisions occur as suggested with ZO-1 loss. Its likely that ZO-1 null Eph4 cells divide in planar orientation. This suggests the mechanism of reintegration in Kif18b KO epithelial cells is likely ZO-1-dependent since they also have intact ZO-1 and are able to reintegrate. Tissue differences may necessitate different mechanisms and consequences for oriented division and reintegration as has been seen in *Drosophila* studies [127, 167, 197]. This raises the question of whether the reintegration observed after misoriented division uses the same mechanism as mammary cell intercalation as characterized in chapter 2. Experiments combining both ZO-1 KO and Kif18b KO would answer this question. I anticipate loss of ZO-1 and oriented cell division will result in multilayering.

While I show loss of oriented cell division (by Kif18b KO) does not affect normal mammary gland epithelium formation, I did not observe the larger organization of branching in transplant regenerated mammary glands. It has been suggested that perpendicular divisions and tubular accumulation of luminal cells play a role in mammary side branching during pubertal morphogenesis [28, 122, 198]. Kif18b KO in luminal mammary cells during branching morphogenesis seems like an ideal model to test this hypothesis since more cells will likely be dividing in a perpendicular fashion, therefore inducing greater side branching if the hypothesis is correct. This can be observed by analyzing a whole mounted mouse mammary gland after pubertal development with Kif18b KO. It has also been suggested that mammary stem cells located at the cap of the TEB divide in a symmetric or asymmetric fashion and then self-

renew or differentiate, respectively [125, 199, 200]. This form of oriented division has been shown to be important in development of other tissues [31, 64]. Using a promoter that is specific to mammary cap cells could enable Cre recombinase activity to ablate Kif18b in mammary stem cells to determine how the stem cells in the cap respond to loss of division alignment.

An outstanding question in the field of cancer cell biology is how early tumors are formed. Epithelium is relatively rigid and constrained and how this organization is broken is not well understood. It has been postulated that misoriented divisions drive multilayering in transformed cells and this process promotes the displacement of cells to disrupt normal epithelial architecture as seen in early tumors. In my live imaging experiments of transformed mouse epithelial cell lines, division orientation is unaffected yet cells still multilayer. A closer examination suggests mechanisms other than misoriented divisions cause multilayering. One area of future investigation is the mechanism by which cells are multilayered. Live imaging data suggests monolayer density builds up to a critical level before cells multilayer but uncontrolled proliferation in transformed cells complicates this interpretation. Future experiments may involve condensing similar density wildtype or transformed monolayers through release of a pre-applied stretch in order to determine over a very short time interval if density induces transformed cell multilayering independent of proliferation compared to control cells. Several factors may be at play in this process which must be accounted for in future experiments such as cell-cell and cell-matrix binding strength in transformed vs. control cells.

One key finding that suggests multilayering occurs at a high density is the observation that transformed cells will intercalate into normal (wildtype) monolayers at a confluent but lower density than is seen at the time of multilayering. These integrated cells display relatively normal epithelial morphology despite having oncogenic stimulation. This suggests that at least briefly, these transformed cells are able to behave much the same as normal cells, showing multilayering is context-dependent – likely meaning density of the surrounding cells is an important context. Other mechanisms of multilayering besides misoriented division include extrusion by surrounding monolayer cells, which has been observed in oncogenic-Ras-transformed

cells [120]. Neighbor cell context has also been shown to influence transformed cell growth in mammary acinar culture. Transformed cell neighbors with low p120, a critical adherens junction component, fail to displace transformed cells into the lumen, resulting in their more extensive proliferation [182].

While loss of oriented cell division alone does not perturb normal mammary epithelial organization, it would be interesting to determine whether combining a mild oncogenic stimulus with Kif18b KO to induce misoriented division, would result in quicker tumor generation time. The result from this experiment would help to rule out the possibility that loss of division orientation has any effect on the formation of primary tumors.

## 4.3 Concluding Remarks

While many questions remain unanswered about the processes controlling epithelial development and homeostasis in the mammary gland, there have been several key advances from the work presented in this dissertation. One key finding is that most of the cells within the TEB must contribute to the developing ductal monolayer, promoting its elongation and lumen clearance. The predominant theory in the field is that most cells in the interior TEB die to clear the lumen but this seems to only count for a small fraction of luminal clearance. To study this, a simple, modular, quantitative model of intercalation was developed, and it was found that ZO-1 is required for this process. Also shown is the ability for cells to intercalate in a ZO-1-dependent manner after intraductal transplantation. Another critical observation is that mammary epithelial cells are resistant to misalignment of normal planar cell division – which was previously hypothesized to be a key step in tumor formation. It was found that intercalation (and reintegration) is a pivotal cellular behavior of mammary epithelial cells that supports proper epithelial organization and acts as a defense against dysplasia induced by misoriented division.

## References


1. Alberts, B., et al., *Molecular biology of the cell*. Seventh edition ed. 2022, New York, NY: W. W. Norton & Company.
2. Dickinson, D.J., W.J. Nelson, and W.I. Weis, *A Polarized Epithelium Organized by β- and α-Catenin Predates Cadherin and Metazoan Origins.* Science, 2011. **331**(6022): p. 1336-1339.
3. Izumi, Y., et al., *An Atypical PKC Directly Associates and Colocalizes at the Epithelial Tight Junction with ASIP, a Mammalian Homologue of Caenorhabditis elegans Polarity Protein PAR-3.* Journal of Cell Biology, 1998. **143**(1): p. 95-106.
4. Kemphues, K.J., et al., *Identification of genes required for cytoplasmic localization in early C. elegans embryos.* Cell, 1988. **52**(3): p. 311-20.
5. Joberty, G., et al., *The cell-polarity protein Par6 links Par3 and atypical protein kinase C to Cdc42.* Nature Cell Biology, 2000. **2**(8): p. 531-539.
6. Lin, D., et al., *A mammalian PAR-3–PAR-6 complex implicated in Cdc42/Rac1 and aPKC signalling and cell polarity.* Nature Cell Biology, 2000. **2**(8): p. 540-547.
7. Rodriguez-Boulan, E. and I.G. Macara, *Organization and execution of the epithelial polarity programme.* Nature Reviews Molecular Cell Biology, 2014. **15**(4): p. 225-242.
8. Campanale, J.P., T.Y. Sun, and D.J. Montell, *Development and dynamics of cell polarity at a glance.* Journal of Cell Science, 2017. **130**(7): p. 1201-1207.
9. Larue, L., et al., *E-cadherin null mutant embryos fail to form a trophectoderm epithelium.* Proceedings of the National Academy of Sciences, 1994. **91**(17): p. 8263-8267.
10. Shamir, E.R., et al., *Twist1-induced dissemination preserves epithelial identity and requires E-cadherin.* Journal of Cell Biology, 2014. **204**(5): p. 839-856.
11. Martin, A.C. and B. Goldstein, *Apical constriction: themes and variations on a cellular mechanism driving morphogenesis.* Development, 2014. **141**(10): p. 1987-1998.
12. Daniel, C.W., P. Strickland, and Y. Friedmann, *Expression and functional role of E- and P-cadherins in mouse mammary ductal morphogenesis and growth.* Dev Biol, 1995. **169**(2): p. 511-9.
13. Kurley, S.J., et al., *p120-catenin is essential for terminal end bud function and mammary morphogenesis.* Development, 2012. **139**(10): p. 1754-1764.
14. Runswick, S.K., et al., *Desmosomal adhesion regulates epithelial morphogenesis and cell positioning.* Nature Cell Biology, 2001. **3**(9): p. 823-830.
15. Neumann, N.M., et al., *Coordination of Receptor Tyrosine Kinase Signaling and Interfacial Tension Dynamics Drives Radial Intercalation and Tube Elongation.* Developmental Cell, 2018. **45**(1): p. 67-82.e6.
16. Ewald, A.J., et al., *Mammary collective cell migration involves transient loss of epithelial features and individual cell migration within the epithelium.* J Cell Sci, 2012. **125**(Pt 11): p. 2638-54.
17. Guillot, C. and T. Lecuit, *Mechanics of epithelial tissue homeostasis and morphogenesis.* Science, 2013. **340**(6137): p. 1185-9.
18. Paine, I.S. and M.T. Lewis, *The Terminal End Bud: the Little Engine that Could.* J Mammary Gland Biol Neoplasia, 2017. **22**(2): p. 93-108.

19. Shamir, E.R. and A.J. Ewald, *Adhesion in mammary development: novel roles for E-cadherin in individual and collective cell migration.* Curr Top Dev Biol, 2015. **112**: p. 353-82.
20. Singhai, R., et al., *E-Cadherin as a diagnostic biomarker in breast cancer.* N Am J Med Sci, 2011. **3**(5): p. 227-33.
21. Moll, R., et al., *Differential loss of E-cadherin expression in infiltrating ductal and lobular breast carcinomas.* Am J Pathol, 1993. **143**(6): p. 1731-42.
22. Fischer, K.R., et al., *Epithelial-to-mesenchymal transition is not required for lung metastasis but contributes to chemoresistance.* Nature, 2015. **527**(7579): p. 472-6.
23. Padmanaban, V., et al., *E-cadherin is required for metastasis in multiple models of breast cancer.* Nature, 2019. **573**(7774): p. 439-444.
24. Gilcrease, M.Z., *Integrin signaling in epithelial cells.* Cancer Lett, 2007. **247**(1): p. 1-25.
25. Boudreau, N., et al., *Suppression of ICE and apoptosis in mammary epithelial cells by extracellular matrix.* Science, 1995. **267**(5199): p. 891-3.
26. Taddei, I., et al., *Integrins in mammary gland development and differentiation of mammary epithelium.* J Mammary Gland Biol Neoplasia, 2003. **8**(4): p. 383-94.
27. Reginato, M.J., et al., *Integrins and EGFR coordinately regulate the pro-apoptotic protein Bim to prevent anoikis.* Nat Cell Biol, 2003. **5**(8): p. 733-40.
28. Cellurale, C., et al., *Role of JNK in mammary gland development and breast cancer.* Cancer Res, 2012. **72**(2): p. 472-81.
29. Girnius, N. and R.J. Davis, *JNK Promotes Epithelial Cell Anoikis by Transcriptional and Post-translational Regulation of BH3-Only Proteins.* Cell Rep, 2017. **21**(7): p. 1910-1921.
30. Toyoshima, F. and E. Nishida, *Integrin-mediated adhesion orients the spindle parallel to the substratum in an EB1- and myosin X-dependent manner.* The EMBO Journal, 2007. **26**(6): p. 1487-1498.
31. Lechler, T. and E. Fuchs, *Asymmetric cell divisions promote stratification and differentiation of mammalian skin.* Nature, 2005. **437**(7056): p. 275-280.
32. Akhtar, N. and C.H. Streuli, *An integrin–ILK–microtubule network orients cell polarity and lumen formation in glandular epithelium.* Nature Cell Biology, 2013. **15**(1): p. 17-27.
33. Gudjonsson, T., et al., *Normal and tumor-derived myoepithelial cells differ in their ability to interact with luminal breast epithelial cells for polarity and basement membrane deposition.* Journal of Cell Science, 2002. **115**(1): p. 39-50.
34. Hsu, J.C. and K.M. Yamada, *Salivary gland branching morphogenesis--recent progress and future opportunities.* Int J Oral Sci, 2010. **2**(3): p. 117-26.
35. Wang, S., et al., *Budding epithelial morphogenesis driven by cell-matrix versus cell-cell adhesion.* Cell, 2021. **184**(14): p. 3702-3716.e30.
36. Nerger, B.A., et al., *Local accumulation of extracellular matrix regulates global morphogenetic patterning in the developing mammary gland.* Current Biology, 2021. **31**(9): p. 1903-1917.e6.
37. Conklin, M.W., et al., *Aligned collagen is a prognostic signature for survival in human breast carcinoma.* Am J Pathol, 2011. **178**(3): p. 1221-32.
38. Schedin, P. and P.J. Keely, *Mammary gland ECM remodeling, stiffness, and mechanosignaling in normal development and tumor progression.* Cold Spring Harb Perspect Biol, 2011. **3**(1): p. a003228.

39. Ilina, O., et al., *Cell–cell adhesion and 3D matrix confinement determine jamming transitions in breast cancer invasion.* Nature Cell Biology, 2020. **22**(9): p. 1103-1115.
40. Katsuno-Kambe, H., et al., *Collagen polarization promotes epithelial elongation by stimulating locoregional cell proliferation.* Elife, 2021. **10**.
41. di Pietro, F., A. Echard, and X. Morin, *Regulation of mitotic spindle orientation: an integrated view.* EMBO Rep, 2016. **17**(8): p. 1106-30.
42. Rappaport, R., *Experiments concerning the cleavage furrow in invertebrate eggs.* J Exp Zool, 1966. **161**(1): p. 1-8.
43. Hertwig, O., *Das Problem der Befruchtung und der Isotropie des Eies, eine Theorie der Vererbung*. Untersuchungen zur Morphologie und Physiologie der Zelle. 1884.
44. Hertwig, O., *Ueber den Werth der ersten Furchungszellen für die Organbildung des Embryo Experimentelle Studien am Frosch-und Tritonei.* Archiv für mikroskopische Anatomie, 1893. **42**(4): p. 662-807.
45. Minc, N., D. Burgess, and F. Chang, *Influence of cell geometry on division-plane positioning.* Cell, 2011. **144**(3): p. 414-26.
46. Bosveld, F., et al., *Epithelial tricellular junctions act as interphase cell shape sensors to orient mitosis.* Nature, 2016. **530**(7591): p. 495-498.
47. Finegan, T.M., et al., *Tissue tension and not interphase cell shape determines cell division orientation in the Drosophila follicular epithelium.* Embo j, 2019. **38**(3).
48. Fink, J., et al., *External forces control mitotic spindle positioning.* Nat Cell Biol, 2011. **13**(7): p. 771-8.
49. Campinho, P., et al., *Tension-oriented cell divisions limit anisotropic tissue tension in epithelial spreading during zebrafish epiboly.* Nat Cell Biol, 2013. **15**(12): p. 1405-14.
50. Fleming, E.S., et al., *Planar spindle orientation and asymmetric cytokinesis in the mouse small intestine.* J Histochem Cytochem, 2007. **55**(11): p. 1173-80.
51. Du, Q., P.T. Stukenberg, and I.G. Macara, *A mammalian Partner of inscuteable binds NuMA and regulates mitotic spindle organization.* Nature Cell Biology, 2001. **3**(12): p. 1069-1075.
52. Zheng, Z., et al., *LGN regulates mitotic spindle orientation during epithelial morphogenesis.* Journal of Cell Biology, 2010. **189**(2): p. 275-288.
53. Toyoshima, F. and E. Nishida, *Integrin-mediated adhesion orients the spindle parallel to the substratum in an EB1- and myosin X-dependent manner.* Embo j, 2007. **26**(6): p. 1487-98.
54. Haren, L. and A. Merdes, *Direct binding of NuMA to tubulin is mediated by a novel sequence motif in the tail domain that bundles and stabilizes microtubules.* Journal of Cell Science, 2002. **115**(9): p. 1815-1824.
55. Seldin, L., A. Muroyama, and T. Lechler, *NuMA-microtubule interactions are critical for spindle orientation and the morphogenesis of diverse epidermal structures.* eLife, 2016. **5**: p. e12504.
56. Hao, Y., et al., *Par3 Controls Epithelial Spindle Orientation by aPKC-Mediated Phosphorylation of Apical Pins.* Current Biology, 2010. **20**(20): p. 1809-1818.
57. Qin, Y., et al., *Tuba, a Cdc42 GEF, is required for polarized spindle orientation during epithelial cyst formation.* Journal of Cell Biology, 2010. **189**(4): p. 661-669.
58. Cerruti, B., et al., *Polarity, cell division, and out-of-equilibrium dynamics control the growth of epithelial structures.* Journal of Cell Biology, 2013. **203**(2): p. 359-372.

59. Guilgur, L.G., et al., *Drosophila aPKC is required for mitotic spindle orientation during symmetric division of epithelial cells.* Development, 2012. **139**(3): p. 503-513.
60. Peyre, E., et al., *A lateral belt of cortical LGN and NuMA guides mitotic spindle movements and planar division in neuroepithelial cells.* Journal of Cell Biology, 2011. **193**(1): p. 141-154.
61. Siegrist, S.E. and C.Q. Doe, *Microtubule-Induced Pins/Gαi Cortical Polarity in Drosophila Neuroblasts.* Cell, 2005. **123**(7): p. 1323-1335.
62. Saadaoui, M., et al., *Dlg1 controls planar spindle orientation in the neuroepithelium through direct interaction with LGN.* Journal of Cell Biology, 2014. **206**(6): p. 707-717.
63. Schaefer, M., et al., *A protein complex containing Inscuteable and the Gα-binding protein Pins orients asymmetric cell divisions in Drosophila.* Current Biology, 2000. **10**(7): p. 353-362.
64. Kraut, R., et al., *Role of inscuteable in orienting asymmetric cell divisions in Drosophila.* Nature, 1996. **383**(6595): p. 50-55.
65. Williams, S.E., et al., *Par3–mInsc and Gαi3 cooperate to promote oriented epidermal cell divisions through LGN.* Nature Cell Biology, 2014. **16**(8): p. 758-769.
66. Kotak, S., C. Busso, and P. Gönczy, *Cortical dynein is critical for proper spindle positioning in human cells.* J Cell Biol, 2012. **199**(1): p. 97-110.
67. Nguyen-Ngoc, T., K. Afshar, and P. Gönczy, *Coupling of cortical dynein and G alpha proteins mediates spindle positioning in Caenorhabditis elegans.* Nat Cell Biol, 2007. **9**(11): p. 1294-302.
68. Okumura, M., et al., *Dynein–Dynactin–NuMA clusters generate cortical spindle-pulling forces as a multi-arm ensemble.* eLife, 2018. **7**: p. e36559.
69. Tame, M.A., et al., *Astral microtubules control redistribution of dynein at the cell cortex to facilitate spindle positioning.* Cell Cycle, 2014. **13**(7): p. 1162-70.
70. Hirokawa, N., et al., *Kinesin superfamily motor proteins and intracellular transport.* Nature Reviews Molecular Cell Biology, 2009. **10**(10): p. 682-696.
71. Ali, I. and W.-C. Yang, *The functions of kinesin and kinesin-related proteins in eukaryotes.* Cell Adhesion & Migration, 2020. **14**(1): p. 139-152.
72. Stout, J.R., et al., *Kif18B interacts with EB1 and controls astral microtubule length during mitosis.* Molecular Biology of the Cell, 2011. **22**(17): p. 3070-3080.
73. Marvin, et al., *A Complex of Kif18b and MCAK Promotes Microtubule Depolymerization and Is Negatively Regulated by Aurora Kinases.* Current Biology, 2011. **21**(16): p. 1356-1365.
74. Lee, Y.M., et al., *Cell cycle-regulated expression and subcellular localization of a kinesin-8 member human KIF18B.* Gene, 2010. **466**(1-2): p. 16-25.
75. McHugh, T., A.A. Gluszek, and J.P.I. Welburn, *Microtubule end tethering of a processive kinesin-8 motor Kif18b is required for spindle positioning.* Journal of Cell Biology, 2018. **217**(7): p. 2403-2416.
76. Moreci, R.S. and T. Lechler, *KIF18B is a cell type–specific regulator of spindle orientation in the epidermis.* Molecular Biology of the Cell, 2021. **32**(21): p. mbc.E21-06-0291.
77. Ouspenskaia, T., et al., *WNT-SHH Antagonism Specifies and Expands Stem Cells prior to Niche Formation.* Cell, 2016. **164**(1-2): p. 156-169.

78. Bergstralh, D.T., H.E. Lovegrove, and D. St Johnston, *Lateral adhesion drives reintegration of misplaced cells into epithelial monolayers.* Nature Cell Biology, 2015. **17**(11): p. 1497-1503.
79. Nakajima, Y.-I., et al., *Epithelial junctions maintain tissue architecture by directing planar spindle orientation.* Nature, 2013. **500**(7462): p. 359-362.
80. Packard, A., et al., *Luminal Mitosis Drives Epithelial Cell Dispersal within the Branching Ureteric Bud.* Developmental Cell, 2013. **27**(3): p. 319-330.
81. Godde, N.J., et al., *Scribble Modulates the MAPK/Fra1 Pathway to Disrupt Luminal and Ductal Integrity and Suppress Tumour Formation in the Mammary Gland.* PLoS Genetics, 2014. **10**(5): p. e1004323.
82. Zhou, P.-J., et al., *Loss of Par3 promotes prostatic tumorigenesis by enhancing cell growth and changing cell division modes.* Oncogene, 2019. **38**(12): p. 2192-2205.
83. Luke, et al., *Loss of the Par3 Polarity Protein Promotes Breast Tumorigenesis and Metastasis.* Cancer Cell, 2012. **22**(5): p. 601-614.
84. Oftedal, O.T., Journal of Mammary Gland Biology and Neoplasia, 2002. **7**(3): p. 253-266.
85. Vorbach, C., M.R. Capecchi, and J.M. Penninger, *Evolution of the mammary gland from the innate immune system?* BioEssays, 2006. **28**(6): p. 606-616.
86. Oftedal, O.T., Journal of Mammary Gland Biology and Neoplasia, 2002. **7**(3): p. 225-252.
87. Telemo, E. and L.A. Hanson, *Antibodies in milk.* Journal of Mammary Gland Biology and Neoplasia, 1996. **1**(3): p. 243-249.
88. Chu, E.Y., et al., *Canonical WNT signaling promotes mammary placode development and is essential for initiation of mammary gland morphogenesis.* Development, 2004. **131**(19): p. 4819-4829.
89. Jerome-Majewska, L.A., et al., *Tbx3, the ulnar-mammary syndrome gene, andTbx2interact in mammary gland development through a p19<sup>Arf</sup>/p53-independent pathway.* Developmental Dynamics, 2005. **234**(4): p. 922-933.
90. Mailleux, A.A., et al., *Role of FGF10/FGFR2b signaling during mammary gland development in the mouse embryo.* Development, 2002. **129**(1): p. 53-60.
91. Hogg, N.A., C.J. Harrison, and C. Tickle, *Lumen formation in the developing mouse mammary gland.* J Embryol Exp Morphol, 1983. **73**: p. 39-57.
92. Debnath, J., et al., *The Role of Apoptosis in Creating and Maintaining Luminal Space within Normal and Oncogene-Expressing Mammary Acini.* Cell, 2002. **111**(1): p. 29-40.
93. Macias, H. and L. Hinck, *Mammary gland development.* Wiley Interdisciplinary Reviews: Developmental Biology, 2012. **1**(4): p. 533-557.
94. Howard, B.A., Journal of Mammary Gland Biology and Neoplasia, 2000. **5**(2): p. 119-137.
95. Humphreys, R.C., et al., *Apoptosis in the terminal endbud of the murine mammary gland: a mechanism of ductal morphogenesis.* Development, 1996. **122**(12): p. 4013-22.
96. Mailleux, A.A., et al., *BIM regulates apoptosis during mammary ductal morphogenesis, and its absence reveals alternative cell death mechanisms.* Dev Cell, 2007. **12**(2): p. 221-34.
97. Ewald, A.J., et al., *Collective Epithelial Migration and Cell Rearrangements Drive Mammary Branching Morphogenesis.* Developmental Cell, 2008. **14**(4): p. 570-581.

98. Huebner, R.J., T. Lechler, and A.J. Ewald, *Developmental stratification of the mammary epithelium occurs through symmetry-breaking vertical divisions of apically positioned luminal cells.* Development, 2014. **141**(5): p. 1085-1094.
99. Schedin, P. and P.J. Keely, *Mammary Gland ECM Remodeling, Stiffness, and Mechanosignaling in Normal Development and Tumor Progression.* Cold Spring Harbor Perspectives in Biology, 2011. **3**(1): p. a003228-a003228.
100. Ruan, W. and D.L. Kleinberg, *Insulin-like growth factor I is essential for terminal end bud formation and ductal morphogenesis during mammary development.* Endocrinology, 1999. **140**(11): p. 5075-81.
101. Daniel, C.W., G.B. Silberstein, and P. Strickland, *Direct action of 17 beta-estradiol on mouse mammary ducts analyzed by sustained release implants and steroid autoradiography.* Cancer Res, 1987. **47**(22): p. 6052-7.
102. Lydon, J.P., et al., *Mice lacking progesterone receptor exhibit pleiotropic reproductive abnormalities.* Genes Dev, 1995. **9**(18): p. 2266-78.
103. Ciarloni, L., S. Mallepell, and C. Brisken, *Amphiregulin is an essential mediator of estrogen receptor alpha function in mammary gland development.* Proc Natl Acad Sci U S A, 2007. **104**(13): p. 5455-60.
104. Lu, P., et al., *Genetic mosaic analysis reveals FGF receptor 2 function in terminal end buds during mammary gland branching morphogenesis.* Dev Biol, 2008. **321**(1): p. 77-87.
105. Silberstein, G.B. and C.W. Daniel, *Reversible inhibition of mammary gland growth by transforming growth factor-beta.* Science, 1987. **237**(4812): p. 291-3.
106. Joseph, H., et al., *Overexpression of a kinase-deficient transforming growth factor-beta type II receptor in mouse mammary stroma results in increased epithelial branching.* Mol Biol Cell, 1999. **10**(4): p. 1221-34.
107. Sung, H., et al., *Global Cancer Statistics 2020: GLOBOCAN Estimates of Incidence and Mortality Worldwide for 36 Cancers in 185 Countries.* CA: A Cancer Journal for Clinicians, 2021. **71**(3): p. 209-249.
108. Ellis, I.O., *Intraductal proliferative lesions of the breast: morphology, associated risk and molecular biology.* Mod Pathol, 2010. **23 Suppl 2**: p. S1-7.
109. Lopez-Garcia, M.A., et al., *Breast cancer precursors revisited: molecular features and progression pathways.* Histopathology, 2010. **57**(2): p. 171-92.
110. Cowell, C.F., et al., *Progression from ductal carcinoma in situ to invasive breast cancer: revisited.* Mol Oncol, 2013. **7**(5): p. 859-69.
111. *Comprehensive molecular portraits of human breast tumours.* Nature, 2012. **490**(7418): p. 61-70.
112. Javadi, A., et al., *PTEN controls glandular morphogenesis through a juxtamembrane β-Arrestin1/ARHGAP21 scaffolding complex.* Elife, 2017. **6**.
113. Toyoshima, F., et al., *PtdIns(3,4,5)P3 Regulates Spindle Orientation in Adherent Cells.* Developmental Cell, 2007. **13**(6): p. 796-811.
114. Attalla, S., et al., *Insights from transgenic mouse models of PyMT-induced breast cancer: recapitulating human breast cancer progression in vivo.* Oncogene, 2021. **40**(3): p. 475-491.
115. Guy, C.T., R.D. Cardiff, and W.J. Muller, *Induction of mammary tumors by expression of polyomavirus middle T oncogene: a transgenic mouse model for metastatic disease.* Mol Cell Biol, 1992. **12**(3): p. 954-61.

116. Pfefferle, A.D., et al., *Transcriptomic classification of genetically engineered mouse models of breast cancer identifies human subtype counterparts.* Genome Biology, 2013. **14**(11): p. R125.
117. Guy, C.T., et al., *Activation of the c-Src tyrosine kinase is required for the induction of mammary tumors in transgenic mice.* Genes Dev, 1994. **8**(1): p. 23-32.
118. Halaoui, R., et al., *Progressive polarity loss and luminal collapse disrupt tissue organization in carcinoma.* Genes Dev, 2017. **31**(15): p. 1573-1587.
119. Shore, A.N., et al., *PTEN is required to maintain luminal epithelial homeostasis and integrity in the adult mammary gland.* Dev Biol, 2016. **409**(1): p. 202-217.
120. Kajita, M., et al., *Interaction with surrounding normal epithelial cells influences signalling pathways and behaviour of Src-transformed cells.* Journal of Cell Science, 2010. **123**(2): p. 171-180.
121. Mailleux, A.A., et al., *BIM Regulates Apoptosis during Mammary Ductal Morphogenesis, and Its Absence Reveals Alternative Cell Death Mechanisms.* Developmental Cell, 2007. **12**(2): p. 221-234.
122. Villegas, E., et al., *Plk2 regulates mitotic spindle orientation and mammary gland development.* Development, 2014. **141**(7): p. 1562-1571.
123. Packard, A., et al., *Luminal mitosis drives epithelial cell dispersal within the branching ureteric bud.* Dev Cell, 2013. **27**(3): p. 319-30.
124. Ragkousi, K. and M.C. Gibson, *Cell division and the maintenance of epithelial order.* J Cell Biol, 2014. **207**(2): p. 181-8.
125. Ballard, M.S., et al., *Mammary Stem Cell Self-Renewal Is Regulated by Slit2/Robo1 Signaling through SNAI1 and mINSC.* Cell Rep, 2015. **13**(2): p. 290-301.
126. Fischer, E., et al., *Defective planar cell polarity in polycystic kidney disease.* Nature Genetics, 2006. **38**(1): p. 21-23.
127. Bergstralh, D.T., H.E. Lovegrove, and D. St Johnston, *Lateral adhesion drives reintegration of misplaced cells into epithelial monolayers.* Nat Cell Biol, 2015. **17**(11): p. 1497-1503.
128. Macara, I.G., et al., *Epithelial Homeostasis.* Curr Biol, 2014. **24**(17): p. R815-R825.
129. Pei, D., et al., *Mesenchymal-epithelial transition in development and reprogramming.* Nat Cell Biol, 2019. **21**(1): p. 44-53.
130. Sutherland, A., R. Keller, and A. Lesko, *Convergent extension in mammalian morphogenesis.* Semin Cell Dev Biol, 2020. **100**: p. 199-211.
131. Wilson, T.J. and D.T. Bergstralh, *Cell reintegration: Stray epithelial cells make their way home.* Bioessays, 2017. **39**(6).
132. Bruce, A.E.E. and C.P. Heisenberg, *Mechanisms of zebrafish epiboly: A current view.* Curr Top Dev Biol, 2020. **136**: p. 319-341.
133. Geldmacher-Voss, B., et al., *A 90-degree rotation of the mitotic spindle changes the orientation of mitoses of zebrafish neuroepithelial cells.* Development, 2003. **130**(16): p. 3767-80.
134. Stubbs, J.L., et al., *Radial intercalation of ciliated cells during Xenopus skin development.* Development, 2006. **133**(13): p. 2507-2515.
135. Silberstein, G.B., *Postnatal mammary gland morphogenesis.* Microsc Res Tech, 2001. **52**(2): p. 155-62.
136. Hinck, L. and G.B. Silberstein, *Key stages in mammary gland development: the mammary end bud as a motile organ.* Breast Cancer Res, 2005. **7**(6): p. 245-51.

137. Sreekumar, A., et al., *WNT-Mediated Regulation of FOXO1 Constitutes a Critical Axis Maintaining Pubertal Mammary Stem Cell Homeostasis.* Dev Cell, 2017. **43**(4): p. 436-448 e6.
138. Paine, I., et al., *A Geometrically-Constrained Mathematical Model of Mammary Gland Ductal Elongation Reveals Novel Cellular Dynamics within the Terminal End Bud.* PLoS Comput Biol, 2016. **12**(4): p. e1004839.
139. Baena-López, L.A., A. Baonza, and A. García-Bellido, *The Orientation of Cell Divisions Determines the Shape of Drosophila Organs.* Current Biology, 2005. **15**(18): p. 1640-1644.
140. Prater, M.D., et al., *Mammary stem cells have myoepithelial cell properties.* Nature Cell Biology, 2014. **16**(10): p. 942-950.
141. Umeda, K., et al., *ZO-1 and ZO-2 Independently Determine Where Claudins Are Polymerized in Tight-Junction Strand Formation.* Cell, 2006. **126**(4): p. 741-754.
142. Pasic, L., et al., *Sustained activation of the HER1–ERK1/2–RSK signaling pathway controls myoepithelial cell fate in human mammary tissue.* Genes & Development, 2011. **25**(15): p. 1641-1653.
143. Murrell, M., et al., *Forcing cells into shape: the mechanics of actomyosin contractility.* Nature Reviews Molecular Cell Biology, 2015. **16**(8): p. 486-498.
144. Sedzinski, J., et al., *Emergence of an Apical Epithelial Cell Surface In Vivo.* Developmental Cell, 2016. **36**(1): p. 24-35.
145. Ventura, G., et al., *Multiciliated cells use filopodia to probe tissue mechanics during epithelial integration in vivo.* Nature Communications, 2022. **13**(1).
146. Takeichi, M., *Dynamic contacts: rearranging adherens junctions to drive epithelial remodelling.* Nature Reviews Molecular Cell Biology, 2014. **15**(6): p. 397-410.
147. Ahmed, S.M. and I.G. Macara, *The Par3 polarity protein is an exocyst receptor essential for mammary cell survival.* Nature Communications, 2017. **8**(1): p. 14867.
148. Engl, W., et al., *Actin dynamics modulate mechanosensitive immobilization of E-cadherin at adherens junctions.* Nature Cell Biology, 2014. **16**(6): p. 584-591.
149. Efimova, N. and T.M. Svitkina, *Branched actin networks push against each other at adherens junctions to maintain cell–cell adhesion.* Journal of Cell Biology, 2018. **217**(5): p. 1827-1845.
150. Beutel, O., et al., *Phase Separation of Zonula Occludens Proteins Drives Formation of Tight Junctions.* Cell, 2019. **179**(4): p. 923-936.e11.
151. Tornavaca, O., et al., *ZO-1 controls endothelial adherens junctions, cell–cell tension, angiogenesis, and barrier formation.* Journal of Cell Biology, 2015. **208**(6): p. 821-838.
152. Balda, M.S. and K. Matter, *The tight junction protein ZO-1 and an interacting transcription factor regulate ErbB-2 expression.* EMBO J, 2000. **19**(9): p. 2024-33.
153. Remue, E., et al., *TAZ interacts with zonula occludens-1 and -2 proteins in a PDZ-1 dependent manner.* FEBS Letters, 2010. **584**(19): p. 4175-4180.
154. McCaffrey, L.M. and I.G. Macara, *The Par3/aPKC interaction is essential for end bud remodeling and progenitor differentiation during mammary gland morphogenesis.* Genes Dev, 2009. **23**(12): p. 1450-60.
155. Pease, J.C. and J.S. Tirnauer, *Mitotic spindle misorientation in cancer--out of alignment and into the fire.* J Cell Sci, 2011. **124**(Pt 7): p. 1007-16.
156. Quyn, A.J., et al., *Spindle orientation bias in gut epithelial stem cell compartments is lost in precancerous tissue.* Cell Stem Cell, 2010. **6**(2): p. 175-81.

157. Seldin, L. and I. Macara, *Epithelial spindle orientation diversities and uncertainties: recent developments and lingering questions.* F1000Res, 2017. **6**: p. 984.
158. Bergstralh, D.T. and D. St Johnston, *Spindle orientation: what if it goes wrong?* Semin Cell Dev Biol, 2014. **34**: p. 140-5.
159. McCaffrey, L.M. and I.G. Macara, *Epithelial organization, cell polarity and tumorigenesis.* Trends Cell Biol, 2011. **21**(12): p. 727-35.
160. Polyak, K., *Breast cancer: origins and evolution.* J Clin Invest, 2007. **117**(11): p. 3155-63.
161. Casasent, A.K., M. Edgerton, and N.E. Navin, *Genome evolution in ductal carcinoma in situ: invasion of the clones.* J Pathol, 2017. **241**(2): p. 208-218.
162. Dontu, G. and T.A. Ince, *Of mice and women: a comparative tissue biology perspective of breast stem cells and differentiation.* J Mammary Gland Biol Neoplasia, 2015. **20**(1-2): p. 51-62.
163. Cheffings, T.H., N.J. Burroughs, and M.K. Balasubramanian, *Actomyosin Ring Formation and Tension Generation in Eukaryotic Cytokinesis.* Curr Biol, 2016. **26**(15): p. R719-r737.
164. Zheng, Z., et al., *LGN regulates mitotic spindle orientation during epithelial morphogenesis.* J Cell Biol, 2010. **189**(2): p. 275-88.
165. McCaffrey, L.M. and I.G. Macara, *The Par3/aPKC interaction is essential for end bud remodeling and progenitor differentiation during mammary gland morphogenesis.* Genes & Development, 2009. **23**(12): p. 1450-1460.
166. Liu, W.A., et al., *PARD3 dysfunction in conjunction with dynamic HIPPO signaling drives cortical enlargement with massive heterotopia.* Genes Dev, 2018. **32**(11-12): p. 763-780.
167. Nakajima, Y., et al., *Epithelial junctions maintain tissue architecture by directing planar spindle orientation.* Nature, 2013. **500**(7462): p. 359-62.
168. Kuo, C.S. and M.A. Krasnow, *Formation of a Neurosensory Organ by Epithelial Cell Slithering.* Cell, 2015. **163**(2): p. 394-405.
169. Macias, H. and L. Hinck, *Mammary gland development.* Wiley Interdiscip Rev Dev Biol, 2012. **1**(4): p. 533-57.
170. Inman, J.L., et al., *Mammary gland development: cell fate specification, stem cells and the microenvironment.* Development, 2015. **142**(6): p. 1028-42.
171. Stout, J.R., et al., *Kif18B interacts with EB1 and controls astral microtubule length during mitosis.* Mol Biol Cell, 2011. **22**(17): p. 3070-80.
172. McHugh, T., A.A. Gluszek, and J.P.I. Welburn, *Microtubule end tethering of a processive kinesin-8 motor Kif18b is required for spindle positioning.* J Cell Biol, 2018. **217**(7): p. 2403-2416.
173. Tanenbaum, M.E., et al., *A complex of Kif18b and MCAK promotes microtubule depolymerization and is negatively regulated by Aurora kinases.* Curr Biol, 2011. **21**(16): p. 1356-65.
174. Sanjana, N.E., O. Shalem, and F. Zhang, *Improved vectors and genome-wide libraries for CRISPR screening.* Nat Methods, 2014. **11**(8): p. 783-784.
175. Walczak, C.E., et al., *Spatial regulation of astral microtubule dynamics by Kif18B in PtK cells.* Mol Biol Cell, 2016. **27**(20): p. 3021-3030.
176. Nguyen-Ngoc, K.V., et al., *3D culture assays of murine mammary branching morphogenesis and epithelial invasion.* Methods Mol Biol, 2015. **1189**: p. 135-62.

177. Rodriguez-Fraticelli, A.E., et al., *The Cdc42 GEF Intersectin 2 controls mitotic spindle orientation to form the lumen during epithelial morphogenesis.* J Cell Biol, 2010. **189**(4): p. 725-38.
178. Qin, Y., et al., *Tuba, a Cdc42 GEF, is required for polarized spindle orientation during epithelial cyst formation.* J Cell Biol, 2010. **189**(4): p. 661-9.
179. Zhu, J., et al., *LGN/mInsc and LGN/NuMA complex structures suggest distinct functions in asymmetric cell division for the Par3/mInsc/LGN and Gαi/LGN/NuMA pathways.* Mol Cell, 2011. **43**(3): p. 418-31.
180. Halaoui, R., et al., *Progressive polarity loss and luminal collapse disrupt tissue organization in carcinoma.* Genes & Development, 2017. **31**(15): p. 1573-1587.
181. Kon, S., et al., *Cell competition with normal epithelial cells promotes apical extrusion of transformed cells through metabolic changes.* Nature Cell Biology, 2017. **19**(5): p. 530-541.
182. Leung, C.T. and J.S. Brugge, *Outgrowth of single oncogene-expressing cells from suppressive epithelial environments.* Nature, 2012. **482**(7385): p. 410-413.
183. Tang, N., et al., *Control of mitotic spindle angle by the RAS-regulated ERK1/2 pathway determines lung tube shape.* Science, 2011. **333**(6040): p. 342-345.
184. Villegas, E., et al., *Plk2 regulates mitotic spindle orientation and mammary gland development.* Development, 2014. **141**(7): p. 1562-71.
185. Nishio, S., et al., *Loss of oriented cell division does not initiate cyst formation.* J Am Soc Nephrol, 2010. **21**(2): p. 295-302.
186. Fedeles, S. and A.R. Gallagher, *Cell polarity and cystic kidney disease.* Pediatric Nephrology, 2013. **28**(8): p. 1161-1172.
187. Marciano, D.K., *A holey pursuit: lumen formation in the developing kidney.* Pediatr Nephrol, 2017. **32**(1): p. 7-20.
188. Fankhaenel, M., et al., *Annexin A1 is a polarity cue that directs mitotic spindle orientation during mammalian epithelial morphogenesis.* Nature Communications, 2023. **14**(1).
189. Hartsock, A. and W.J. Nelson, *Adherens and tight junctions: structure, function and connections to the actin cytoskeleton.* Biochim Biophys Acta, 2008. **1778**(3): p. 660-9.
190. Collins, C., et al., *Tubulin acetylation promotes penetrative capacity of cells undergoing radial intercalation.* Cell Rep, 2021. **36**(7): p. 109556.
191. Sedzinski, J., et al., *Emergence of an Apical Epithelial Cell Surface In Vivo.* Dev Cell, 2016. **36**(1): p. 24-35.
192. Noatynska, A., M. Gotta, and P. Meraldi, *Mitotic spindle (DIS)orientation and DISease: Cause or consequence?* Journal of Cell Biology, 2012. **199**(7): p. 1025-1035.
193. Compton, D.A. and D.W. Cleveland, *NuMA is required for the proper completion of mitosis.* Journal of Cell Biology, 1993. **120**(4): p. 947-957.
194. Rajeevan, A., et al., *NuMA interaction with chromatin is vital for proper chromosome decondensation at the mitotic exit.* Molecular Biology of the Cell, 2020. **31**(22): p. 2437-2451.
195. Kuo, W.T., et al., *The Tight Junction Protein ZO-1 Is Dispensable for Barrier Function but Critical for Effective Mucosal Repair.* Gastroenterology, 2021. **161**(6): p. 1924-1939.
196. Odenwald, M.A., et al., *ZO-1 interactions with F-actin and occludin direct epithelial polarization and single lumen specification in 3D culture.* J Cell Sci, 2017. **130**(1): p. 243-259.

197. Zhou, Z., H. Alégot, and K.D. Irvine, *Oriented Cell Divisions Are Not Required for Drosophila Wing Shape.* Curr Biol, 2019. **29**(5): p. 856-864.e3.
198. Sternlicht, M.D., *Key stages in mammary gland development: The cues that regulate ductal branching morphogenesis.* Breast Cancer Research, 2005. **8**(1).
199. Chhabra, S.N. and B.W. Booth, *Asymmetric cell division of mammary stem cells.* Cell Div, 2021. **16**(1): p. 5.
200. Cicalese, A., et al., *The tumor suppressor p53 regulates polarity of self-renewing divisions in mammary stem cells.* Cell, 2009. **138**(6): p. 1083-95.